Aus der Neurochirurgischen Klinik und Poliklinik
der Ludwig-Maximilians-Universität München

Vorstand: Prof. Dr. med. Jörg-Christian Tonn

APLN-APLNR signaling controls tumor angiogenesis and glioblastoma cell invasion

Dissertation
zum Erwerb des Doktorgrades der Naturwissenschaften
an der Medizinischen Fakultät der
Ludwig-Maximilians-Universität zu München

Vorgelegt von
Giorgia Mastrella
aus
Castelfranco Veneto
2019

Mit Genehmigung der Medizinischen Fakultät

der Universität München

Betreuer: Prof. Dr. rer. nat. Rainer Glaß

Zweitgutachter: Prof. Dr. rer. nat. Heiko Hermeking

Dekan: Prof. Dr. med. dent. Reinhard Hickel

Tag der mündlichen Prüfung: 13. Dezember 2019

Zusammenfassung

Das Glioblastoma multiforme (GBM) ist ein tödlicher Tumor, der 2,5 Personen von 100000 Erwachsenen pro Jahr betrifft. Trotz der aggressiven Interventionen hat ein Patient eine Lebenserwartung von 14-16 Monaten. Die GBM-Zellen dringen in das Tumorparenchym ein und breiten sich von der ursprünglichen Masse zu entfernten Stellen aus. Der wachsende Tumor induziert das Aussprossen der vorhandenen Blutgefäße und die vaskuläre Proliferation, die als das Phänomen der "Tumorangiogenese“ bekannt ist. Angesichts der ausgeprägten Vaskularisierung des Glioblastoms stellen antiangiogene Wirkstoffe eine vielversprechende therapeutische Strategie dar und viele Medikamente werden derzeit untersucht, um diese Malignität zu behandeln. Die meisten Interventionen zielen auf das Vascular Endothelial Growth Factor (VEGF) Signal ab, aber ihre langfristigen Vorteile haben den Erwartungen nicht entsprochen: der Tumor kommt immer wieder, unterstützt von der Hochregulation anderer angiogener Signale und der zusätzlichen Hilfe der Tumor-assoziierten myeloiden Zellen. Deshalb ist die Validierung alternativer Ziele ein drängendes Thema in der präklinischen Forschung, um effizientere Therapien gegen das GBM zu finden. Unter den vielen neuen antiangiogenen Signalen, die an der GBM-Neoangiogenese beteiligt sind, hat die aktuelle Forschung neue Aufmerksamkeit auf den Apelin - Apelin Rezeptor (APLN-APLNR) Signalweg gelenkt. Das APLN-APLNR-Signal spielt eine wichtige Rolle bei der Entwicklung des vaskulären Systems während der Embriogenese, aber auch bei verschiedenen pathologischen Zuständen.

In meiner Doktorarbeit habe ich eine ausführliche Charakterisierung der Expression von APLN und APLNR in *in vitro* Zellkulturen aus GBM-Patienten und in GBM Maus- und menschlichen Proben durchgeführt. Ligand und Rezeptor sind im GBM-Gewebe hochreguliert und diese Hochregulation ist mit dem angiogenen GBM-Phänotyp assoziiert. Die Erzeugung mehrerer primärer GBM-Zellen mit Verlust der APLN-Expression hat dabei die Notwendigkeit des APLN-Signals für die GBM-Neoangiogenese bestätigt. Außerdem, führte der Verlust eines autokrinen APLN-APLNR-Signals in den implantierten GBM-Zellen zu einer erhöhen Tumorinvasion.

In verschiedenen humanen GBM-Proben wies die besondere Verteilung von Ligand und Rezeptor in der Tumormasse auf die Doppelrolle dieses Signals sowohl bei der Tumorangiogenese als auch der Tumorzell-Invasion hin. Die invasive Fähigkeit der GBM-Zellen mit APLN-Verlust wurde *in vitro* umfassend charakterisiert, wobei, analog zu den *in vivo* Resultaten, das Fehlen eines autokrinen APLN-APLNR-Signals die Zellinvasion antreibt.

Zusätzlich fand ich heraus, dass die Blockade von APLNR die Zellinvasion *in vitro* beeinflusst und dass die intrazelluläre Rezeptorverteilung sich dabei ändert. Daher könnte der Aktivierungsstatus des Rezeptors selbst eine zentrale Funktion bei der Bestimmung des GBM-Zellverhaltens haben. Die zusätzlich hergestellten primären GBM-Zellen mit APLNR-Verlust werden in zukünftigen Studien eine bessere Charakterisierung des APLNR Rezeptors und seiner Rolle als Treiber der Tumorinvasion ermöglichen.

Die Analyse verschiedener Proben von Patienten und Mausmodelle, die aus Studien über die Behandlung des GBMs mit antiangiogenen Mitteln kommen, zeigte, dass der APLN-APLNR-Signalweg auch an der Rekurrenz des Tumors beteiligt ist.

Des Weiteren konnte ich darlegen, dass die therapeutische Blockade von APLNR *in vivo,* die die Tumorinvasion und Angiogenese reduzierte, eine erhöhte Akkumulation von intratumoralen myeloiden Zellen auslöst, welche mit der Tumorrekurrenz nach Verabreichung von antiangiogenen Behandlungen verbunden zu sein scheint.

Insgesamt, zeigte es sich in meiner Arbeit, dass der APLN-APLNR-Signalweg, mit seiner prominenten Expression in GBM-Gewebe und seiner Rolle bei der Eindämmung der GBM-Invasion und –Angiogenese, ein interessantes Ziel für zukünftige Tumortherapien darstellt. Weitere Studien sind jedoch notwendig, um die Konsequenzen und das therapeutische Potenzial seiner Blockade vollständig zu offenbaren.

Preamble

Part of the work collected in this thesis is included in a manuscript entitled "*Targeting APLN/APLNR Improves Antiangiogenic Efficiency and Blunts Proinvasive Side Effects of VEGFA/VEGFR2 Blockade in Glioblastoma*", where my colleagues Min Li, Mengzhuo Hou, and I are three first authors. The manuscript is cited as reference 147.

Abstract

Glioblastoma multiforme (GBM) is a deadly tumor that affects 2.5 people every 100000 adults per year. Despite the aggressive interventions, a GBM patient has a life expectancy of 14-16 months. GBM cells invade the tumor parenchyma and spread to distant sites from the original mass. The growing tumor induces sprouting of the existing vessels and vascular proliferation, the phenomenon known as "tumor angiogenesis". Given the prominent vascularization of glioblastoma, anti-angiogenic agents are a promising strategy for the treatment of this malignancy and many drugs are under evaluation. The majority of these interventions, which target the vascular endothelial growth factor (VEGF) signaling pathway, do not show long-term benefits: tumor rebound always occurs, supported by the upregulation of other angiogenic pathways and the tumor-promoting role of the tumor-associated myeloid cells. Therefore, the validation of alternative targets for more efficient therapies is an urgent need in preclinical research. Among other emerging angiogenic pathways involved in GBM neo-angiogenesis, recent findings brought attention to the apelin-apelin receptor (APLN-APLNR) signaling, which has a primary role in the development of the vascular system during embryogenesis, but it is also associated to different pathological conditions.

In the present thesis, I performed an extensive characterization of the expression of APLN and APLNR in *in vitro* cultures of patient-derived GBM cells and in mouse and human GBM specimens. Ligand and receptor were up-regulated in the GBM tissue and this upregulation was associated with the GBM angiogenic phenotype. The generation of several primary GBM cells with loss of APLN expression confirmed that GBM neo-angiogenesis *in vivo* depends on APLN function. Moreover, the loss of an autocrine APLN-APLNR signaling in the implanted GBM cells drove tumor invasion.

In various human GBM samples, the peculiar distribution of both ligand and receptor across the tumor mass hinted to the dual role of the pathway in tumor angiogenesis and invasion. The invasive ability of the GBM cells with loss of APLN was extensively characterized *in vitro*, where, as demonstrated *in vivo*, the absence of an autocrine APLN-APLNR signaling increased cell invasion.

In addition, the *in vivo* intratumoral administration of the receptor antagonist apelin-F13A was able to reduce tumor invasion and angiogenesis. *In vitro*, the exposure to apelin-F13A reduced the invasive abilities of the cells tested.

Moreover, the administration of apelin-13 and apelin-F13A did not only modify the *in vitro* and *in vivo* behavior of the GBM cells, but also the intracellular distribution of APLNR. Therefore,

the distribution/activation status of the receptor itself may have a central function in the determination of the GBM phenotype.

Next, the analysis of various samples obtained from different studies of GBMs therapeutically-treated with anti-angiogenic agents, demonstrated that the APLN-APLNR signaling, aside from being a driver of tumor progression, may also be involved in therapy resistance.

Overall, the prominent expression of the APLN-APLNR signaling in GBM tissue and its role in driving GBM invasion and angiogenesis indicate its promising function as target of future tumor therapies. Further studies, however, are required to fully disclose the consequences and the therapeutic potential of its blockade.

Contents

1. Abbreviations

aCSF	Artificial cerebrospinal fluid
ACV	Anterior cardinal vein
Ang-2	Angiopoietin 2
Apelin-13scr	Apelin-13 scrambled
APLN	Apelin
APLNR	Apelin receptor
ATCC	American Type Culture Collection
BBB	Blood brain barrier
bFGF	Basic fibroblastic growth factor
cAMP	Cyclic adenosine monophosphate
CD68, 11b	Cluster of differentiation 68, 11b
CHO	Chinese hamster ovary cells
CNS	Central nervous system
CSF	Colony stimulating factor
ECs	Endothelial cells
EGF	Endothelial growth factor
EMA	European Medicine Agency
FDA	Food and Drug Administration (United States)
GBM	Glioblastoma multiforme
GFP	Green fluorescent protein
GPCR	G protein-coupled receptor
GSCs	Glioma stem cells
HEK293	Human embryonic kidney 293 cells
HIF	Hypoxia-inducible factor
HS	Homo sapiens

IDH	Isocitrate dehydrogenase
IBA1	Ionized calcium-binding adapter molecule 1
IFNγ	Interferon γ
IL	Interleukin
ISVs	Intersomitic vessels
EG5	Kinesin-5
KD	Knock down
KO	Knock out
MM	Mus musculus
NOS	Nitric oxygen synthase
NPCs	Neural precursor cells
NSCLC	Non-small cell lung cancer
OPN	Osteopontin
OS	Overall survival
PCV	Posterior cardinal vein
PDGF	Platelet-derived growth factor
PDX	Patient-derived xenograft
PFS	Progression-free survival
PIGF	Placenta growth factor
(pyr^{1})apelin-13	Pyroglutamylated apelin-13
qPCR	Quantitative PCR
siRNA	Small interfering RNA
SVZ	Subventricular zone
TAMs	Tumor-associated myeloid cells
TMZ	Temozolomide

VEGF	Vascular endothelial growth factor
VSMCs	Vascular smooth muscle cells
WHO	World health organization
WT	Wild type

2. List of figures

Supplementary Information:

3. List of tables

Materials and methods:

4. Introduction

4.1 Glioblastoma multiforme

Gliomas are the most common primary brain cancers among adults, accounting for 80% of all brain tumors. Among them, glioblastoma multiforme (GBM) is diagnosed in 65% of the cases [1-3]. The World Health Organization (WHO) classifies GBMs as grade IV gliomas and, according to the new guidelines of the 2016 Classification of Tumors of the Central Nervous System (CNS WHO), divides them into isocitrate dehydrogenase gene (IDH)-wildtype (WT) and IDH-mutant. IDH-WT GBMs originate *de novo*, while IDH-mutants are secondary tumors developed from a low-grade glioma. The average survival rates of IDH-wildtype and IDH-mutant GBMs are approximatively 14-16 and 27 months, respectively [4]. Typical features of grade IV gliomas are abundant necrosis, the highly invasive behavior, and the presence of numerous microvascular proliferations [5, 6].

Neovascularization is a fundamental step in the distinction between low-grade and high-grade gliomas: the progression from a low-grade to a high-grade tumor is not only associated with an increased infiltrative behavior, but also with increased vascular proliferation [7-9]. This phenomenon, known as the "angiogenic switch", defines GBM as a fatal disease and explains the recent attempts in cancer research to block angiogenesis with anti-angiogenic agents [9, 10].

Tumor transformation to a fatal high-grade status is a matter of intense study and the possibility to predict disease progression would be an important achievement for patient-specific therapeutic interventions. *Rees* and colleagues demonstrated that two reliable factors for malignancy prediction of gliomas are tumor volume and its growth rate, this latter showing an exponential curve for the brain tumors that will undergo a low- to high-grade evolution [11].

GBM was classified by gene expression profiling into four different subclasses: proneural, neural, classical, and mesenchymal. Recent studies, however, dismissed the "neural" category as a proper subgroup because of its lack of typical genetic abnormalities that would allow a GBM classification under this name [12]. In fact, the neural subtype expresses genes that are also found in non-tumor tissue and it is mostly represented by the marginal tumor regions, where GBM cells alternate with brain parenchyma. It is therefore a less-defined GBM subgroup, in contrast to the other ones that are mostly found in the contrast-enhancing regions of the tumor core [13].

The GBM subgroups do not only differ in the altered expression of molecular pathways, but also in the therapeutic responses to treatments and in clinical outcomes, with an average

survival advantage in the proneural subtype and a worse outcome in mesenchymal GBM [14]. It is important to underline that often a tumor mass does not belong to a single subtype, but presents itself as a heterogeneous mass containing tumor areas with different subtypes [12, 15, 16]. GBM subgroup heterogeneity, a major challenge to therapeutic efficacy, is not restricted to a spatial axis, but develops along the temporal one too: the evolution of the disease after recurrence implies changes in the subgroup features with a typical progress to the mesenchymal classification [17].

Characteristic pathological features of these GBM subtypes can be recapitulated by genetic manipulations of neural precursor cells (NPCs): these manipulations include the ablation or mutation of the tumor suppressor p53, deletion of neurofibromatosis-1 (NF1), or loss of cdkn2a genes. Concomitant with these loss-of-function mutations, gliomagenesis requires the upregulation of a proto-oncogenic gene, such as the epidermal growth factor receptor (EGFR), the platelet derived growth factor receptor-A (PDGFRA), or a constantly-activated form of EGFR (EGFR-variant-3, EGFRvIII) [16, 18].

Intratumoral heterogeneity is enhanced by the presence of non-tumoral cells that contribute to GBM growth or suppression: natural killer cells, dendritic cells, $CD8^+$ or $CD4^+$ T-cells, microglia, macrophages, Treg cells, and endothelial cells (ECs) (Figure 1). The latter five are generally involved in GBM progression and represent the major targets for innovative therapeutic interventions [19-21].

Currently, the standard treatment for GBMs consists in surgical resection (when possible), followed by combined radiotherapy and temozolomide (TMZ) chemotherapy, and TMZ alone as adjuvant at the end of irradiation. Corticosteroids are administered in case of brain edema and when necessary also after tumor resection [22, 23], but a recent study performed by *Pitter et al.* reported corticosteroid adverse effects on patient overall survival (OS) [24]. Despite the aggressive therapeutic regimen, relapse normally occurs in proximity to the first lesion, specifically in close association with the invasive margins of the resected tumor mass [25-27].

The absence of a successful treatment that provides a significant improvement in the length of the progression-free survival (PFS) period, if not a complete cure, for GBM patients, makes the discovery and testing of new drugs an urgent need in the field of cancer research.

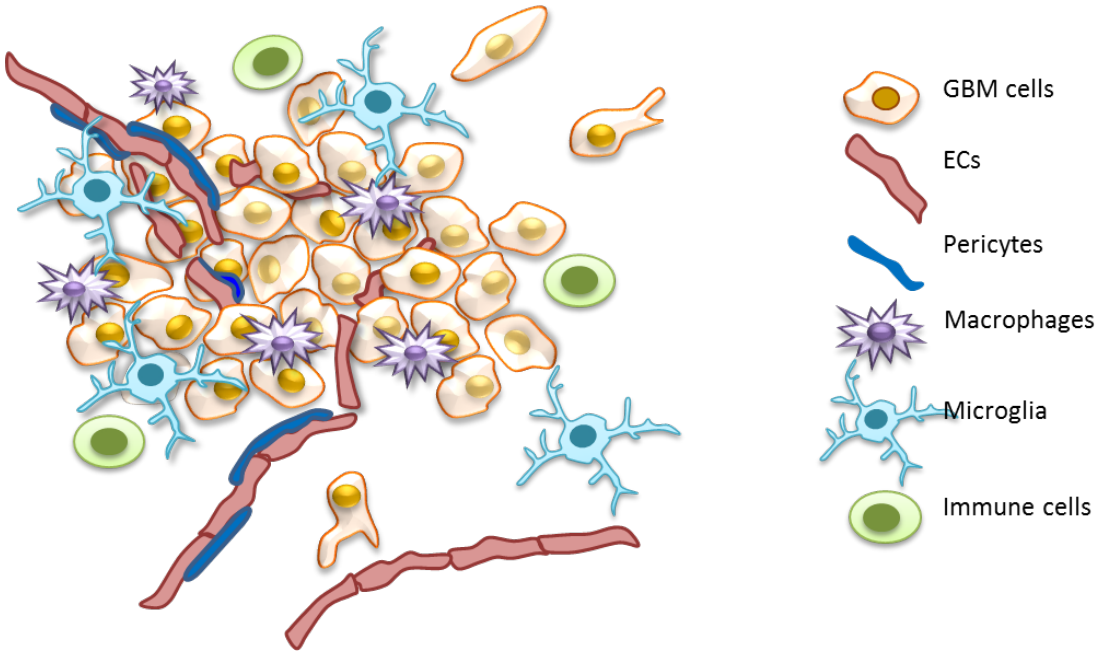

Figure 1: The heterogeneity of the GBM microenvironment. The microenvironment of glioblastoma multiforme is very heterogeneous and characterized by the presence of numerous non-neoplastic cells: ECs and pericytes belonging to co-opted blood vessels or newly-synthesized vessels induced by the tumor-secreted angiogenic signals; tumor-associated microglia and macrophages, attracted by numerous cues released by the tumor cells; other tumor-associated immune cells, such as Tregs, natural killer cells, CD4+ and CD8+ cells, and dendritic cells. All these cells participate in the generation of GBM by acting in a pro-tumorigenic or anti-tumorigenic way.

4.1.1 Tumor angiogenesis

The formation of new vessels is a fundamental process during embryogenesis and childhood, to sustain organ development and growth. In adulthood, vessels are quiescent and actively proliferate only during healing, ovarian cycle, pregnancy, and disease [28].

In brain malignancies, it is believed that the tumor cells migrate along the existing vessels in order to assure blood supply, in a phenomenon known as "vessel co-option" [29]. Soon the growing tumor mass may reach a point when the level of oxygenation is not sufficient anymore, thus entering a hypoxic phase [30]. The production of the hypoxia-inducible transcription factors (HIFs) induces the secretion of growth factors that stimulate ECs to form new branching vessels for adequate sustainment of the tumor. ECs do not only support tumor growth by delivering oxygen and nutrients, but also by releasing important cytokines for maintenance of the cancer initiating and propagating cells [31, 32]. The ongoing angiogenic signaling generates an abnormal and unbalanced proliferation of ECs that form disorganized vessels characterized by high permeabilization, irregular pericyte coverage, and heterogeneous blood flow. The newly formed vessels are mostly nonfunctional and generate a vicious cycle that leads to increased hypoxia and tissue necrosis [33, 34]. The formation of such abnormal vessels lacking

proper tight junctions causes the disruption of the blood brain barrier (BBB) [35, 36] and the accumulation of interstitial fluid that enhances intra-tumoral pressure and originates a brain edema, one of the main causes of morbidity [30, 37].

4.1.2 Anti-angiogenic therapies in GBMs

Due to its high vascularization, GBM is considered a perfect candidate to be targeted with antiangiogenic therapies [38]. Current treatments mainly target the VEGF - VEGFR signaling that, together with other pathways only more recently taken under consideration, plays a central role in GBM angiogenesis [31, 39].

VEGFA is the best known component of the VEGF family and has a central role in maintaining the homeostasis of vessel growth and branching, acting as a growth factor to stimulate EC proliferation [40]. When VEGFA expression is induced by HIF1α in the hypoxic tissue, it acts in a paracrine fashion activating quiescent ECs [31, 40-42]. Inhibitors of VEGF and its receptors are widely approved by the United States Food and Drug Administration (FDA) and the European Medicines Agency (EMA) for the treatment of numerous malignancies, often in concomitance with chemotherapy [43].

The FDA approved bevacizumab (a humanized monoclonal antibody against VEGFA, also known under the trade name of Avastin®) for recurrent GBM, also as monotherapy. The EMA, however, rejected its use in glioblastoma [44, 45]. Phase II and III clinical trials for recurrent and primary GBMs reported increased PFS of patients treated with bevacizumab in combination with chemotherapy, or bevacizumab in combination with chemotherapy and radiation. These studies, however, did not detect any improvements in patient OS and the number of adverse events following therapies was higher in the bevacizumab-treated group [39, 46]. Sorafenib and sunitinib, two inhibitors of receptor protein tyrosine kinases, did not give better outcomes: sorafenib trials in GBM are ongoing and results are not available yet [47], while the administration of sunitinib as monotherapy in phase II trials for GBM was unsuccessful [48].

The regimen of bevacizumab administration for GBM was adopted from the standard therapy of other tumors, but for improvements in clinical results the dose may need adjustments and the agent might not work with the same efficacy in the different GBM subtypes [39]. In fact, a deeper analysis of the results obtained in the Avaglio (Avastin® in Glioblastoma) study revealed that the use of bevacizumab in addition to the standard chemotherapy-TMZ regimen

significantly increased the OS of patients with a proneural *IDH1* wild-type tumor, in comparison to the placebo group [49].

The general unchanged OS following the administration of an antiangiogenic agent can be explained by the increased invasive/aggressive tumor behavior [50]. This assumption is supported by a study on bevacizumab administration in an orthotopic GBM mouse model, where the antiangiogenic treatment selected a more invasive mesenchymal tumor phenotype [51]. Other studies in tumor-bearing mice reported an increase of metastasis formation following antiangiogenic treatments [52, 53] or VEGFA ablation [52].

As mentioned in the beginning of this paragraph, VEGF signaling, despite playing a major role in tumor vascularization, does not act alone: there are many other factors that act in parallel to the VEGF axis and are upregulated in GBM neo-angiogenesis. Among these are e.g. the basic fibroblast growth factor (bFGF), the platelet-derived growth factor (PDGF), the placenta growth factor (PIGF), angiopoietin 2 (ang-2), and APLN [30, 54, 55]. Some of these have been found overexpressed in patient-derived GBM samples following bevacizumab administration [54, 56] and are under evaluation as alternative targets in different tumor mouse models and clinical trials for multi-targeting anti-angiogenic treatments [30, 54, 57, 58]. These treatments, which combine the targeting of the VEGF-VEGFR pathway and an additional angiogenic factor, already showed beneficial effects on animal survival in laboratory studies [54, 59]. Importantly, as I will describe in the next paragraphs, also the stromal cells involved in tumor progression as fibroblasts and myeloid cells contribute to tumor resistance to antiangiogenic therapies and GBM recurrence [60-63].

4.2 APLN-APLNR signaling

The APLN gene encodes for a 77 amino acid pre-propeptide that is cleaved into the different isoforms apelin-13, apelin-17, and apelin-36. The pyroglutamylated (Pyr[1])apelin-13, which originates through post-translational modifications, is the most abundant form in the human cardiac tissue and, together with apelin-13, the most potent activator of APLN receptor [64]. Apelin-13 sequence is conserved among mammals [65] and comparison of human and *Xenopus* apelin-13 reveals sequence identity among vertebrates [55]. Mouse and human APLNR receptors show 91% of protein sequence homology [64].

APLN peptides bind to the receptor APLNR, a G-protein-coupled receptor that has the highest sequence homology to the angiotensin II receptor but does not bind angiotensin II [66].

Both ligand and receptor are abundantly expressed in the adult human central nervous system (CNS) and in various peripheral organs [65, 67, 68]. APLNR activation inhibits the production of cyclic adenosine monophosphate (cAMP), activates the PI3K/Akt and the proteinase kinase C (PKC) signaling pathways [69, 70], and increases intracellular calcium concentration [67]. The PKC pathway acts through the mitogen-activated protein kinase (MAPK) and the extracellular-regulated kinase (ERK) in the regulation of angiogenesis [71, 72] (Figure 2). In rats, intravenous administration of APLN lowers the blood pressure in a dose-dependent manner, by inducing nitric oxide synthase (NOS) phosphorylation [73]. APLN transcription is activated by hypoxia, which acts through a hypoxia-responsive element at the first intron [74, 75].

Studies showed that the fate of the activated APLNR and its responsiveness to a persistent stimulus depends on the isoform of the binding APLN peptide: binding assays with APLNR fused to the green fluorescent protein (GFP) demonstrated that apelin-13 and apelin-36 recruit different β-arrestins, causing either the receptor internalization and rapid recycling to the cell surface, or its stable intracellular sequestration, respectively [76, 77]. Another study by *Pope et al.* reported that the fast mechanism of receptor internalization after stimulation with (Pyr[1])apelin-13 is not mediated by β-arrestins, but dynamin-dependent clathrin-coated vesicles [78]. Hence, the heterogeneity of APLNR intracellular pathways increases the varieties of cellular responses and the possible physiological outcomes in consequence to the activation of the receptor.

In addition to these numerous responses to the stimulation with the agonist peptides, *in vitro* and *in vivo* studies showed that the administration of the peptide apelin-F13A, where the

carboxyl-terminal phenylalanine is substituted with an alanine, has an antagonistic effect on APLNR activation [67, 79, 80].

A recent crystallography study on the structure of the APLNR revealed a 2-sites binding mode of the APLN peptides [81]. Contrary to previous findings [67], in this latest study the antagonist peptide apelin-F13A did not show any decreased binding affinity to the APLNR [81].

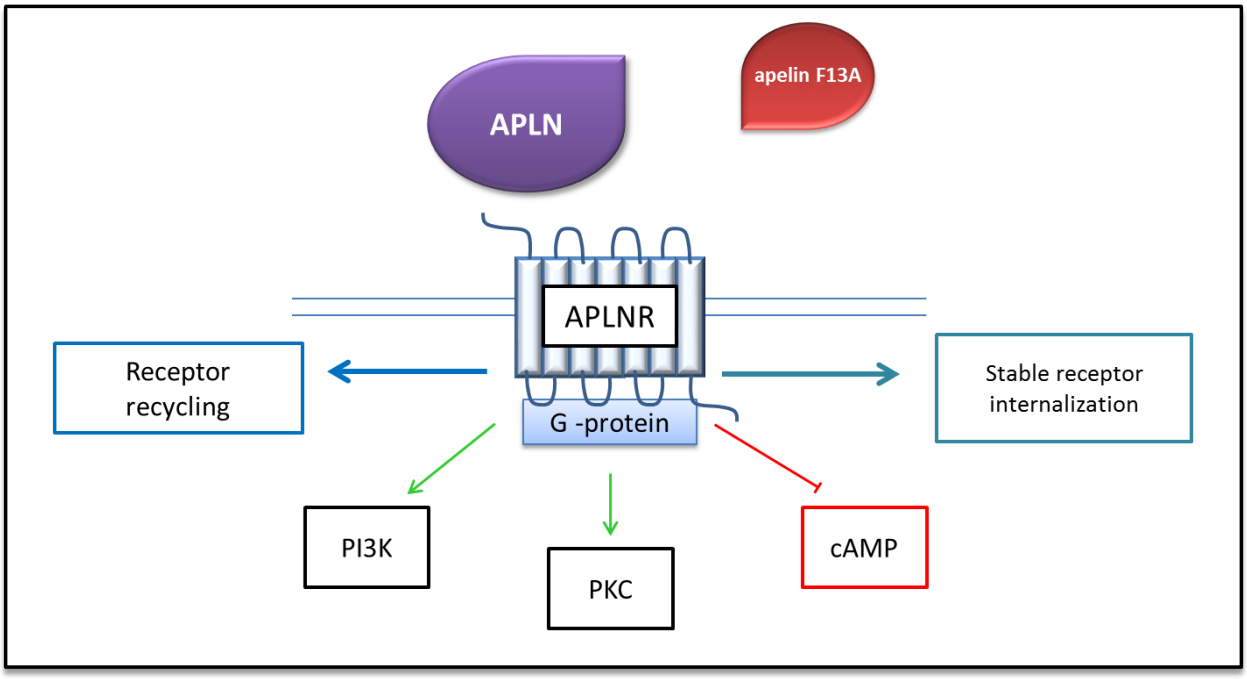

Figure 2: **The APLN-APLNR signaling.** APLN peptides activate the receptor APLNR, a G-protein-coupled receptor, which in turn lowers intracellular cAMP and induces PI3K and PKC. PI3K is associated with vasodilation, while PKC is involved in the control of cell proliferation and angiogenesis, acting through MAPK and ERK. The receptor may undergo different intracellular pathways, depending on the isoform of the binding APLN peptide and, consequently, on the intracellular vesicle-triggering proteins involved.

4.2.1 APLN-APLNR signaling in embryonic development

In *Xenopus laevis*, *Cox et al.* and *Kälin et al* demonstrated that the APLN-APLNR signaling plays a role in the development of the intersomitic vessels (ISVs): APLN expressed in the dermatomes first acts in an autocrine way to stimulate APLNR-expressing vessels coming from the posterior cardinal vein (PCV). The use of APLN- and APLNR-knock-down (APLN-KD, APLNR-KD) models revealed a disruption in ISVs, PCV and ventral plexus vessels in the absence of a proper APLN-APLNR signaling. *Inui et al.* reported a role of the APLN-APLNR signaling in the development and organization of the *Xenopus* cardiovascular system [82].

In the developing cardiovascular system of the zebrafish, the APLN-APLNR signaling is a critical factor for the migration of myocardial progenitors [83].

Saint-Geniez et al. found that both APLN and the APLNR are strongly expressed in vessels and capillaries of the mouse developing retina, where they display differential staining patterns that hint to a migratory effect of APLN on APLNR-expressing endothelial cells. Their expression, however, decreases at later developmental stages [84]. In the mouse embryo, APLNR is expressed in the ECs sprouting from the dorsal aorta and in the migrating end of the anterior cardinal vein, but not in the pre-existing ECs of the dorsal aorta. APLNR expression in the sprouting ECs in the dermis of the neonatal mice is lost with maturity [85]. Hence, these findings suggest a transient role of the APLN-APLNR signaling, restricted to the ECs in the stages of angiogenesis. *In vitro* studies confirmed the role of APLN as chemoattractant on APLNR-transfected cell lines [86, 87], and as chemoattractant and mitogen on vascular ECs [55, 88, 89].

Mutant mice lacking APLNR are born at a sub-Mendelian rate and half of the embryos dies *in utero*. The phenotypical characterization of these mice and their developmental defects revealed an impaired vasculature (with abnormalities or absence of important veins and arteries), a decreased number of vascular smooth muscle cells around vessels, and marked cardiac malformations [90].

On the contrary, APLN ablation does not show increased lethality in embryogenesis, and APLN mutant mice have a normally developed vasculature and cardiac system, even though decreased hart contractility in aged APLN-knock-out (APLN-KO) mice was reported, indicating that the peptide has an important function to maintain a normal cardiac activity in the adult [91]. Postnatal APLN-KO mice show defect in retina vascularization, which recover with time. Ocular malformations, however, are six times more common in APLN-mutant mice, compared with controls [92].

A possible explanation for the viable phenotype of the APLN-KO mice is the presence of another ligand, called apela (or elabela or toddler), that binds to APLNR, thus maintaining the downstream signaling [93]. Apela acts in the very early phases of the embryonic development, hence it is also known as APLN receptor early endogenous ligand. It is expressed in human pluripotent stem cells and is able to induce receptor internalization in human embryonic kidney cells 293 (HEK293) and in Chinese hamster ovary cells (CHO) [94]. In zebrafish, it is the first hormone recognized by APLNR and its mutation causes cardiac malformations comparable to those observed in APLNR-null fish [95]. During zebrafish gastrulation, it is a fundamental signal for cell migration [96]. A recent model of apela-KO pregnant mice showed how the absence of this circulating hormone, which is normally produced by the placenta, induced pre-eclampsia symptoms due to a defective placental angiogenesis, and was able to cause

embryonic malformations similar to the ones observed in the APLNR-KO mice. Importantly, the authors demonstrated that the loss of apela led to the upregulation of other pro-angiogenic factors, APLN included. Therefore, this early ligand, which may be responsible for the vascular integrity of both mother and fetus, plays an intertwined role together with APLN in the angiogenic process [97].

4.2.2 APLN-APLNR signaling in pathological angiogenesis

In addition to its physiological functions described in the previous paragraphs, the APLN-APLNR signaling is involved in recovery and formation of new vessels during cerebral ischemia, limb ischemia and myocardial infarction [98-100]. This pathway, however, does not always positively affect disease outcome, and it is also associated with disease progression: *Kasai et al.* reported that APLN causes pathological retinal angiogenesis in mice with oxygen-induced retinopathy. When APLN was knocked-down in endothelial cells, these showed decreased proliferation in favor to a maturation state *in vitro*; when implanted *in vivo,* the APLN-KD ECs had increased pericyte coverage, which supports vessel normalization [101]. This result was confirmed in APLN-KO mice that did not develop hypoxia-induced pathological retinal angiogenesis, in comparison with the affected WT controls [102].

Several gain-of-function studies addressed the impact of the angiogenic pathway APLN-APLNR on cancer growth and progression. In 2007, *Sorli et al.* found that the subcutaneous implantation of a murine breast carcinoma cell line with induced APLN over-expression was able to generate tumors with faster onset and progression [103]. In accordance with these findings, APLN over-expression in a non-small cell lung cancer (NSCLC) cell line showed that these cells were able to generate subcutaneous tumors with a faster growth rate and an increased vessel density [104]. Contradictory results were reported in a similar subcutaneous model generated by a murine colorectal cancer cell line with APLN over-expression: the enhanced APLN signal inhibited tumor growth and led to enlarged and more mature tumor vessels. The discrepancies between the studies may be explained by the involvement of different downstream effectors of APLNR activation [105], but also by differences in the expression levels of the endogenous APLN and APLNR in the cell lines, with consequent variations in the paracrine and autocrine signaling generated [103, 106, 107].

A study performed on the use of bevacizumab to treat a subcutaneous mouse model of colon cancer reported an upregulation of APLN expression during the supposed vessel normalization window following the anti-angiogenic treatment [108]. The vessel normalization window is a

time frame obtained by blocking the unbalanced angiogenic signals induced by the tumor hypoxic areas, and it is characterized by more regular and non-leaky vessels, reduced hypoxia and reduced aberrant EC proliferation [33]. The upregulation of APLN as consequence of anti-VEGF treatment may be a useful clinical tool to detect vessel normalization, but may also indicate tumor rebound through an alternative angiogenic pathway.

Aside from the above-mentioned mouse models, numerous observations made on different types of human cancer resections suggested a central role for APLN-APLNR signaling in pathological angiogenesis and in the progression of malignancies [55, 80, 104, 109-111].

APLN was found to be upregulated in patient-derived samples of NSCLC, in comparison with normal lung tissue, and associated with a poor prognosis [104]. The analysis of 62 samples of patient-derived oral squamous cell carcinoma revealed a correlation between hypoxia-induced APLN expression upregulation and tumor recurrence [109]. *Picault et al.* reported an upregulation of APLN and APLNR in human colon adenocarcinomas and in colorectal cancer cell lines, suggesting the existence in these cells of a loop of autocrine signal that sustain tumor development [80]. An expression profile analysis of 1250 human cancer samples including head and neck squamous cells carcinoma, breast cancer, and clear cell renal cell carcinoma, reported APLNR as a signature gene of tumor angiogenesis [110]. A recent work done by *Patel et al.* identified a link between APLNR and the efficacy of immunotherapy administered to patients with metastatic melanoma and lung cancer. In particular, the authors found that the tumor samples from patients refractory to the therapy had multiple loss-of-function mutations in the APLNR gene, thus rendering tumor cells and vessels less responsive to interferon γ (IFNγ) released by T-cells. This finding highlights a new possible role of the APLN-APLNR signaling in the regulation of the tumor-associated immune-compartment, thus rendering the pathway an even more promising target for cancer therapy [111]. A study of our group on patient-derived GBM sections reported upregulated APLN and APLNR expression in tumor tissue and tumor vessels, with a co-localized expression of APLN and VEGFA in the tumor necrotic areas [55].

Altogether, these data indicate a role of the APLN-APLNR signaling in the progression of different malignancies and in the growth and angiogenesis of glioblastoma. Therefore, a better characterization of the pathway in the context of GBM is essential to unravel another potential suitable target for future interventions. While the above-mentioned results were limited to the study of subcutaneously-implanted cell lines or primary tumor cells, the use of orthotopically-implanted primary GBM cells allows a higher reproducibility of the human disease in the GBM mouse models. Moreover, in this doctoral work I present for the first time the use of primary

GBM cells with a manipulated expression of APLN, in order to better understand the role of this ligand and the activation of its receptor in the context of glioblastoma progression.

4.3 GBM-associated myeloid cells

Myeloid cells, which account for resident microglia and peripheral macrophages, are the most abundant non-neoplastic cells identifiable in a glioma, representing up to the 50% of the total number of cells in the tumor mass [63]. Microglia cells are resident cells of the central nervous system (CNS), while peripheral macrophages are circulating monocytes that enter the nervous system through the disrupted BBB [112]. The abundance of tumor-associated myeloid cells (TAMs) drove the attention on their role in the history of glioma progression. Studies using transgenic mouse models with depletion of the myeloid cell pool through the herpes simplex virus thymidine kinase (HSVTK) – glancicovir system gave contradictory results in terms of glioma growth, depending on a specific depletion of the resident microglia or of the circulating macrophages [113, 114]. As a consequence, these studies opened multiple possibilities on the individual role of each subpopulation, or on their specific activation status, in the panorama of GBMs.

Traditionally, myeloid cell activation states were classified according to two categories, M1 and M2, described as a classical inflammatory activation and a pro-tumorigenic activation, respectively. Recent discoveries, however, defined this classification as too artificial, as mainly deduced on gene expression profiles obtained *in vitro*, but not reproducible in a complex and heterogeneous setting as the *in vivo* tumor microenvironment, where transitions between states are less defined and in a persistent change [115, 116] . Thus, in this thesis I will not refer to the macrophage/microglia-polarization states, but I will simply refer to them as TAMs.

4.3.1 The tumor-supportive role of TAMs

Most studies on TAMs in GBM (*in vitro*, *in vivo*, and in the clinical setting) point to a tumor-supportive role of these cells: TAMs, in fact, release matrix metalloproteases (MMPs) and EGF that increase glioma invasion [63, 117-119] and cooperate with growth factors such as VEGF, PDGF, FGF, and the transforming growth factor β (TGF β) in the promotion of tumor angiogenesis [62, 117, 120] (Figure 3).

Nishie et al. demonstrated that the level of intratumoral macrophages correlated with glioma grade, being higher in grade IV gliomas in comparison to the lower grade ones. Moreover, the increase in TAMs also correlated with an increase in the vascular density measured in these samples, suggesting a direct effect of TAMs on neovascularization. The author postulated that IL8, the expression of which correlated with the increase of macrophages found in high-grade GBM samples, may have a role in their attraction to the tumor [121]. It is now known that IL8

expressed by glioma cells attracts myeloid cells and promotes angiogenesis [122], together with other molecules such as the colony-stimulating factor 1 (CSF1), the glial cell-derived neurotropic factor (GDNF), the granulocyte-macrophage colony-stimulating factor (GM-CSF), VEGFA, and ATP [63, 117, 123].

In vivo studies performed on orthotopic GBM mouse models demonstrated that TAMs are recruited by high levels of intratumoral hypoxia, and their presence is associated with tumor resistance to anti-angiogenic therapies [124, 125]. The role of TAMs in recurrent GBMs was further assessed in a study conducted on a cohort of autopsies from GBM patients: the tumor resections after treatment with bevacizumab showed increased numbers of TAMs, quantified by staining with cluster of differentiation 68 (CD68) and CD11b, in comparison with the pre-treatment samples. Moreover, the higher number of infiltrating myeloid cells inversely correlated with the OS of these patients [61]. The association between TAMs and resistance to anti-angiogenic therapy may also be indirectly deduced by the fact that, as already mentioned, resistance to anti-VEGF therapies correlates with a transition to the GBM mesenchymal subtype, which is characterized by ample intratumoral heterogeneity [12, 51].

In conclusions, targeting TAMs is a promising strategy in the field of cancer research, given the evidences in support of their pro-tumorigenic and immunosuppressive role and their involvement in tumor resistance to anti-angiogenic therapies [123, 126]. There are already some data available on the blockage of single pathways involved in TAMs recruitment in peripheral solid tumor and GBMs, which showed beneficial effects restricted to specific tumor typologies [127, 128].

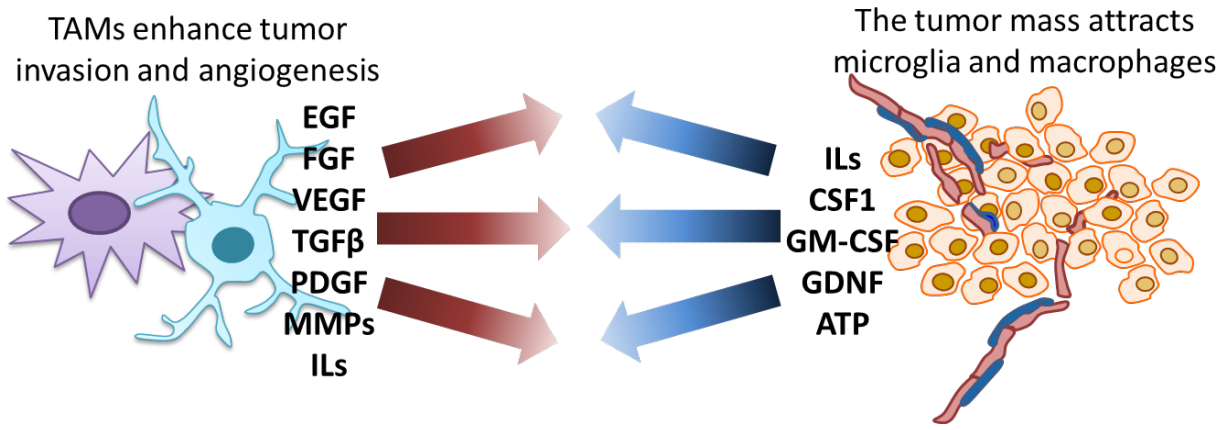

Figure 3: The tumor-associated myeloid cells. Glioblastoma secretes numerous attractive cues that induce microglia and macrophage migration to the tumor. Myeloid cells sustain GBM growth and progression by releasing growth factors, cytokines, and metalloproteases that support tumor invasion and angiogenesis.

4.3.2 APLN-APLNR signaling and tumor-associated myeloid cells

A recent study conducted by *Szulzewsky* and colleagues analyzed the genetic expression of microglia and macrophages in the context of glioblastoma and identified two novel genes strongly upregulated in GBM-associated myeloid cells: these genes encode for the transmembrane glycoprotein NMB, also known as osteoactivin, and the secreted phosphoprotein 1 (SPP1), also known as osteopontin (OPN), respectively. The latter, in particular, acts on tumor cell invasion and binds to CD44, increasing the stemness properties of glioblastoma stem cells (GSCs) [129].

The induction of macrophage proliferation and migration by different chemokines acting through OPN has been demonstrated in pathological contexts (obesity and diabetes) [130, 131]; in an *in vitro* study, apelin-13 upregulated OPN on rat vascular smooth muscle cells (VSMCs), [132].

Therefore, given that both APLN-APLNR signaling and TAMs have important roles in tumor progression and angiogenesis, the exploration of the possible role of APLN and of the blockade of the APLN-APLNR signaling on TAM recruitment is a fundamental step to evaluate and fully understand how the pathway is implicated in GBM evolution.

5. Objectives of the study

The short survival expectancy of glioblastoma patients and the absence of a successful therapeutic intervention with long term benefits make the discovery of new GBM treatments an urgent topic in cancer research.
In this thesis, to fully characterize the effects of the APLN-APLNR signaling on GBM growth, I pursued three main objectives:

1- The analysis of APLN and APLNR expression and distribution in human and mouse primary GBM cells as well as in murine and patient GBM tissue;
2- The study of the function of APLN-APLNR signaling by generating new models of human primary GBM cells depleted for APLN expression for *in vitro* and *in vivo* experimentation;
3- The study of APLNR activation or blockade for potential GBM therapy, alone or in combination with anti-angiogenic approaches, and its effects on the tumor microenvironment.

In the objectives n.1, the analysis of APLN and APLNR expression was performed on human and mouse primary GBM cells by quantitative PCR (qPCR); in addition, I extensively characterized the expression of both APLN and APLNR in human and mouse GBM samples, by qPCR and *in situ* hybridization. This last technique, when used on mouse xenografts with implanted human GBM cells, allowed me to distinguish between the tumor- and brain parenchyma-derived signals.

In the objectives n.2, the new human primary GBM cell models with APLN loss were obtained by lentiviral transduction. After the assessment of the viability and proliferative abilities of the generated cells, their invasive potential was analyzed *in vitro* and the cells were orthotopically implanted to study *in vivo* the impact of APLN loss in GBM angiogenesis and growth. The *in vivo* and *in vitro* findings, demonstrating an enhanced tumor invasion detected after loss of APLN expression, brought me to the following secondary objectives:

- The generation of human and mouse primary GBM cells with APLNR loss: the human primary GBM cells with APLNR loss were generated by lentiviral transduction and characterized *in vitro* for cell viability and proliferative potential;

- The analysis of the intracellular distribution of APLNR was evaluated after the up-take of GFP-linked apelin-13 peptides.

In the objectives n.3, I focused on the use of anti-angiogenic therapies against the VEGF-signaling and assessed the possible consequent upregulation of alternative angiogenic pathways or of the recruitment of TAMs.
These objectives were divided into the following parts:

- The analysis of APLN and APLNR expression in human- and mouse-derived GBM samples of tumors treated with anti-VEGF-signaling agents: this analysis was performed by qPCR in patient-derived GBM samples and mouse-derived GBM xenografts, previously treated with anti-VEGFA antibodies or VEGFR-2-blocking compounds;
- The quantification of TAMs in mouse xenografts: given the possible direct role of the APLN-APLNR signaling on myeloid cell recruitment and some preliminary promising data obtained by my colleague Jonathan Muffler, I performed some experiments of immunostaining and quantified the ionized calcium-binding adapter molecule 1 (Iba1)-positive cells in two different orthotopic GBM mouse models treated with the antagonistic peptide apelin-F13A.

6. Materials and methods

6.1 List of materials

*6.1.1 Cells culture – **Table 1***

Material	Brand	Catalog Number
B27	Invitrogen	17504-044
Collagenase	Serva	17456
DMEM	Biochrom	FG0415
DMEM-F12	Invitrogen	11320-074
EGF	R&D systems	236-EG
Fetal Bovine Serum	Life Technologies	102270-106
FGF	PeproTech	100-18B
MEM non-essential amino acids	Life Technologies	11140-035
penicillin-streptomycin	Life Technologies	15140-122

*6.1.2 Cloning of GIPZ lentiviral DNA vectors – **Table 2***

Material	Brand	Catalog Number
GIPZ APLN shRNA, hs	Dharmacon GE Life Sciences	RHS4430-EG187 V3LHS_401190
GIPZ APLNR shRNA, hs	Dharmacon GE Life Sciences	RHS4531- EG187 V3LHS_634451
GIPZ APLNR shRNA, hs	Dharmacon GE Life Sciences	RHS4531- EG187 V3LHS_34449
GIPZ APLNR shRNA, mm	Dharmacon GE Life Sciences	RMM4532-EG23796 V2LMM_218787
GIPZ APLNR shRNA, mm	Dharmacon GE Life Sciences	RMM4532-EG23796 V3LMM_517943
GIPZ non-silencing Lentiviral shRNA Control	Dharmacon GE Life Sciences	RHS4346
LB medium	Sigma Aldrich	L-3397
Midi Prep kit	Qiagen	12143

6.1.3 Lentivirus production and cell transduction –**Table 3**

Material	Brand	Catalog Number
Accutase	Sigma Aldrich	A6964
Hs PDGFB primers	Eurofins Genomics	-
Puromycin	Sigma Aldrich	P8833
TransLenti Viral GIPZ Packaging System	Dharmacon GE Life Sciences	TPLP4614
Trypsin/EDTA	Merck Millipore	L2153

6.1.4 Quantitative PCR – **Table 4**

Material	Brand	Catalog Number
QuantiTec Reverse Transcription Kit	Qiagen	205313
TaqMan Gene Expression Master Mix	Applied Biosystems	4369016
Trizol	ThermoFisher Scientific	15596-026
Trypsin/EDTA	Merck Millipore	L2153

	Gene	***Catalog Number***
TaqMan Gene Expression Assays – Applied Biosystems	Hs Actin	Hs99999903_m1
	Hs APLN	Hs00936329_m1
	Hs EG5	Hs00189698_m1
	Hs GAPDH	Hs99999905_m1
	Hs HPRT1	HS99999909_m1
	Hs KDR	Hs009117_m1
	Hs VEGFA	Hs00900054_m1
	Hs APLNR	Hs00945496_s1
	Mm apela	Mm04278373_m1
	Mm APLN	Mm00443562_m1
	Mm APLNR	Mm00442191_s1
	Mm GAPDH	Mm99999915_g1
	Rn APLN	Rn00581093_m1
	Rn APLNR	Rn00580252_s1
	Rn GAPDH	Rn01775763_g1
	Rn KDR	RN00564986_m1

6.1.5 Assessment of RNA quality – **Table 5**

Material	Brand	Catalog Number
Agilent RNA 6000 Nano kit	Agilent Technologies	5067-1511

6.1.6 Viability and proliferation assays – **Table 6**

Material	Brand	Catalog Number
CellTiter 96 Non-Radioactive Cell Proliferation Assay	Promega	G4000

6.1.7 Invasion assays – **Table 7**

Material	Brand	Catalog Number
(Ala13)apelin-13	Bachem	H-6308.005
Collagen I	Gibco	A10483-01
pyroglutamylated apelin-13	Bachem	H-4568

6.1.8 GBM mouse specimens – **Table 8**

Material	Brand	Catalog Number
Cryomatrix	ThermoFisher Scientific	6769006
Narcoren	Merial	-

6.1.9 Immunostaining – **Table 9**

Material	Brand	Catalog Number
Alexa Fluor® 647 AffiniPure Donkey anti-goat	Jackson Immunoresearch	705-607-003
Alexa Fluor® 594 Streptavidin	Jackson Immunoresearch	016-580-084
Alexa Fluor® 488 Streptavidin	Jackson Immunoresearch	016-540-084
Alexa Fluor® 647 Streptavidin	Jackson Immunoresearch	016-600-084
Anti-APLNR made in rabbit	Abcam	Ab66218
Anti-iba1 made in goat	Abcam	Ab5076

Biotin-SP AffiniPure Donkey Anti-Rabbit	Jackson Immunoresearch	711-065-152
DAB 2-components kit	DCS Innovative Diagnostik-Systeme	DC137C100
DAPI	Fluka	32670
Donkey Serum	Jackson Immunoresearch	017-000-121
Entellan	Merck Millipore	107960
Dako Fluorescent Mounting Medium	Dako	S3023
Hemalaun	Sigma	HAT1101128
Peroxidase AffiniPure Donkey anti-goat	Jackson Immunoresearch	705-035-003
Peroxidase Streptavidin	Jackson Immunoresearch	016-030-084
RotiHistol	Roth	6640.1
To-Pro™-3 Iodide	ThermoFisher Scientific	T3605
Triton-X	Fluka	93418
Wheat germ agglutinin (WGA) Alexa Fluor® 594	ThermoFisher Scientific	W11262

*6.1.10 Probe generation for in situ hybridization – **Table 10***

Material	Brand	Catalog Number
DIG RNA labeling mix	Roche Diagnostics	11277073910
EcorI Fast Digest	ThermoFisher Scientific	FD0274
KpnI Fast Digest	ThermoFisher Scientific	FD0524
Mini Elute Reaction Clean-up Kit	Quiagen	28204
NotI Fast Digest	Thermo Scientific	FD0594
Polymerase T3	Roche Diagnostics	11031163001
Polymerase T7	Roche Diagnostics	10881775001
Polymerase SP6	Roche Diagnostics	10810274001
Quick Spin Columns	Roche Diagnostics	11273990001
SalI Fast Digest	Thermo Scientific	FD0644

6.1.11 In situ hybridization – **Table 11**

Material	Brand	Catalog Number
Acetic anhydride	Sigma Aldrich	320102
Anti-DIG antibody	Roche Diagnostics	11093274910
BCIP/NBT substrate	Vector Laboratories	SK-5400
Proteinase K	PeqLab	04-1070
RNAse-Zap	Sigma Aldrich	R2020
ssDNA – salmon sperm DNA	Ambion	AM9680
co-precipitate RNA – Yeast RNA	Ambion	AM7118
Triethanolamine	Sigma Aldrich	09278

6.2 List of devices – Table 12

Device / Software	Brand
Agilent 2100 Bioanalyzer	Agilent Technologies
Agilent 2100 Expert software	Agilent Technologies
Axiovert25	Zeiss
Axiocam MRm	Zeiss
Axiocam 105 color	Zeiss
Axioskop2	Zeiss
Axiovision Rel. 4.8 software	Zeiss
Axiovision SE64 Rel. 4.9 software	Zeiss
LAS AF software	Leica Microsystems
LAS X software	Leica Microsystems
Leica SP5 confocal microscope	Leica Microsystems
Leica SP8X WLL upright confocal microscope	Leica Microsystems
Microtome	Pfm Medicals
SofMax Pro Software	Molecular Devices
StepOnePlus Instrument	Applied Biosystems
StepOne Software v2.2.2	Applied Biosystems
Versa Max reader	Molecular devices

6.3 Techniques

6.3.1 Animals

All experiments were performed in compliance with the National Guidelines for Animal Protection, Germany, with approval of the local animal care committee of the Government of Oberbayern (Regierung von Oberbayern), the "Landesamt für Gesundheit und Soziales (LaGeSO)" in Berlin and every experiment was conducted after the guidelines of the UK Co-ordinating Committee on Cancer Research [133].

All mice were kept in a 12 h light/dark cycle with *ad libitum* access to food and water. Mice were sacrificed at defined pre-symptomatic time points or at humane end-point for the survival experiments.

6.3.2 Cell culture

Human primary GBM cells were obtained from surgically resected tumor samples at the Medical Faculty Heidelberg [134] and the Charité Medical University of Berlin, according to local ethical regulations. NPCs were isolated from the subventricular zone (SVZ) of Bl6/J or FVB mice bearing homozygous deletion in p53 or cdkn2a and APLN genes respectively, and subsequently transduced to obtain GBM specific subtypes.

Human and mouse primary cells were cultured as floating neurospheres in DMEM-F12 supplemented with 1X B27, 5% penicillin-streptomycin, 10 ng/ml EGF, and 10 ng/ml FGF.

U87 MG cells were obtained from the American Type Culture Collection (ATCC). U87 APLN-KD and non-silencing control (NSC) cells had been previously obtained by transduction with lentiviral vectors carrying the short-hairpin RNA (shRNA) of interest. For some experiments mentioned in this doctorate thesis, U87 MG, U87 APLN-KD, and U87 NSC cells were cultures under spheroid conditions with DMEM-F12 medium supplemented as mentioned above.

All cells were maintained at 37 °C in a humidified atmosphere of 95% O2 and 5% CO2.

6.3.3 Cloning of GIPZ lentiviral DNA vectors

The plasmids of interest carrying the shRNA constructs for Homo sapiens (Hs) APLN-KD, Hs APLNR-KD, and NSC were acquired as glycerol stocks. Each glycerol stock was plated in LB medium containing ampicillin at a final concentration of 100 µg/ml and left on the shaker for 16 hours maximum. Plasmid amplification and purification were performed according to the midi prep protocol of the manufacturer.

6.3.4 Lentivirus production and cell transduction

Lentiviral vectors carrying APLN-KD (V3LHS_401190), APLNR-KD (V3LHS_634451, V3LHS_34449, V2LMM_218787, V3LMM_517943), or NSC GFP-micro-RNA-adapted shRNA with the puromycin-resistance gene were produced in HEK293T cells using the TransLenti Viral GIPZ Packaging System according to the manufacturer´s instructions. Virus-containing supernatant was harvested two days after transfection, filtered with a 0,22 µm filter to avoid cellular contamination and preserved at -80°C. For GBM cell transduction, the primary spheroids (GBM14, GBM#1, NCH644, and p53KO PDGFB) were dissociated with Accutase. $8x10^4$ cells were incubated with 500 µl of virus [multiplicity of infection (MOI) = 0,6-0,7] for six hours in a 24-well plate, then 1ml of medium was added and cells left overnight at 37°C. The day after, cells were centrifuged and resuspended in 1ml of fresh F12 medium. On the second day after transduction, cells were treated with 50 µl of Accutase and resuspended in fresh F12 medium.

After cell recovery, puromycin was added to culture medium and selection maintained for 3 weeks. The concentrations of the antibiotics had been previously determined by a kill curve and differed for each cell type.

6.3.5 Generation of mouse primary GBM cells

NPCs were isolated from the SVZ of 30-day-old Bl6/J mice carrying homozygous deletion in the cdkn2a and the APLN genes. The isolated tissue was treated with trypsin for 15 min at 37°C, then homogenized with a glass pipette and incubated with collagenase for other 10 min at 37°C.

DMEM with 10% FSC was added to inactivate trypsin, centrifuged and substitute with DMEM F12 supplemented with growth factors.

Once cells recovered and formed spheres, the transduction with retroviral particles carrying human PDGFB-GFP or -dsRed gene was performed: 200000 cells were resuspended in 5 µl of medium and incubated for 2 hours at 37°C with 0,8 µl of viral particle, for a MOI of 80.
VSV-G pseudotyped retroviral particles were kindly provided by F.Calzolari/M.Götz. The cDNA of human PDGFB was derived from the RCAS-pBIG plasmid (kindly provided by E. Holland, Fred Hutchinson Cancer Research Center Seattle, WA; USA).
Fresh medium was added after 2 hours and cells left overnight at 37°C, until the complete change of medium on the next day.
After transduction, red- or green-fluorescent neurospheres were selected to have a 100% transduced culture. The correct insertion of the human PDGFB gene was verified by PCR amplification (primers: HsPDGFB f2 5´-CAGCTGAAAGGGTGGCAACT-3´; HsPDGFB r2 5´-ATGGTTCGTCTTCACTCGCC-3´) and ran on a 2% agarose gel.

6.3.6 Quantitative PCR (qPCR)

RNA extraction was performed using the Trizol protocol according to the manufacturer´s instructions. 1µg RNA per cell pellet or tumor sample was reverse-transcribed into cDNA using the QuantiTect Reverse Transcription Kit. The cDNAs were analyzed by quantitative PCR using the TaqMan Gene Expression Assays for the following Hs, Mm and Rattus norvegicus (Rn) genes: APLN, APLNR, apela, KDR, VEGFA, EG5, HPRT1 and GAPDH, with TaqMan Gene Expression Master Mix in a StepOnePlus Instrument. Samples were amplified with the standard running method provided by StepOne Software v2.2.2, increasing the cycle numbers to 45. In every run, the expression levels of the gene of interest were normalized to the housekeeping gene GAPDH, HPRT1, or actin.

6.3.7 Assessment of RNA quality

To verify the extraction procedure and the quality of the extracted RNA, some of the isolated RNA samples (from cell pellets and tissue samples) were run on the Agilent Bioanalyzer with the Agilent RNA 6000 Nano kit according to manufacturer´s instructions.

6.3.8 Viability and proliferation assays

6000 cells/well were plated in 96-well plates in DMEM-F12 on day 0. Cell viability was measured after 24, 48, 72 and 96 hours using a tetrazolium compound-based assay (3(4,5-dimethylthiazol-2-yl)2,5-diphenyl-tetrazoliumbromide, MTT) for cell metabolic activity according to manufacturer´s instruction, incubating the cells for one hour with the Stop Mix solution. Absorbance was measured with Versa Max microplate reader and SoftMax Pro with a reference wavelength of 630 nm. Background absorbance from empty wells was subtracted from all measurements and six replicate/samples were used in each experiment. Three experiments per cell type were done.

6.3.9 Limiting dilution assay

GBM14 APLN-KD (V3LHS_401190) and NSC cells were dissociated with Accutase, counted, and plated in triplicates at decreasing densities of 2000, 1500, 1000, 500, 200, 100 and 10 cells/well in 200 µl of DMEM F12 in 96-well plates.
Pictures were taken after 7 days under an Axiovert25 microscope with Axiocam MRm and Axiovision Rel. 4.8 software at 10x magnification. Sphere were quantified with Fiji (https://fiji.sc/, [135, 136]) and their umber adjusted for well area. The Extreme Limiting Dilution Analysis (ELDA), for the analysis of the stem cell frequency [137], was performed by uploading the data of the sphere-dilution assay to the software at http://bioinf.wehi.edu.au/software/elda/.

6.3.10 Invasion assays

For these assays, also U87 cells have been maintained in spheroid conditions with DMEM-F12 medium. Cellular spheres were picked up under an Axiovert25 microscope. In 24-well plates, each spheroid was plated into a 50 µl drop mixture of 1 mg/ml Rat Tail Collagen I, 10X PBS, 1N NaOH and dH_2O, diluted according to manufacturer´s instructions.
To create an APLN-enriched environment, two conditions have been used: either an U87 MG sphere was plated in 75 µl of collagen mix with an APLN-KD (V3LHS_401190) or NSC sphere, or apelin-13 200 nM (pyroglutamylated apelin-13) was added to the collagen mix. For blocking conditions, apelin-F13A 200 nM ((Ala13)apelin-13) was added to the collagen mix. Collagen matrix was left gelling for 50 min at 37°C, then covered with 600 µl DMEM-F12.

Cell invasion was followed over a 7-days period and pictures taken every day under an Axiovert25 microscope with Axiocam MRm and Axiovision Rel. 4.8 software.
Pictures were analyzed with Fiji and the invasive area (mm^2) calculated as ΔA= (area covered on day n) – (sphere area at day0).

6.3.11 APLN up-take experiments

The APLN up-take experiments were performed with GBM14 cells. The cells were plated at a density of 10.000 cells/well on a glass coverslip previously coated with poly-D-lysin 50 µg/ml followed by laminin 50 µg/ml. The day after, the medium was replaced with 200 µl of fresh medium and the GFP-conjugated peptides or the polyplexes containing a Cy5-labelled siRNA were added at a final concentration of 1 µM. The Cy5-polyplexes and the GFP-conjugated peptides were kindly provided by Sören Reinhard, from the group of Prof. Dr. Ernst Wagner at the Department of Pharmacy, LMU Munich.
Cy5-polyplexes: after plating on the cells, they were incubated on ice for 15 min, then medium was replaced with 250 µl of fresh medium and incubated for 45 min at 37 °C.
GFP-labelled peptides: for the condition of competition, the non-labelled apelin-13 peptide was added at a concentration of 20 µM 30 min prior to the addition of the GFP-labelled apelin-13. The cells were incubated with the GFP-peptides for 120 min at 37 °C.
After the incubation at 37°C, cells in both conditions were washed and fixed for 30 min with 4% PFA. Afterwards, they were incubated for 10 min at room temperature with WGA-594 1:200 and DAPI 1:1000 diluted in PBS. After staining, cells were washed and mounted on a glass slide with Dako Fluorescent Mounting Medium. The pictures were taken at the Leica SP8X WLL upright confocal microscope or at the Leica SP5 inverted confocal microscope, with the LAS X software, and analyzed with ImageJ.
For the quantification of the GFP-positive cells, 6 pictures per condition were used, and for each picture the data were measured as number of GFP-positive cells (with bound or internalized GFP-particles) on the total number of cells, which were approximatively 20/picture.

6.3.12 Mouse GBM specimens and immunofluorescent staining

Tumor-bearing mice were transcardially perfused under Narcoren anesthesia with 1x PBS followed by 4% phosphate buffered PFA. Brains were post-fixed for two days in 4% PFA and then left in 30% sucrose for at least 24 hours at 4 °C. Freezing was performed embedding the

tissue in Cryomatrix and brains were preserved at -20°C. Tissue was sectioned horizontally in 40 µm-thick slices on a microtome. Floating sections were washed with PBS, blocked for 1h at room temperature in 1X PBS containing 5% donkey serum and 0,3% Triton-X, and then incubated overnight at 4°C with the primary antibodies. On the second day, slices were washed in PBS and incubated for 3h at room temperature with the secondary (and tertiary when necessary) antibody, then washed with PBS and mounted with mounted with Dako Fluorescent Mounting Medium. All secondary antibodies were diluted in blocking solution.

6.3.13 Immunofluorescent staining on mouse GBM floating sections

Slice were incubated overnight at 4°C with goat anti-Iba1 and rabbit anti-APLNR primary antibodies, both diluted 1:100. On the second day, they were incubated for 3h at room temperature with donkey anti-rabbit biotynilated 1:250, then for 2h at room temperature with Alexa Fluor® donkey anti-goat 647 1:500, Alexa Fluor® conjugated streptavidin 594 1:500, and Dapi nuclear staining 1:10000. The pictures were taken at the Leica SP8X WLL upright confocal microscope, with the LAS X software.
For immunostaining for the detection of the invading APLNR-positive GBM cells or the APLNR-positive NPCs in the SVZ, the same protocol with the primary antibodies rabbit anti-APLNR was used. In these two experiments, the pictures were taken at the confocal microscope at Leica SP5 inverted confocal microscope with the LAS AF software.

6.3.14 Human GBM specimens

GBM samples were obtained from the Neurosurgery Department of the University Clinics LMU Munich. Samples were classified as “center” or “border” of the original tumor mass, according to their position at the time of surgical resection. Necrotic tumor tissue as evaluated by H&E was excluded from the analysis. Paraffin slides of the GBM sample that underwent stereotactic resection were obtained from the Center for Neuropathology and Prion Research (ZNP) LMU Munich. With each section obtained from this specimen a surgical depth (indicated as distance in mms from the target point 0 defined by the neurosurgeon) and a histopathological description was attributed. The studies were conducted according to the local standard ethical regulations.

6.3.15 Immunohistochemistry with horseradish peroxidase (HRP) on mouse GBM floating sections

Human paraffin-embedded tissue was left in isopropanol heated to 60°C for 30 min, then in acetone at -20°C for 10 min. After one wash in distilled water, it was washed in PBS. At this point, the human mounted tissue or the mouse floating sections were incubated for 10 minutes with H_2O_2 0,3%, methanol 50%. After washing with PBS, slices were blocked for 1h at room temperature in 1X PBS containing 5% donkey serum and 0,3% Triton-X, then incubated overnight at 4°C with goat anti-Iba1 primary antibodies diluted 1:100.

On the next day, after rinsing with PBS, the human tissue was incubated with the secondary antibodies donkey anti-rabbi biotynilated 1:250 for 3h at room temperature, and subsequently with the third antibodies streptavidin HRP-conjugated, 1:500 for 2h at room temperature.

On the second day, after rinsing with PBS, the mouse slices were incubated for 3h at room temperature with the secondary antibodies donkey anti-goat HRP-conjugated, 1:500.

After the incubation with the respective antibodies, the slices were washed with PBS and the chromogenic reaction was obtained by incubating the tissue for 10 min with DAB: DAB chromogen was mixed with DAB substrate according to manufacturer´s instructions.

After being washed with PBS and ethanol 70%, tissue was incubated in hematoxylin for 2 min, then in graded alcohol (70-100%) and Roti Histol. Slides were mounted with Entellan.

For the quantification of the iba1-positive cells, pictures were taken at 40x magnification at the Axioskop2 microscope with Axiocam 105 Color and Axiovision SE64 Rel. 4.9 software and quantified with Fiji. For each mouse, 3 to 4 slices were considered. Slices in which the tumor was located in the ventricular space were excluded from counting. For each slice, three areas were analyzed: intratumoral, defined as the area with densely-distributed tumor cells; peritumoral, defined as the area lining the mass of dense tumor cells; contralateral, defined as the area in the hemisphere opposite to the tumor-bearing one. For each area, 2 to 4 pictures were taken, depending on the dimension of the tumor mass. In the graphs, the quantification is shown as number of cells/area of the picture (μm^2).

6.3.16 Hematoxylin and Eosin staining

Paraffin-embedded samples were cut into 15 µm-thick slices and mounted on slides. Deparaffination was done with serial passages into Roti-Histol and graded alcohol (100%-70%) for a Hematoxylin & Eosin staining (H&E) according to the standard protocol. Slides were mounted with Entellan.

6.3.17 Probe generation for in situ hybridization

Probes were generated as previously described [55]. Briefly, for linearization, the plasmids (Life Technologies) carrying the genes of interest were incubated with the restriction enzymes Fast Digest for the time and at the temperatures indicated in the table below:

Table 13 **– Plasmid linearization for *in situ* probe synthesis**

Gene	Enzyme	Temperature	Time (min)	Enzyme inactivation	
				Temperature	Time (min)
Hs APLN anti-sense	EcoRI	37°C	30	80°C	15
Hs APLN sense	NotI	37° C	60	80°C	
Hs APLNR anti-sense	EcoRI	37° C	30	80°C	
Hs APLNR sense	KpnI	37° C	30	80°C	
Mm APLN anti-sense	SalI	37° C	30	65°C	
Mm APLN sense	NotI	37° C	60	80°C	
Mm APLNR anti-sense	SalI	37° C	30	65°C	
Mm APLNR sense	NotI	37° C	60	80°C	
Hs VEGFA anti-sense	SalI	37° C	30	65°C	

For confirmation, the linearized plasmids ran onto a 1% agarose gel and were purified with the MinElute Reaction Clean-up Kit according to the manufacturer´s instructions. 1 µg of each purified linearized plasmid was taken for probe synthesis and incubated for 5 hours at 37°C with DIG-labelled RNA according to manufacturer´s instructions. The polymerases T3, T7, or SP6 (Roche Diagnostics) were used according to each promoter.

The enzymes were subsequently inactivated with the addition of EDTA for 5 minutes at 65°C. Probe generation was verified by running on a 1% agarose gel.

The probes were then purified with the Quick Spin Columns according to the manufacturer´s protocol. The concentrations of the purified DIG-labelled probes were measured prior to the performance of the *in situ* hybridization.

6.3.18 In situ hybridization

The bench and the instrumentation were carefully cleaned with RNAse-Zap and solutions were prepared with RNAse free water and sterilized. Sections on slides were deparaffinized by serial passages into Roti-Histol and graded alcohol (100%-25%). Tissue was permeabilized with 10

min incubation in 10 µg/ml of Proteinase K. Slides were fixed for 10 min in 4% paraformaldehyde (PFA) and blocked for 10 min with 2,5 % Acetic Anhydride in 1,5% Triethanolamine. Sections were dried for 2 hours at room temperature, then incubated overnight at 65°C in a humidified chamber with DIG-labelled antisense or sense probes at a final concentration of 7 µg/ml, diluted in a hybridization solution containing 100 µg/ml ssDNA, to mask unspecific binding, and 100 µg/ml co-precipitant RNA. The probe-containing hybridization solution was boiled at 95°C for 10 min before application. On day two, unspecific signal was removed with graded stringency washes with saline sodium citrate from 20x to 0.1x and incubated overnight at 4°C with alkaline phosphatase-conjugated anti-DIG antibody diluted in 10% sheep serum. On day three, slides were washed in PBT (0,1% Tween in 1xPBS) and incubated with BCIP/NBT substrate at 37°C for up to four days. For counterstaining with Eosin, slides underwent serial passages in graded alcohol (70%-100%) till Roti-Histol and were then mounted with Entellan. Pictures were taken under an Axioskop2 microscope with Axiocam 105 Color and Axiovision SE64 Rel. 4.9 software.

6.3.19 Statistical analysis

All statistical analysis was performed with the GraphPad Prism Software. The statistical tests used in each experiment are indicated in the figure legends. P-values were considered statistically significant when <0,05 (*p<0.05, **p<0.005, ***p<0.0005). Analysis was performed with Student's t-test, one-way ANOVA with Newman Keuls post-hoc test, or two-way ANOVA test.

7. Results

The role of the APLN-APLNR signaling in GBM progression

7.1 APLN and APLNR expression in GBM

7.1.1 APLN and APLNR are expressed by primary cultured GBM cells at variable levels

Initially, I verified that both cultured cells and tumor tissue used in the study express APLN and APLNR.

Our research group possesses different human primary GBM cell types derived from patient tumor resections. Moreover, we have murine GBMs obtained from p53-KO or cdkn2a-KO NPCs that were transduced with vectors carrying GBM-specific proto-oncogenes to reproduce the typical human GBM subgroups. The tumorigenicity of the transfected cells was verified *in vivo* and the tumor histology confirmed by a neuropathologist.

The qPCR analysis was performed on primary patient-derived GBM cells, human GBM cell lines, primary NPCs-derived mouse GBM cells, and WT NPCs (Figure 4 A, B, C, D).

I detected APLN expression in all our GBM cell types. In all the analyzed primary GBM cells APLN levels showed inter-group variation, without correlation with any of the GBM genetic subtypes (Figure 4A, B). In the human primary GBM cells, APLNR expression varies among cell groups and does not show any particular correlation with the genetic subtypes (Figure 4C). In NPCs-derived GBM cells, APLNR expression was generally low and did not correlate with either the proneural or classical subgroups; among these cells, however, an extremely high expression of APLNR was shown in the p53-KO PDGFB group, which is extremely invasive when implanted *in vivo* (Figure 4D).

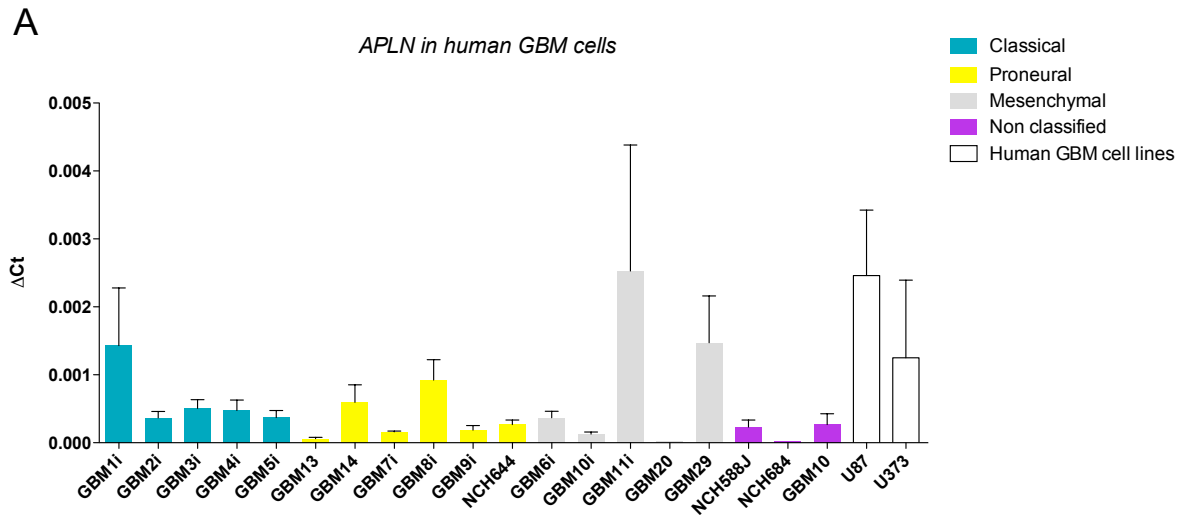
A
APLN in human GBM cells
Classical
Proneural
Mesenchymal
Non classified
Human GBM cell lines
ΔCt
0.005
0.004
0.003
0.002
0.001
0.000
GBM1i
GBM2i
GBM3i
GBM4i
GBM5i
GBM13
GBM14
GBM7i
GBM8i
GBM9i
NCH644
GBM6i
GBM10i
GBM11i
GBM20
GBM29
NCH588J
NCH684
GBM10
U87
U373

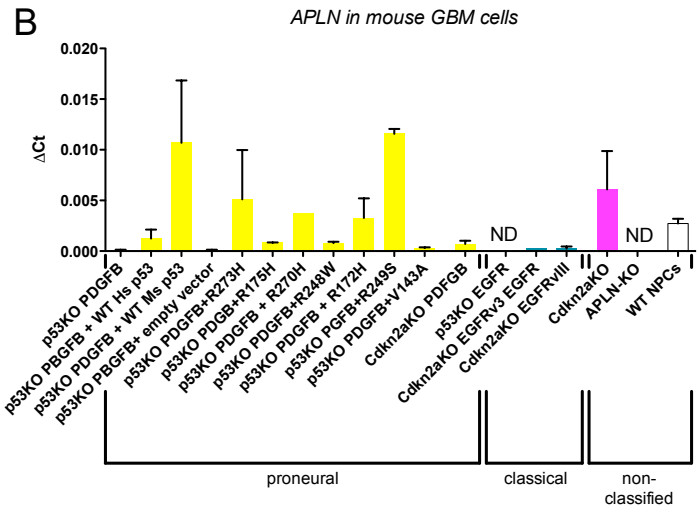
B
APLN in mouse GBM cells
ΔCt
0.020
0.015
0.010
0.005
0.000
ND
ND
p53KO PDGFB
p53KO PBGFB + WT Hs p53
p53KO PDGFB + WT Ms p53
p53KO PBGFB+ empty vector
p53KO PDGFB+R273H
p53KO PDGB+R175H
p53KO PDGFB + R270H
p53KO PDGFB+R248W
p53KO PDGFB + R172H
p53KO PGFB+R249S
p53KO PDGFB+V143A
Cdkn2aKO PDFGB
p53KO EGFR
Cdkn2aKO EGFRv3 EGFR
Cdkn2aKO EGFRvIII
Cdkn2aKO
APLN-KO
WT NPCs
proneural
classical
non-classified

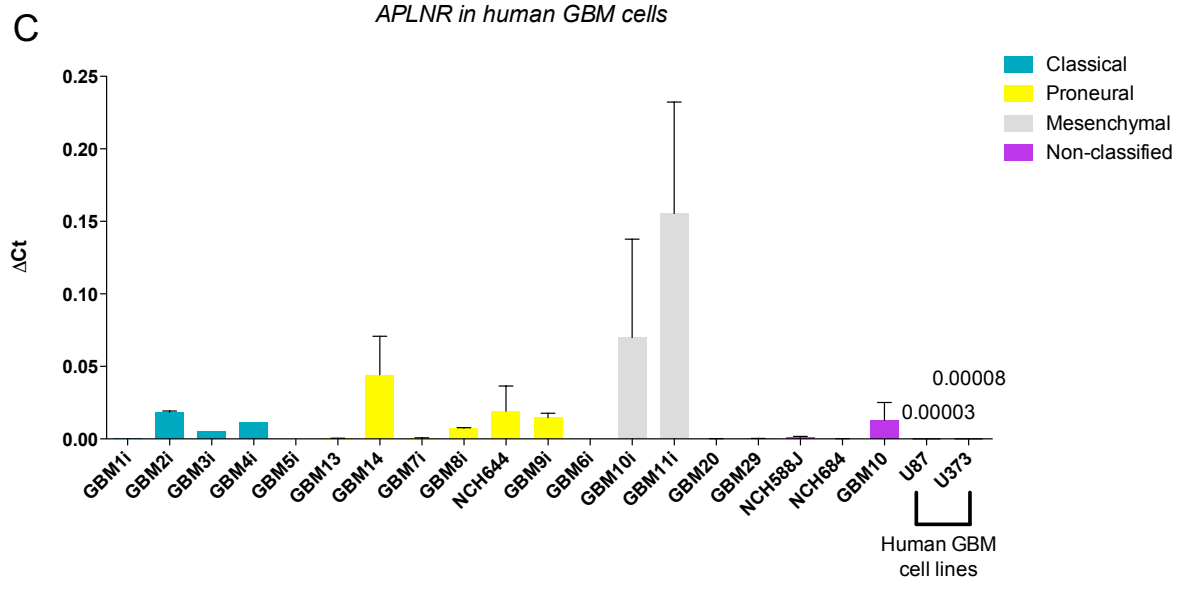
C
APLNR in human GBM cells
Classical
Proneural
Mesenchymal
Non-classified
ΔCt
0.25
0.20
0.15
0.10
0.05
0.00
0.00008
0.00003
GBM1i
GBM2i
GBM3i
GBM4i
GBM5i
GBM13
GBM14
GBM7i
GBM8i
NCH644
GBM9i
GBM6i
GBM10i
GBM11i
GBM20
GBM29
NCH588J
NCH684
GBM10
U87
U373
Human GBM cell lines

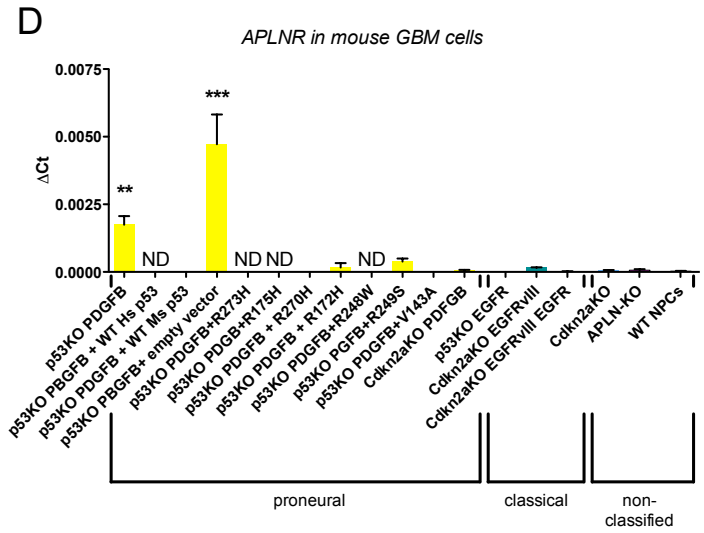

Figure 4: qPCR analysis of APLN and APLNR expression in primary GBM cultures. (A) Expression analysis of APLN was performed by qPCR on patient-derived GBM cells of different genetic subtypes. Experiments were conducted in triplicates; (B) Analysis of APLN expression in different murine glioma cell cultures carrying driver mutations that are representative of different human GBM-subtypes. In APLN-KO NPCs no APLN mRNA was detectable.; (C) APLNR expression analyzed by qPCR also shows variability among the primary human GBM batches divided according to their genetic subtype; (D) The murine GBM cells generally express low levels of APLNR, which was extremely high in the p53KO PDGFB group. One-way ANOVA with Newman Keuls post-hoc test, *$p<0.05$, **$p<0.005$, ***$p<0.0005$ and GAPDH was used as housekeeping gene for all the experiments.

7.1.2 Immunofluorescent detection of APLNR in the NPCs along the SVZ

APLNR expression had already been detected in the mouse hippocampal neurogenic niche [138], and, at paragraph 7.1.1, I demonstrated that APLNR is detectable by qPCR in SVZ-isolated WT NPCs and in NPCs-derived mouse primary GBM cells.

To test if *in vivo* APLNR was detectable in the NPCs of the SVZ neurogenic niche, I performed an immunofluorescent analysis on the SVZ of nestin-GFP reporter mice. Nestin-GFP reporter mice express GFP under the nestin promoter [139]. Nestin is a marker for NPCs along the neurogenic process [140], which were therefore GFP-labelled in the neurogenic niches of these mice.

The results shown in figure 5 demonstrated that, *in vivo*, the NPCs along the SVZ expressed APLNR and may thus be responsive to the ligand APLN. To-Pro™ Iodide was used as nuclear staining. In accordance with the previous findings obtained by qPCR on the analysis of APLNR expression in mouse NPCs, the fluorescent staining demonstrated that APLNR is detectable in some nestin-positive NPCs *in vivo* as well. In addition, the APLNR signal was detectable in other non-nestin-positive cells of the SVZ, thus indicating that the responsiveness to the APLN signal is not restricted to the NPCs (Arrows in figure 5A, B, and C).

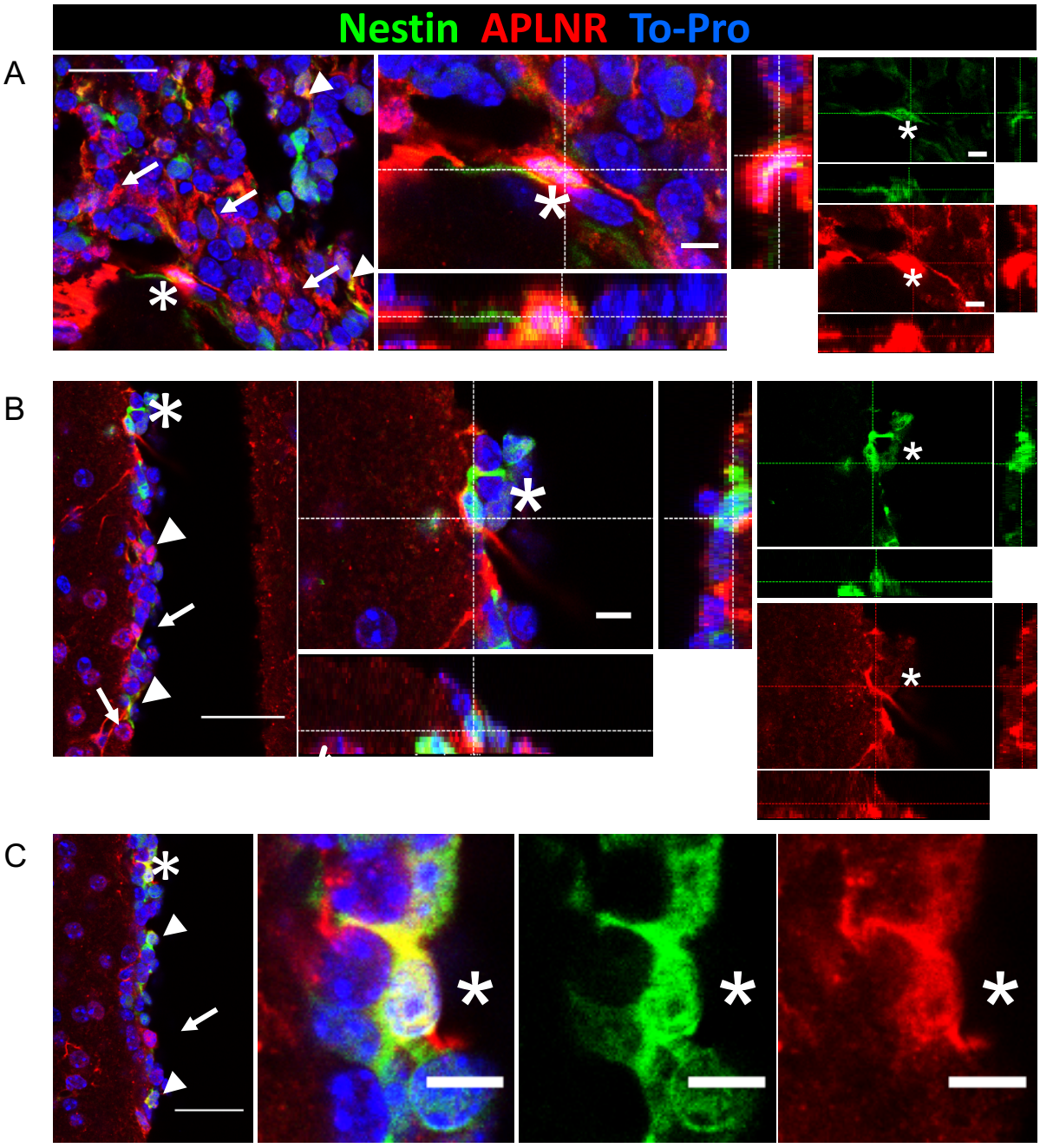

Figure 5: APLNR is expressed in the NPCs lining along the SVZ. (A) In nestin-GFP reporter mice I observed different NPCs co-stained for APLNR, indicated by the arrowheads. The asterisks in the overviews indicate the areas enlarged. In the enlargements, the cross-hair shows a cell positive for nestin and APLNR; In (B) and (C) the overviews and cross-hair show other areas along the SVZ where double-stained NPCs, indicated by arrowheads, are detectable. The asterisks indicate the enlarged cells, which show a strong APLNR signal at the cell body and at the cell protrusions as well. Scale bar in the overviews = 50µm, in the enlargements = 10µm. In A, B, and C the arrows indicate non-nestin-positive cells that express APLNR.

7.1.3 *APLN and APLNR are strongly expressed in GBM cells and in tumor vessels of mouse GBM xenografts – In situ hybridization*

Once APLN and APLNR expression was confirmed in our cultured primary GBM cells, I verified that both ligand and receptor would be detectable in mouse tumor xenografts and checked for their cellular distribution: to do this, I performed *in situ* hybridization on mouse GBMs generated by U87 cells. These xenografts were used as a positive control to establish the protocol, as U87 GBM cells showed the highest level of APLN expression by qPCR analysis (see figure 4A).

On these samples I also verified the presence of VEGFA, which is upregulated by tumor hypoxia [42] and was previously reported to be detected in APLN-expressing regions of human GBM by *in situ* hybridization [55].

The different species of the tumor cells (human) and the brain parenchyma (mouse) allowed me to distinguish between APLN, APLNR, and VEGFA expressed by either the tumor or its microenvironment, by using human (Hs)- or mouse (Mm)-specific antisense RNA probes.

In these mouse xenografts APLN and APLNR were detectable in the U87 tumor mass (Figure 6A): Hs APLN was homogeneously expressed by the GBM cells across the tumor; Mm APLNR was upregulated in the tumor vessels originated in the GBM microenvironment and not detectable in the tumor-free contralateral hemisphere.

In the xenografts in figure 6B, as observed for Mm APLNR, Mm APLN was upregulated in the tumor tissue, in comparison with the tumor-free hemisphere. In addition, the signals of Mm APLN and Hs VEGFA, even though deriving from different sources, showed a similar localization across the tumor mass: while Hs VEGFA was found in human cells of the tumor mass indicative for hypoxic regions, Mm APLN was detected in the tumor vessels of the VEGFA-positive area.

These results allowed me to conclude that the method of *in situ* hybridization is a reliable technique for the detection of APLN, APLNR, and VEGFA expression *in vivo*; moreover, I found that Hs VEGFA and Hs APLN are upregulated in the tumor cells, and Mm APLN and Mm APLNR are upregulated in the newly forming vessels of the xenografts.

Next, I investigated APLN and APLNR expression in a murine GBM model obtained by the implantation of p53-KO PDFGB cells (Figure 6C). These cells generated fast-growing and invasive tumors, where the neo-angiogenic areas of the tumor necrotic regions expressing APLN and APLNR were strongly identified by *in situ* hybridization. In accordance with the previous results shown in figure 6A and B, in the murine GBM model I detected an upregulation

of both APLN and APLNR in the tumor cells and in the newly forming tumor vessels, in comparison to the non-tumor areas of the xenografts (Figure 6C).

I confirm the specificity of the signals by using sense probes that did not hybridize with the tissue (Figure 6D).

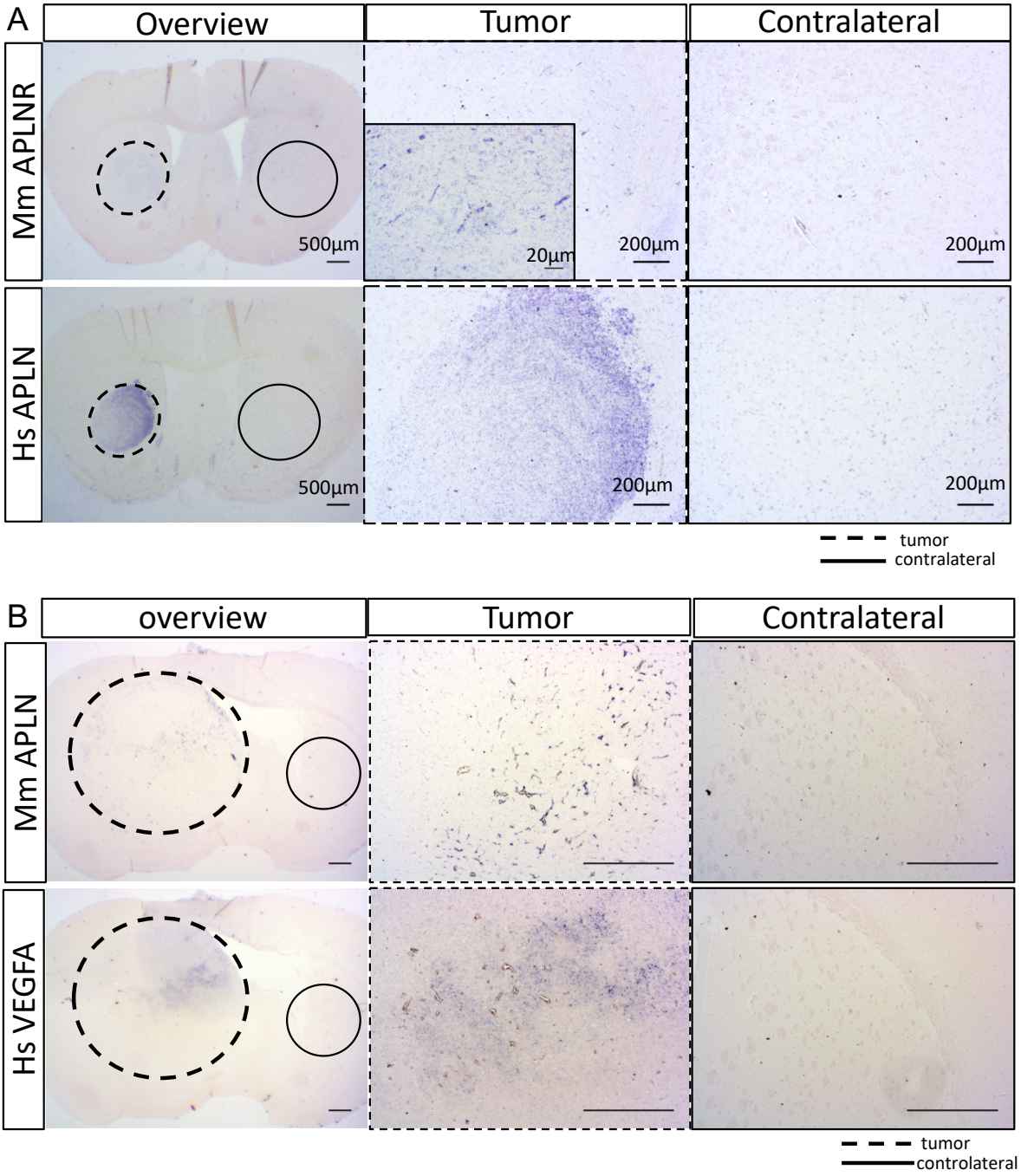

Figure 6: Spatial localization of APLN and APLNR expression in mouse GBM xenografts. (A) The overviews show that the signals of APLN and APLNR obtained by *in situ* hybridization are very strong in the GBM mass. APLN and APLNR show different expression patterns between tumor cell and tumor microenvironment: APLN, detected in the human GBM cells U87, shows a diffuse staining across the tumor, while APLNR, detected in the mouse cells, depicts the mouse blood vessels in the GBM mass, as better illustrated by the enlargement; (B) VEGFA and APLN signals are detectable in the GBM mass originated by U87 cells, but not in the contralateral tumor-free hemisphere. The enlargements show that their expression patterns are similar across the tumor mass. Scale bar = 500µm.

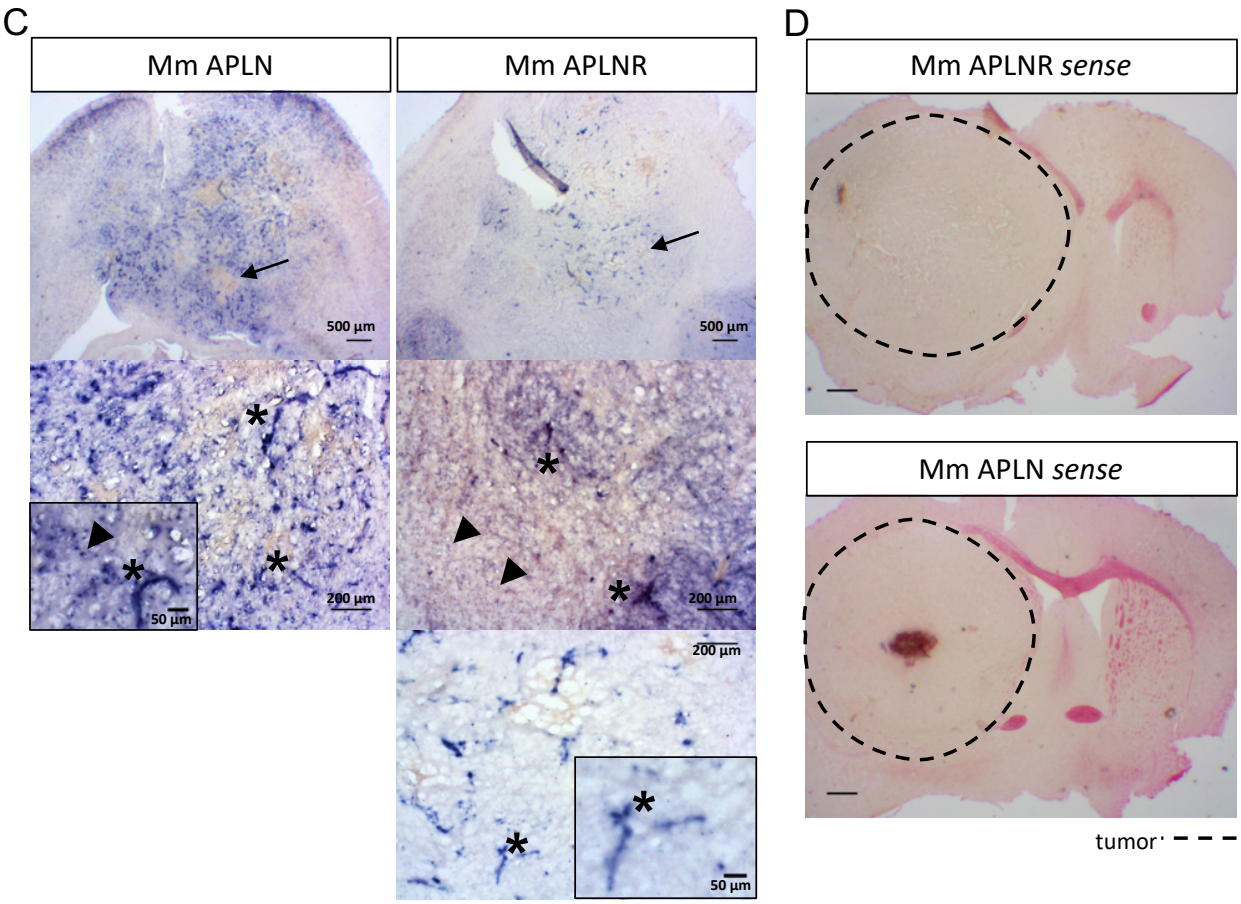

Figure 6 (continued): Spatial localization of APLN and APLNR expression in mouse GBM xenografts. (C) The tumors originated by p53-KO PDGFB cells are highly invasive and give a substantially less compact mass than the ones obtained with U87 cells. The signals of APLN and APLNR in the tumor vessels (asterisks) and tumor cells (arrowheads) are strongly detected by *in situ* hybridization around the necrotic areas (indicated by arrows in the overviews). The enlargements show the details of APLN and APLNR signals in cells and vessels. (D) The sense-control probes did not bind and did not give any signals in the mouse GBM xenografts originated by the implantation of U87 MG cells. Scale bar = 500µm.

7.1.4 *APLN and APLNR are abundantly expressed in patient-derived GBM samples – In situ hybridization*

Next, to evaluate the cellular distribution of the APLN-APLNR signal in human GBMs, I performed *in situ* hybridization on a patient-derived GBM sample obtained from the Neurosurgical Department of the LMU University Clinics. The H&E staining of these GBM sections, used to verify the architecture of the tissue and for comparison with the *in situ* hybridization signal, allowed me to distinguish between an area very dense with tumor cells and a region with healthier tissue (Figure 7A).

The APLN and APLNR signals detected by *in situ* hybridization resembled the H&E features of the sample and showed a clear distinction between the cell-dense tumor areas of the specimen

and the more tumor-free regions, thus indicating a correlation between APLN/APLNR expression and the presence of tumor tissue (Figure 7A).
With inspection at higher magnification, the expression of APLN an APLNR in the tumor-dense area was detectable in the tumor cells and in the ECs (Figure 7B). APLNR signal was very intense at the single-cell level across the tumor and in the regions surrounding the vessels, as shown in the enlargement; APLN signal, instead, although detectable as well in the cells sparse in the tissue, was more intense in the ECs. A similar expression pattern was found on another section of the same GBM analyzed subsequently (Figure 7C). Importantly, APLN and APLNR were not detectable in the control samples obtained from healthy brain, confirming a specific role of the signaling in tumor progression (see Figure 14). Neither APLN nor APLNR sense-probe gave a detectable signal in the control hybridization (Figure 7D).

In conclusion, with the analysis of the mouse tumor xenografts and the patient-derived GBM samples, I demonstrated that APLN and APLNR are upregulated in the tumor mass and this upregulation correlates with the areas of tumor tissue, thus indicating that the APLN-APLNR signaling plays a role in GBM progression. Moreover, their absence or very low detection outside the tumor or in non-tumor-associated blood vessels indicated that the signaling function is restricted to tumor neo-angiogenesis. In the human specimens, the cellular pattern observed for APLN suggested a more prominent detection of the ligand in the tumor vessels, while the APLNR expression, although detectable as well in the ECs, was generally more diffuse across the tissue and gave a very intense signal at the level of single GBM cells.

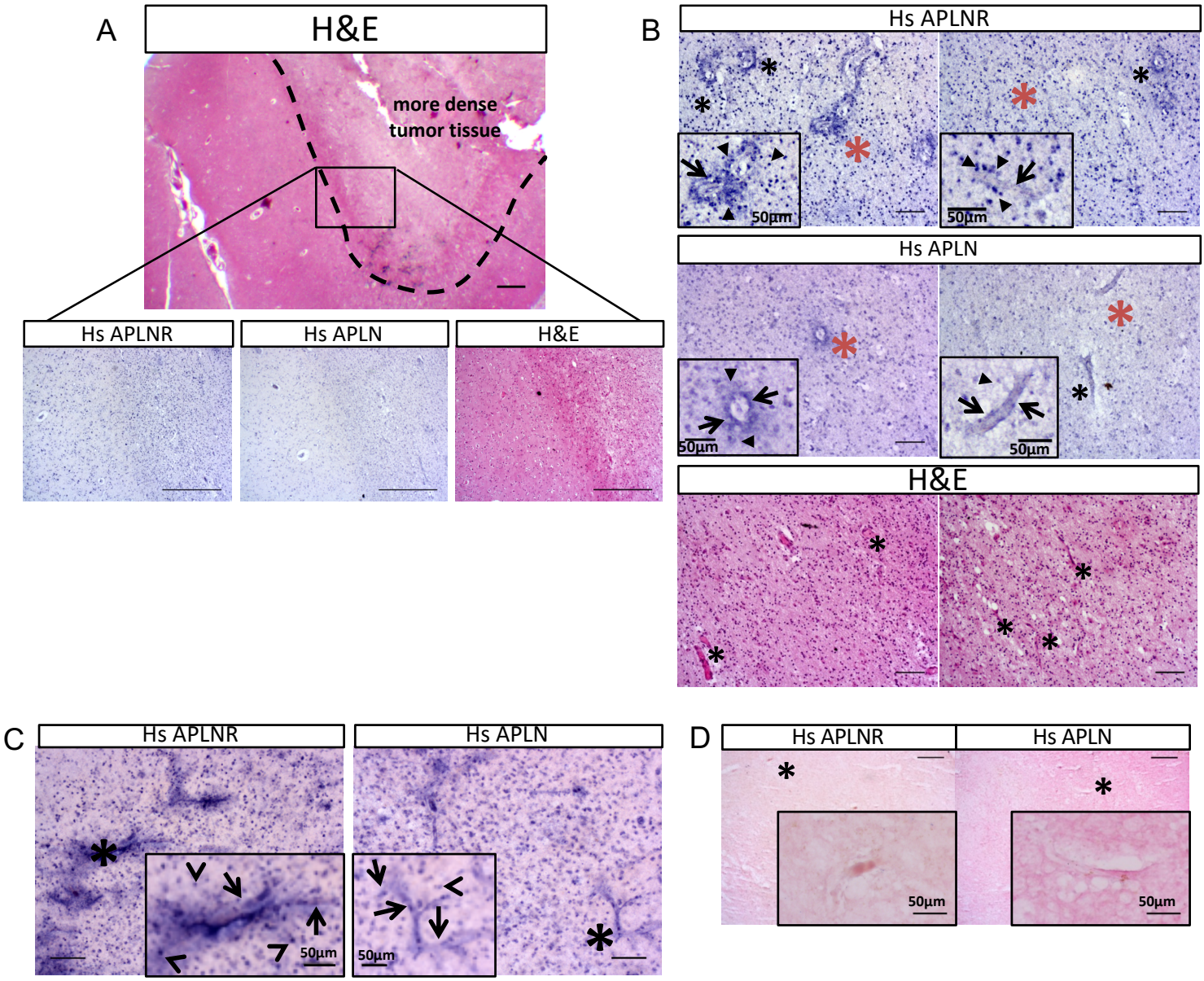

Figure 7: APLN/APLNR expression is upregulated in the cell-dense tumor tissue. (A) *In situ* hybridization for APLN/APLNR characterization was performed on a patient-derived tumor sample: as shown in the H&E staining, the sample presents a tumor-dense area, on the right, opposed to a more-normal-looking region, on the left. The intensity of the *in situ* hybridization signals correlates with the density of the tumor cells; Scale bar = 500µm; (B) As shown in the enlargements indicated by the red asterisks, APLNR signal is very sharp at the single-cell level (arrowheads) surrounding the vessels (arrows); APLN signal, instead, even though equally detectable at the single-cell level (arrowheads), is mostly upregulated on vessels (arrows). The H&E staining is used as reference for the tissue structure and the vessels are indicated by asterisks. Scale bar in the overview = 100µm; (C) Another section of the same specimens analyzed by *in situ* hybridization show the same pattern for the APLN and APLNR staining. The asterisks indicate the enlarged regions, the arrows the ECs and the arrowheads the positive cells in the tumor tissue. Scale bar in the overviews = 100µm; (D) The sense probes tested on these sections did not did not give any detectable signal. The asterisks indicate the enlarged regions. Scale bar in the overviews = 100µm.

7.2 APLN and APLNR expression in GBMs correlates with the angiogenic switch

To further assess the involvement of the APLN-APLNR signaling in tumor angiogenesis, I analyzed various samples obtained from a serial-implantation GBM rat model that allows the study of GBM angiogenic switch [141]. The model was originated with the orthotopic implantation of patient-derived GBM cells, which were sequentially isolated and re-implanted in another receiver. Up to the third re-implantation event, this patient-derived xenograft (PDX) model produces highly infiltrative brain tumors that recruit the pre-existing vasculature without apparent signs of neo-angiogenesis. With serial passaging in animals the tumors gradually transform into a vessel-rich phenotype (angiogenic switch) (Figure 8A) [142]. An advantage of the PDX model is that the gene expression contributed by the GBM cells or by the host can be identified individually by qPCR analysis, by using human or rat (Rn) TaqMan primers.

Furthermore, the modulation of the EGFR signaling can induce the angiogenic phenotype and can be used as an additional model of GBM angiogenic switch, thus providing another method to uncover signaling pathways that control angiogenesis and invasiveness in GBM [143] (Figure 8A). In this last model, the EGFR signaling was inactivated by transducing patient-derived GBM cells presenting EGFR amplification with a lentivirus carrying a dominant-negative form of the receptor. I analyzed the xenografts deriving from both the serial transplantation and the EGFR-blockade models, which had been previously classified by a neuropathologist as either invasive or angiogenic [142, 143], in order to determine changes in the APLN/APLNR expression at the angiogenic switch.

First, I evaluated the gene expression-patterns of the PDX model by comparing the expression levels in the initial generation against the later generation of tumors originated from different patients: I found that tumor cell-derived expression levels of Hs APLN and Hs APLNR were not altered throughout the change from an invasive to an angiogenic phenotype; however, the expression of Rn APLN and Rn APLNR increased dramatically in the tumor microenvironment of the angiogenic GBMs (Figure 8B). Interestingly, tumor-derived VEGFA levels did not change significantly, while the increase of KDR (encoding for VEGFR2) expression level in the tumor microenvironment correlated with the angiogenic switch (Figure 8C). As KDR is an endothelial marker and APLN and APLNR are assumed to be too (see figures 6 and 7), the rat expression seems to reflect the newly formed ECs.

Second, I analyzed the tumor xenografts deriving from the EGFR-blockade model and confirmed the above-mentioned findings: the expression of host-derived Rn APLN and Rn APLNR increased in the tumor microenvironment of the angiogenic GBMs, in comparison to the invasive ones (Figure 8D).

In conclusion, the analysis of the PDX model allowed me to demonstrate that, not only APLN and APLNR are upregulated in the tumor tissue, but also that their signal positively correlates with tumor angiogenesis.

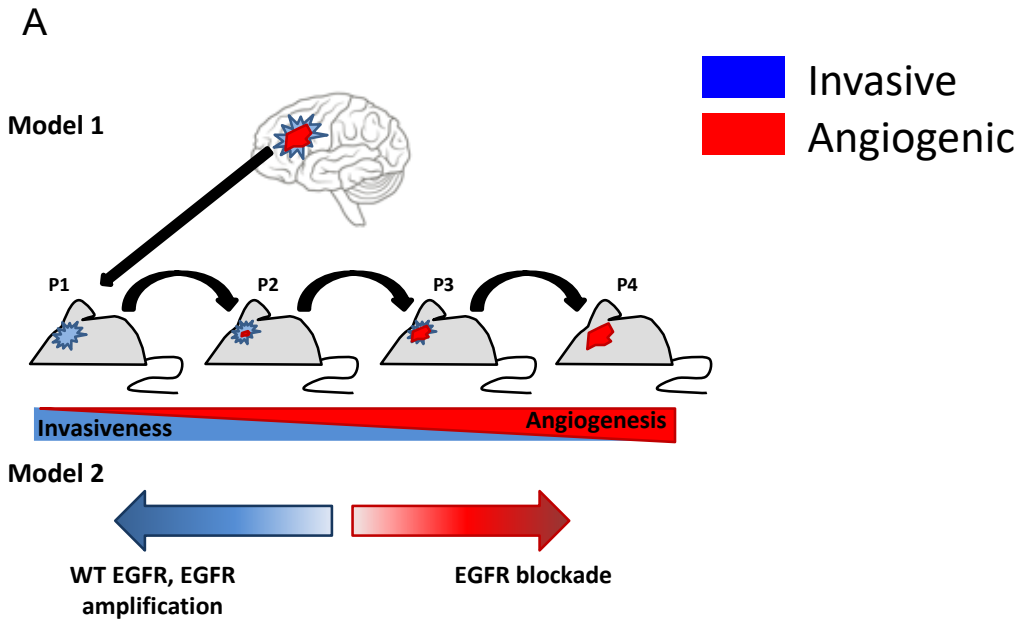

Figure 8: The upregulation of the APLN-APLNR signaling in GBMs correlates with the angiogenic switch. (A) The scheme represents the two models of angiogenic switch used in this analysis: model n.1 refers to the spontaneous angiogenic switch obtained by the passaging of the human tumor GBM cells between rats; model n.2 refers to the switch induced by the implantation of cells previously transduced with a dominant negative form of EGFR.

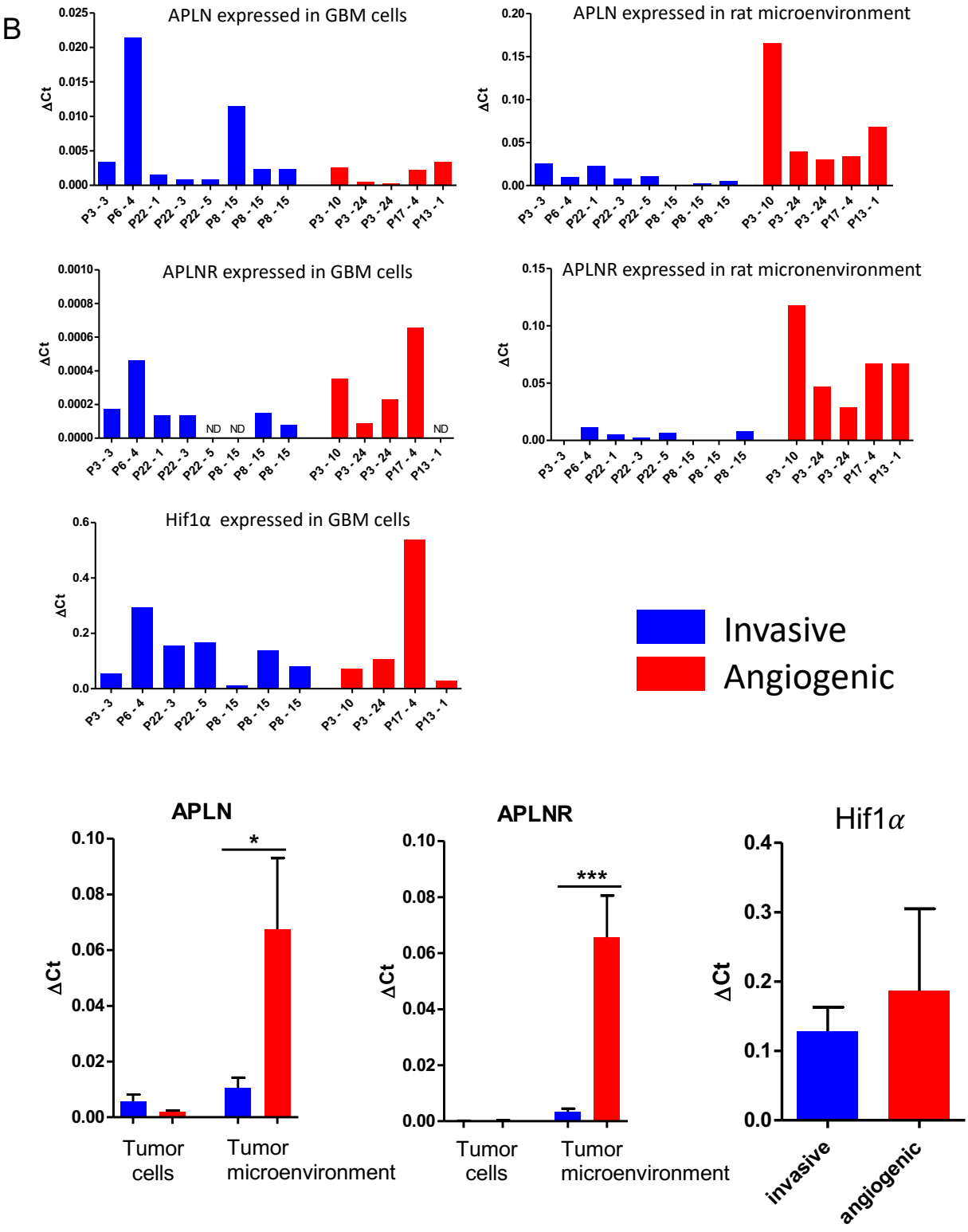

Figure 8 (continued): The upregulation of the APLN-APLNR signaling in GBMs correlates with the angiogenic switch. (B) The results obtained by qPCR show that, in the tumor microenvironment, the angiogenic switch is associated with a significant upregulation of APLN and APLNR. The graphs at the top represent the single samples, which are grouped in the graphs at the bottom for the statistical analysis. Housekeeping gene: GAPDH. For APLN and APLNR samples were 8 and 5 respectively, 3 replicates each sample; for Hif1α samples were 7 and 4, 3 replicates each, Student's t-test, *$p < 0,05$, ***$p < 0,0005$. No significant difference is detectable in APLN and APLNR expressed by the tumor cells.

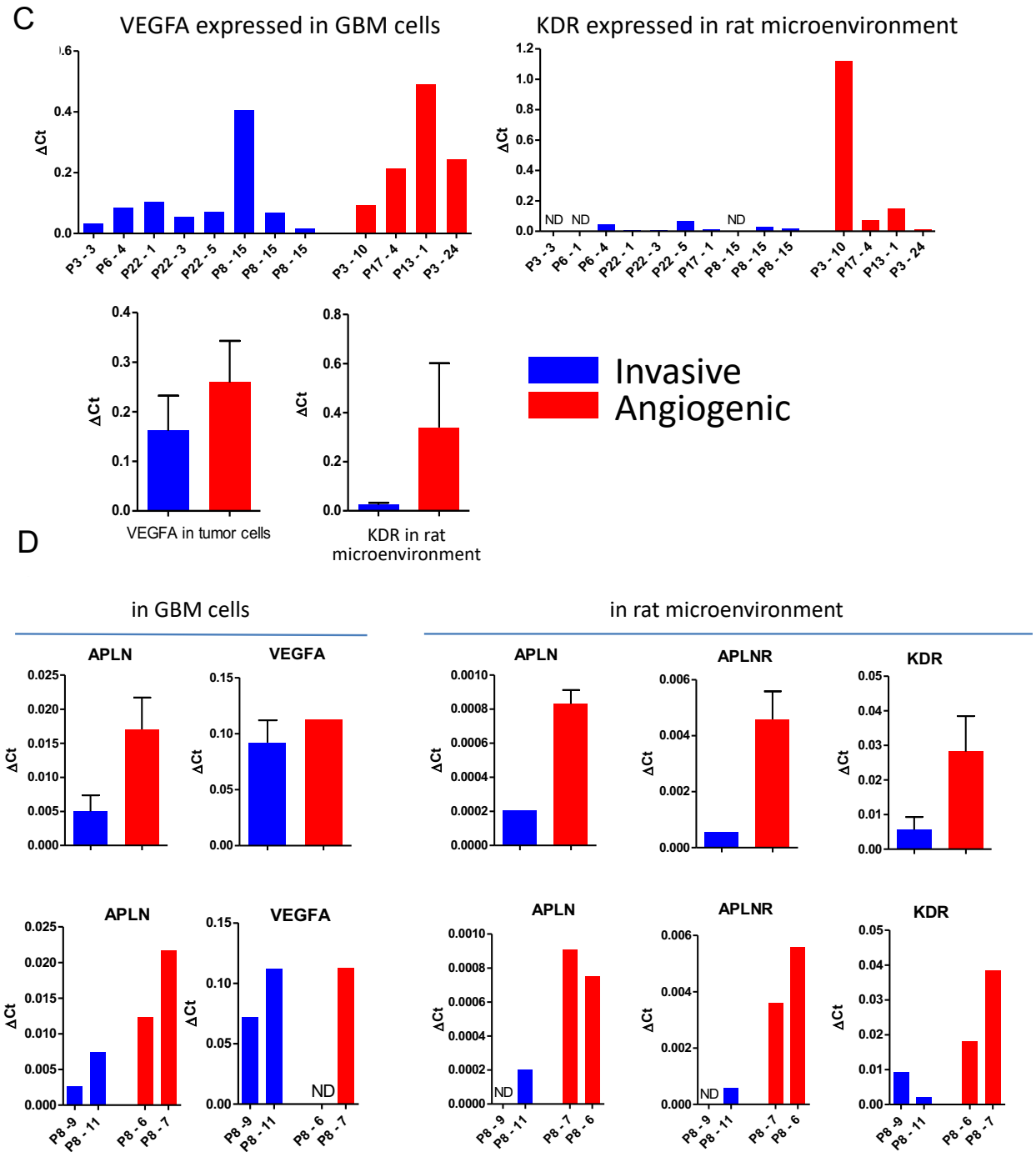

Figure 8 (continued): The upregulation of the APLN-APLNR signaling in GBMs correlates with the angiogenic switch. (C) In the tumor cells and in the rat microenvironment respectively, the expression of VEGFA and KDR shows a tendency to increase, although not significantly, in association with the angiogenic switch. The graphs at the top represent the single samples grouped in the graphs at the bottom for the statistical analysis. Housekeeping gene: GAPDH. 3 replicates each sample, Student's t-test; (D) When the angiogenic switch is induced by EGFR inactivation, a similar tendency to an increased expression of APLN, APLNR, and KDR is observable in the tumor microenvironment. Results are shown as single samples (bottom) and grouped according to their classification as "invasive" or "angiogenic" (top). Unfortunately, the number of samples available in this model was insufficient for a statistical analysis. 3 replicates per sample were used.

7.3 The generation of models to study APLN function in primary GBM cells

7.3.1 *Generation and characterization of primary human GBM cells with APLN loss*

The data presented so far showed a higher expression of both APLN and APLNR in tumor tissue and the correlation of signal upregulation with an angiogenic tumor phenotype. These results however do not provide insights on the direct role of APLN in driving tumor growth and angiogenesis.

The manipulation of APLN expression in either the glioma cells, the healthy brain microenvironment, or both, would allow us to better understand the contribution of the signal and of each compartment to the progression of glioblastoma. In order to reduce APLN expression in the selected GBM cells, I transduced them with a lentivirus carrying a short-hairpin RNA (shRNA) against human APLN, generating APLN-KD primary GBM clones (Figure 9A). The incorporation of the shRNA into a lentivirus allows a stable insertion of the construct into the cell genome. The transcribed shRNA is cleaved by Dicer in the cytoplasm and directs the cleavage and subsequent degradation of the complementary mRNA [144].

From the APLN-expression screening presented in figure 4A, I chose three primary cultures (GBM14, NCH644, and GBM1i) that were relatively high in APLN expression, as indicated in figure 9B. For each cell culture, I also generated the control group transduced with a non-silencing control (NSC) shRNA.

After three weeks of selection with puromycin to eliminate the non-transduced clones, cell pellets were collected for qPCR analysis of gene expression (Figure 9C). As shown in figure 9C, APLN expression was significantly reduced in the APLN-KD cells, in comparison with the NSC and parental groups. Specifically, APLN expression in GBM14 APLN-KD cells was reduced to 14% compared to NSC cells, to 10% in NCH644 APLN-KD, and to 27% in GBM1i APLN-KD.

To verify the specificity of the lentiviral transduction, I performed a qPCR analysis for the expression of different control genes: kinesin-5 (also known as Eg5), an essential protein during mitosis [145]; actin, the cytoskeletal housekeeping gene; and VEGFA, to exclude possible unwanted effects of APLN knock-down on the VEGF-signaling [146]. In all three primary cultures I did not find any differences in the expression of non-targeted genes, meaning that the knock-down of APLN was specific (Figure 9D).

To assess whether the transduction impaired the viability of the cells, which would influence their *in vivo* growth and the results of further experiments, I have used the MTT viability assay: I normalized the absorbance measured for APLN-KD and NSC cells at 24, 48, 72, and 96 hours on their parental group; up to 96 hours after plating, the NSC or APLN-KD GBM14, NCH644, and GBM1i did not shown any decreased viability in comparison with their parental controls (Figure 9E). When comparing the proliferative abilities of the transduced cells and their parental groups, I normalized the absorbance at day 2 (48 hours), 3 (72 hours), and 4 (96 hours), on the absorbance at day 1 (24 hours). After 3 days, GBM14 APLN-KD cells proliferate more than their NSC and parental groups. NCH644 and GBM1i cells did not show any differences in proliferation over 3 days of observation (Figure 9E).
Next, to confirm that the GBM14 APLN-KD cells were equal to the NSC control group in the ability to form spheres, I have performed a sphere-dilution assay, by plating the cells at decreasing density (from 2000 to 10 cells/well) and quantifying the spheres formed after 7 days. Spheres were formed at comparable rate in both groups at all cell dilutions, proving that the transduced cells did not lose the stemness potential also when APLN expression was reduced (Figure 9F). In addition, I used the data from the sphere-dilution assay on the GBM14 cells in the Extreme Limiting Dilution Analysis (ELDA), to assess possible differences in stem cell frequency between GBM14 APLN-KD and NSC cells [137]. The results obtained with the ELDA confirmed no differences between the two cell groups (Figure 9G).

In conclusion, the generation of viable APLN knock-down clones and non-silenced controls was successful, and the two groups were comparable in proliferation, viability, and sphere formation, respectively. The maintenance of the proliferative abilities after the knock-down of APLN expression suggest that the autocrine signal is not responsible for the preservation of the stemness pool. In support to this finding, I observed that the cultured APLN-KO NPCs have a proliferative behavior comparable to the one of APLN-WT NPCs, when kept in standard stem cell culture conditions and without the addition of apelin peptide to the culturing medium.

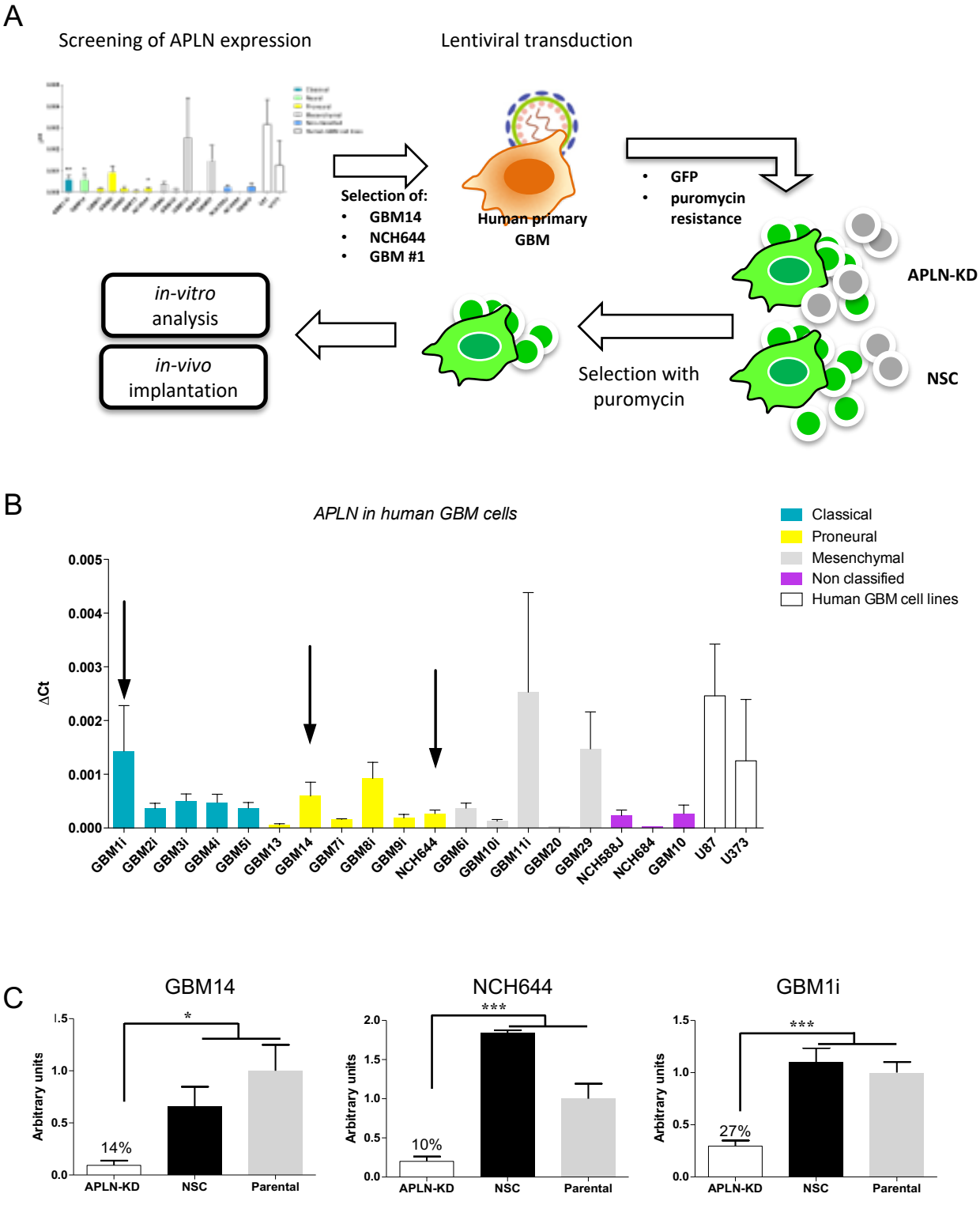

Figure 9: Generation and characterization of new primary GBM models with loss of APLN expression. (A) Schematic representation of the experimental process to obtain APLN-KD and NSC clones; (B) qPCR screening of APLN expression in the primary human GBM cells. The arrows indicate the three cell types chosen for the transduction; (C) After selection with puromycin, the reduction of APLN expression in the three transduced cell groups was confirmed by qPCR. Results are normalized to GAPDH and obtained by at least 3 independent experiments with 3 replicates each. Student's t-test was used to compare APLN expression between APLN-KD cells and NSC or parental cells, *p < 0,05, ***p < 0,0005.

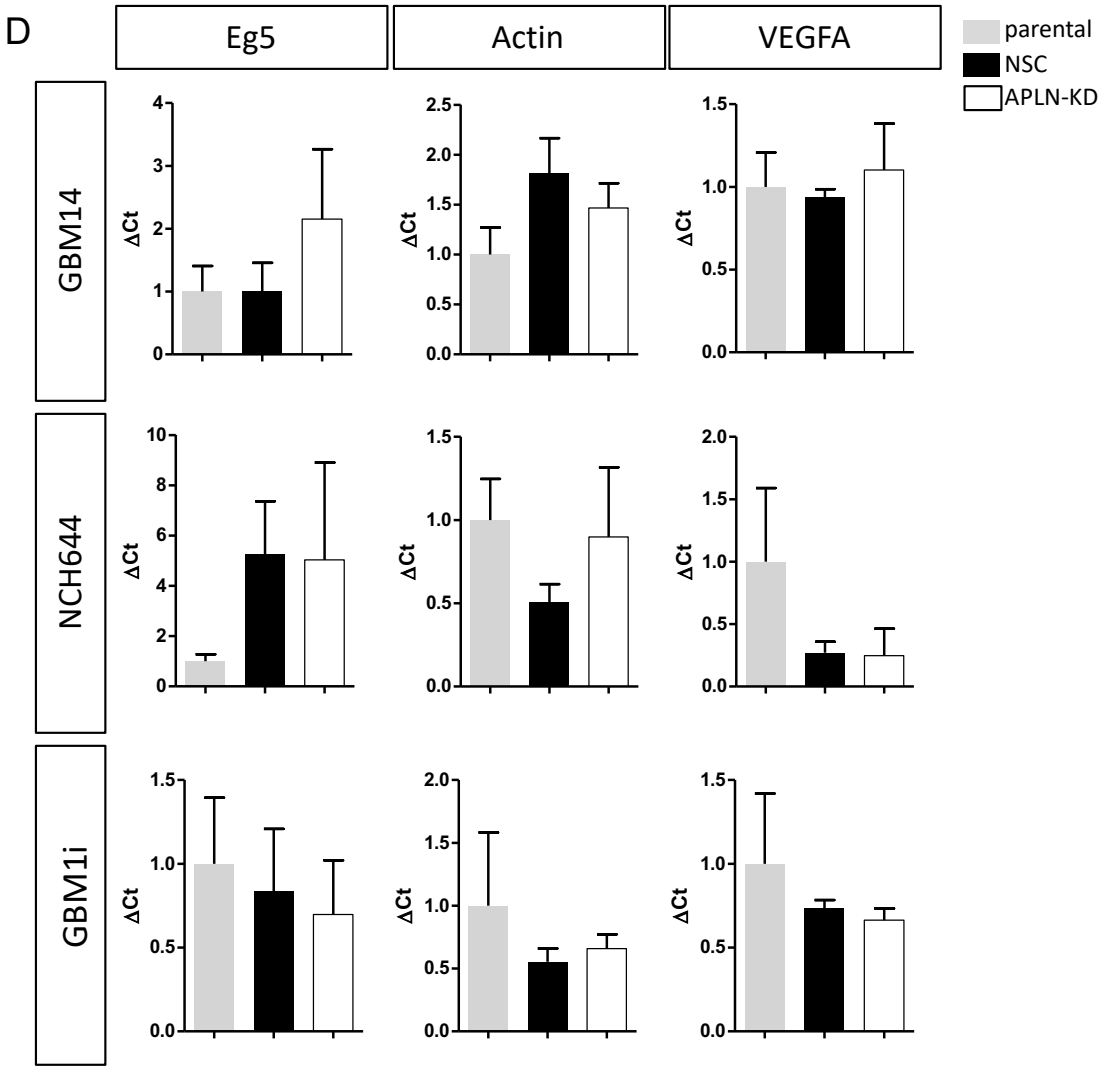

Figure 9 (continued): Generation and characterization of new primary GBM models with loss of APLN expression. (D) qPCR analysis to confirm the specificity of APLN targeting by lentiviral transduction. One-way ANOVA with Newman Keuls post-hoc test, results normalized to GAPDH and obtained from at least 3 independent experiments with 3 replicates each.

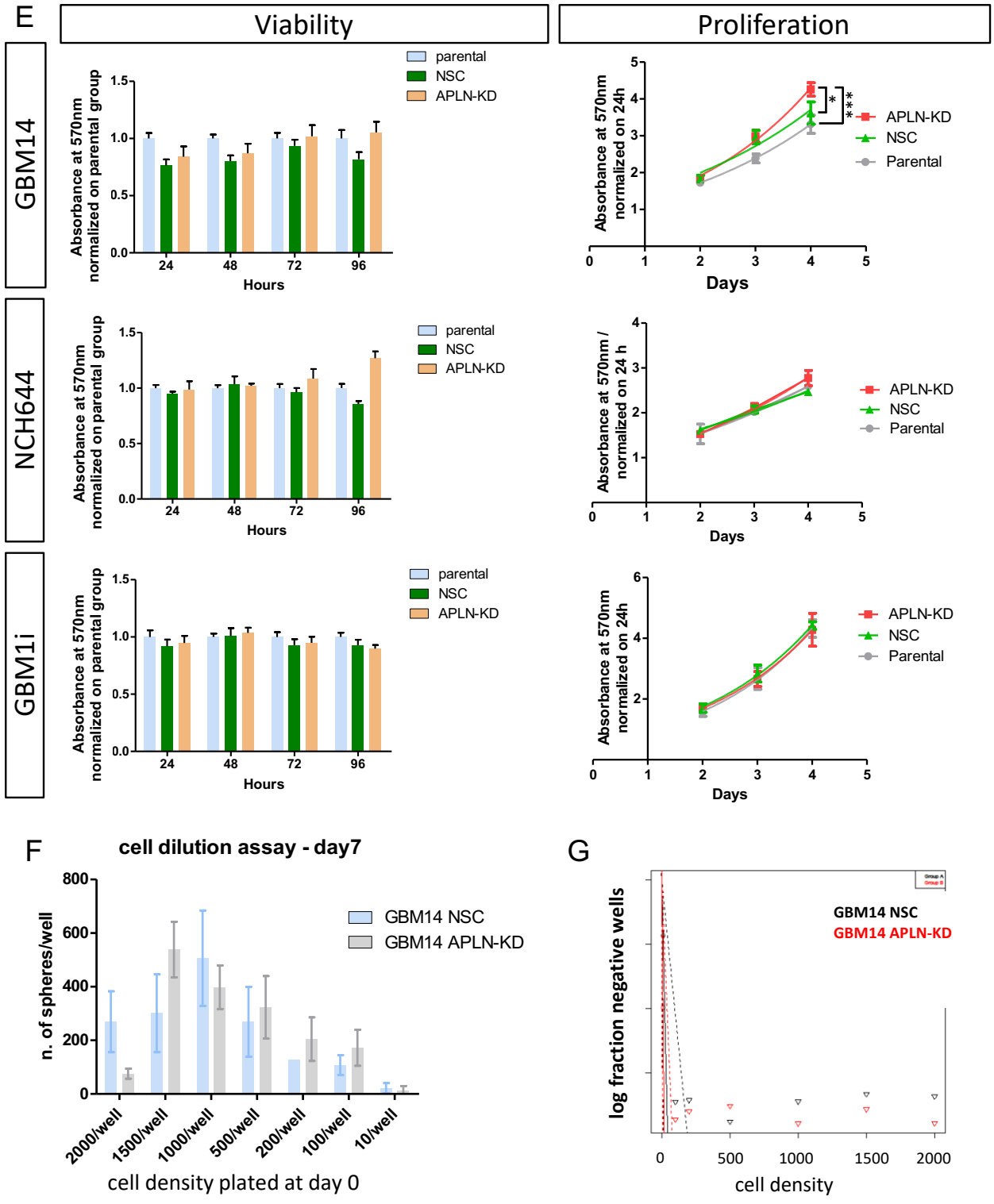

Figure 9 (continued): Generation and characterization of new primary GBM models with loss of APLN expression. (E) The transduction does not affect cell viability. The parental groups are used each day for normalization and indicated as 1. NCH644 and GBM1i cells show no differences in proliferating abilities between groups over a period of 3 days. GBM14 APLN-KD cells, however, have increased proliferative abilities after 3 days, compared to NSC and parental cells. At least 3 independent experiments were performed and analyzed with two-way ANOVA, *p < 0,05, ***p < 0,0005; (F) After 7 days, the ability to form sphere is comparable between GBM14 APLN-KD and NSC cells; 3 replicates/condition; (G) The ELDA analysis, performed at http://bioinf.wehi.edu.au/software/elda/, shows no differences in stem cell frequency between GBM14 APLN-KD and NSC cells; 3 replicates/condition.

7.3.2 APLN loss induces decreased tumor angiogenesis and increased tumor invasion in vivo

The human primary GBM cultures that I generated, GBM14 and NCH644 with and without the loss of APLN expression, have been used for numerous *in vivo* orthotopic implantations to study the role of the APLN-APLNR signaling in tumor progression. In these *in vivo* models, APLN expression was modulated in the tumor cells (by using the APLN-KD or NSC GBM cells), and/or in the tumor microenvironment (by using APLN-KO or WT mice). The *in vivo* results obtained by the implantation of APLN-KD or NSC cells in APLN-KO or WT mice are extensively discussed in our manuscript "*Targeting APLN/APLNR Improves Antiangiogenic Efficiency and Blunts Proinvasive Side Effects of VEGFA/VEGFR2 Blockade in Glioblastoma*" [147].

The implantation of GBM14 and NCH644 APLN-KD cells in APLN-KO or WT mice revealed a direct correlation between the overall level of expressed APLN (contributed by the tumor cells and the host) and the GBM angiogenic phenotype, in confirmation of the results that I reported in the GBM models of the angiogenic switch (chapter 7.2) (Figure 10A and B). When implanted, GBM14 and NCH644 NSC cells generated tumors with a significantly higher vessel density, in comparison with the tumors generated by GBM14 and NCH644 APLN-KD cells, respectively. In addition, the manipulation of APLN expression in the tumor microenvironment, by using APLN-WT or -KO mice, demonstrated that APLN produced by the brain parenchyma partially compensated the decreased APLN levels in the GBM14 APLN-KD cells: in fact, the APLN-KD cells implanted in an APLN-WT parenchyma generated tumor with increased vessel density, when compared to the tumors developed in APLN-KO brains (Figure 10A).

Furthermore, we observed that the APLN-KD GBM cells were able to generate the most invasive tumors (Figure 10C and D). In addition to this, the absence of APLN in the APLN-KO parenchyma significantly increased the invasive behavior of the GBM14 APLN-KD cells (Figure 10C). These results hint to a prominent role of APLNR and the autocrine APLN-APLNR signaling in the determination of an invasive phenotype, aside from its role in angiogenesis.

As discussed in the introduction, the activation of the APLNR can also be triggered by the recently-identified early endogenous ligand apela: to test for apela expression, I performed a qPCR analysis on the brain lysate of APLN-WT, APLN-KO, and K14-APLN brains. The K14-APLN mouse is a transgenic model where APLN is ectopically expressed under the control of the keratin K14 promoter. This model is used to study the effect of epidermal APLN on the regulation of blood vessel caliber [148]. The qPCR results showed that apela is detectable in

all three lysates: in particular, its presence in the APLN-WT type and –KO brains indicated that it may act with or in compensation to APLN in activating APLNR (Figure 10E).

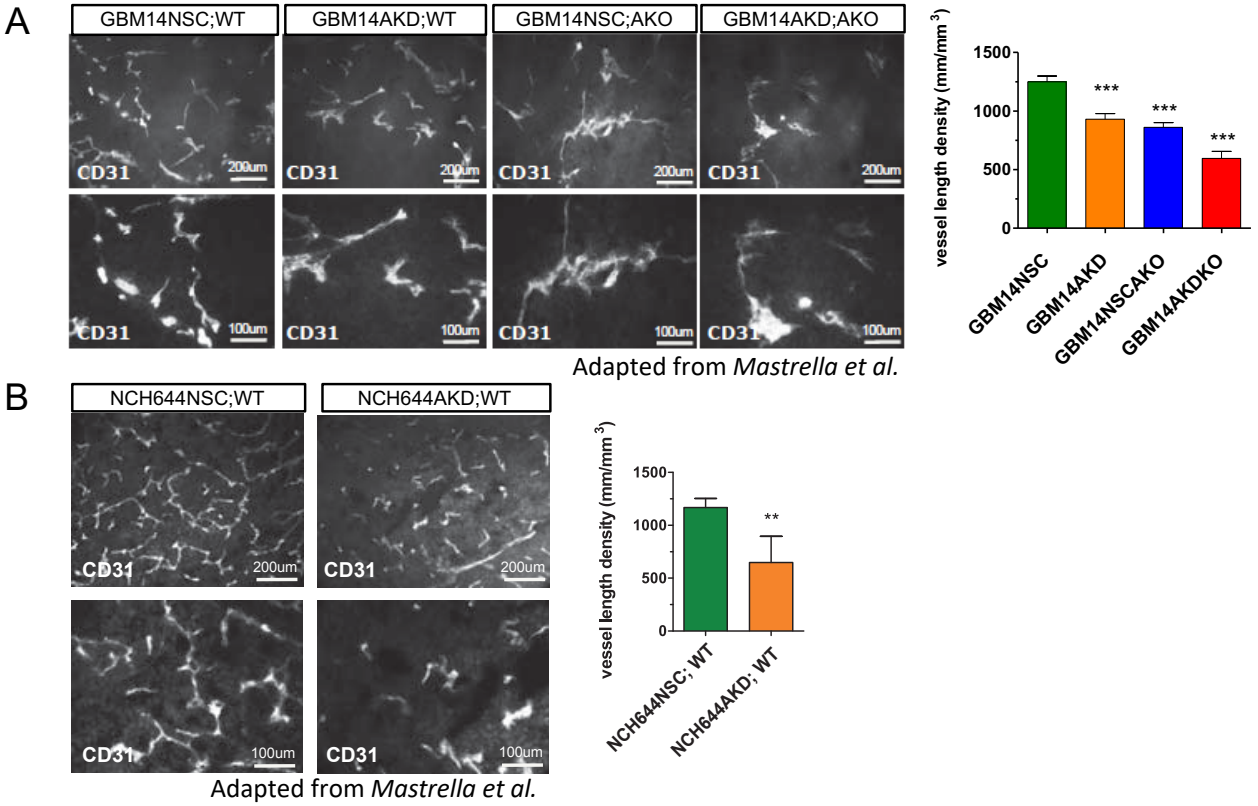

Figure 10: APLN loss induces decreased tumor angiogenesis and increased tumor invasion *in vivo*. In the *in vivo* models generated by GBM14 (A) and NCH644 (B) cells, vessel density decreases in correlation to a decreased APLN expression contributed by the tumor cells and the tumor microenvironment; A: one-way ANOVA with Newman Keuls post-hoc test, APLN-WT n=7/cell type, APLN-KO n=4/cell type; B: Student's t-test, NSC n=8, APLN-KD n=6. **p<0.005, ***p<0.0005.

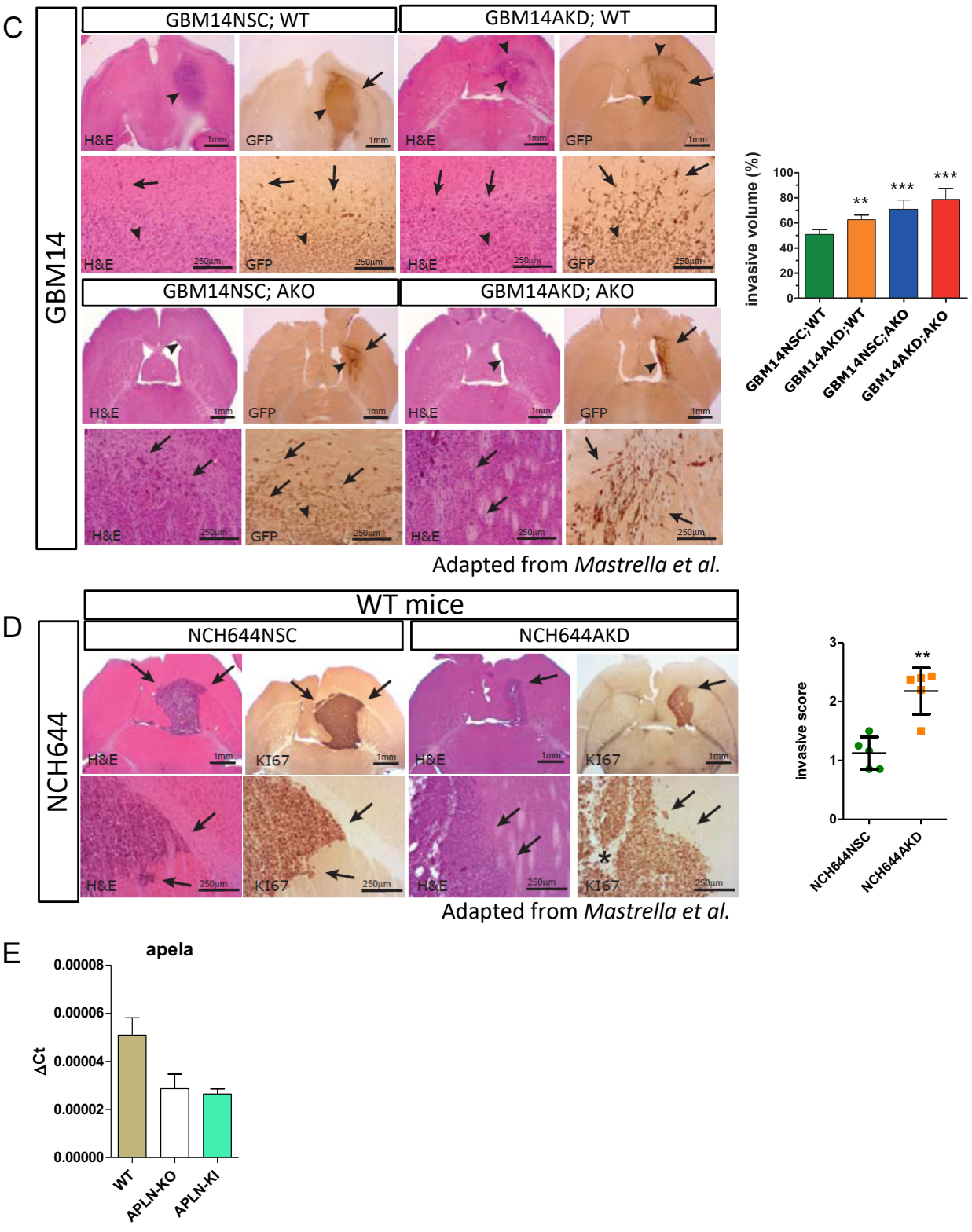

Figure 10 (continued): APLN loss induces decreased tumor angiogenesis and increased tumor invasion *in vivo*. (C) GBM14 cells show increased invasive behavior when the overall level of secreted APLN, from the tumor and the tumor microenvironment, decreases (GBM14 APLN-KD cells in APLN-KO mice). Arrows indicate the invasive borders. One-way ANOVA with Newman Keuls post-hoc test, WT n=7/cell type, APLN-KO n=4/cell type; (D) When implanted, NCH644 APLN-KD cells show increased invasive abilities in comparison with control cells. Arrows indicate the tumor borders. Student's t-test, NSC n=8, NCH644 APLN-KD n=6; (E) The qPCR results confirm the presence of apela in APLN-WT, APLN-KO, and K14-APLN brains. GAPDH was used as housekeeping gene. **p<0.005, ***p<0.0005.

7.3.3 *Generation of mouse proneural primary GBM cells with APLN loss*

To study the role of the APLN-APLNR pathway in an immunocompetent mouse model, I generated mouse primary GBM cells with APLN loss from isolated NPCs (Figure 11A).
Cells were isolated from the SVZ of 30-day-old Bl6/J mice carrying homozygous deletion in cdkn2a or in cdkn2a and APLN genes (cdkn2a-KO and cdkn2a-KO;APLN-KO mice).
Before proceeding with the viral transduction, I verified by qPCR the reliability of the genotyping results by comparing APLN expression in cdkn2a-KO;APLN-KO NPCs with the one measured in a whole-homogenate of APLN-KO brain and in WT NPCs (Figure 11B). Once the genotyping was confirmed, I transduced the isolated NPCs with VSV-G pseudotyped retroviral particles carrying the Hs PDGFB-GFP or -dsRed gene to obtain GBM cells of the proneural subtype, cdkn2a-KO PDGFB and cdkn2a-KO;APLN-KO PDGFB cells (indicated as cdkn2aKO;APLN-KO GFP or cdkn2a-KO;APLN-KO dsRed). Due to the absence of a marker for antibiotic selection in the viral construct, I manually selected the GFP- or dsRed-positive spheres. At last, the success of the transduction was confirmed by verifying the presence of the human PDGFB gene by PCR (Figure 11C). In a first set of *in vivo* experiments, both cell types did not generate a compact tumor mass and further investigation on these clones is required.

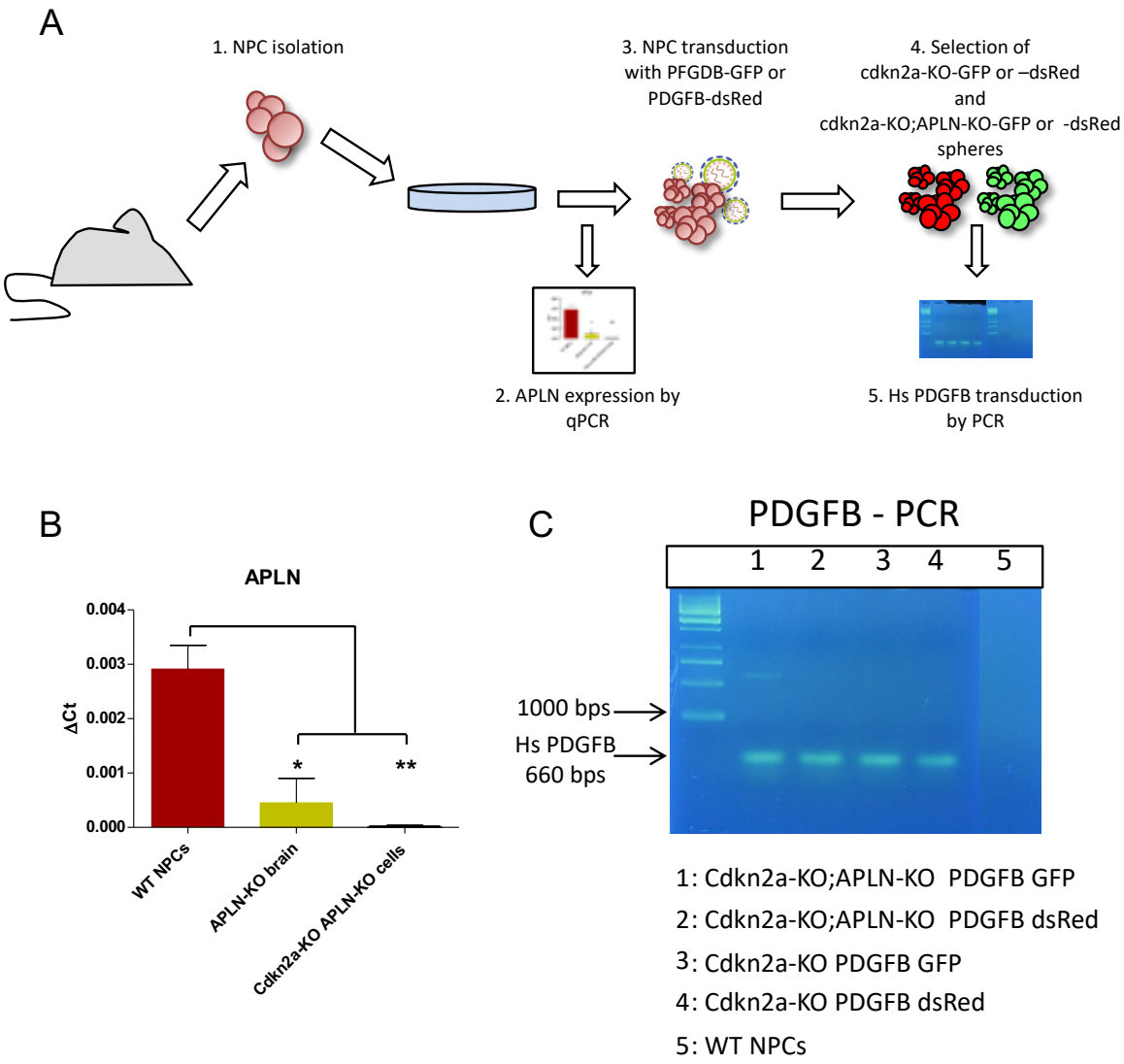

Figure 11: Generation of mouse GBM cells with APLN loss. (A) The scheme shows the experimental process to obtain cdkn2a-KO;APLN-KO PDGFB GFP/dsRed cells and their corresponding controls cdkn2a-KO PDGFB GFP/dsRed; (B) qPCR analysis confirmed the genotyping results and the loss of APLN in the cdkn2a-KO;APLN-KO isolated NPCs. Results are normalized to GAPDH and obtained by 3 independent experiments, n = 9. APLN-KO brain and Cdkn2a-KO APLN-KO cells were compared to WT NPCs with one-way ANOVA with Newman Keuls post-hoc test, *p ≤ 0,05, **p ≤ 0,005; (C) After manual selection under the microscope of GFP/dsRed-positive spheres, I confirmed by PCR the quality of the transduction verifying the presence of the Hs PDGFB gene.

7.4 APLN and APLNR expression differs according to the localization in the tumor mass

7.4.1 Analysis of APLN and APLNR expression in human GBM samples paired as tumor core and tumor border

Our research group previously reported an upregulation of APLN and APLNR in WHO grade IV GBM specimens, especially in hypoxic tumor areas marked by HIF1A and VEGFA expression and in microvascular proliferations [55]. This finding is supported by my results on mouse and human tumor specimens, where APLN and APLNR were upregulated in the tumor tissue. In addition, in the human GBM sections I observed that APLN expression was particularly strong in the ECs (Figure 7B).

To further characterize APLN and APLNR distribution across the tumor, I analyzed GBM biopsies in more detail: the samples were segregated, during neurosurgical resection supported by a neuro-navigation system, into samples derived from the tumor center or from the tumor border (Figure 12A). By qPCR analysis I found that the expression of the marker of hypoxia HIF1A and APLN shared a tendency to be higher in the tumor center, in comparison with the tumor border. The localization of APLN expression in hypoxic areas is in accordance with previous findings reported by me (see figure 6B) and our group [55]. APLNR expression instead tended to increase at the tumor borders (Figure 12B). These results were confirmed with *in situ* hybridization performed on a pair of center and border tumor samples: APLN was detectable at the tumor core, in tumor vessels and tumor cells, and was not detectable at the tumor periphery; on the contrary, APLNR signal was stronger in tumor cells at the tumor borders, but detectable as well in the vessels of the tumor core (Figure 12C). As expected, the frequency of vascular proliferates, visible on H&E, was much higher in the tumor core than in the tumor-periphery. Tumor-free brain tissue did not show considerable expression of APLN or APLNR by *in situ* hybridization (compare also to Figure 13B).

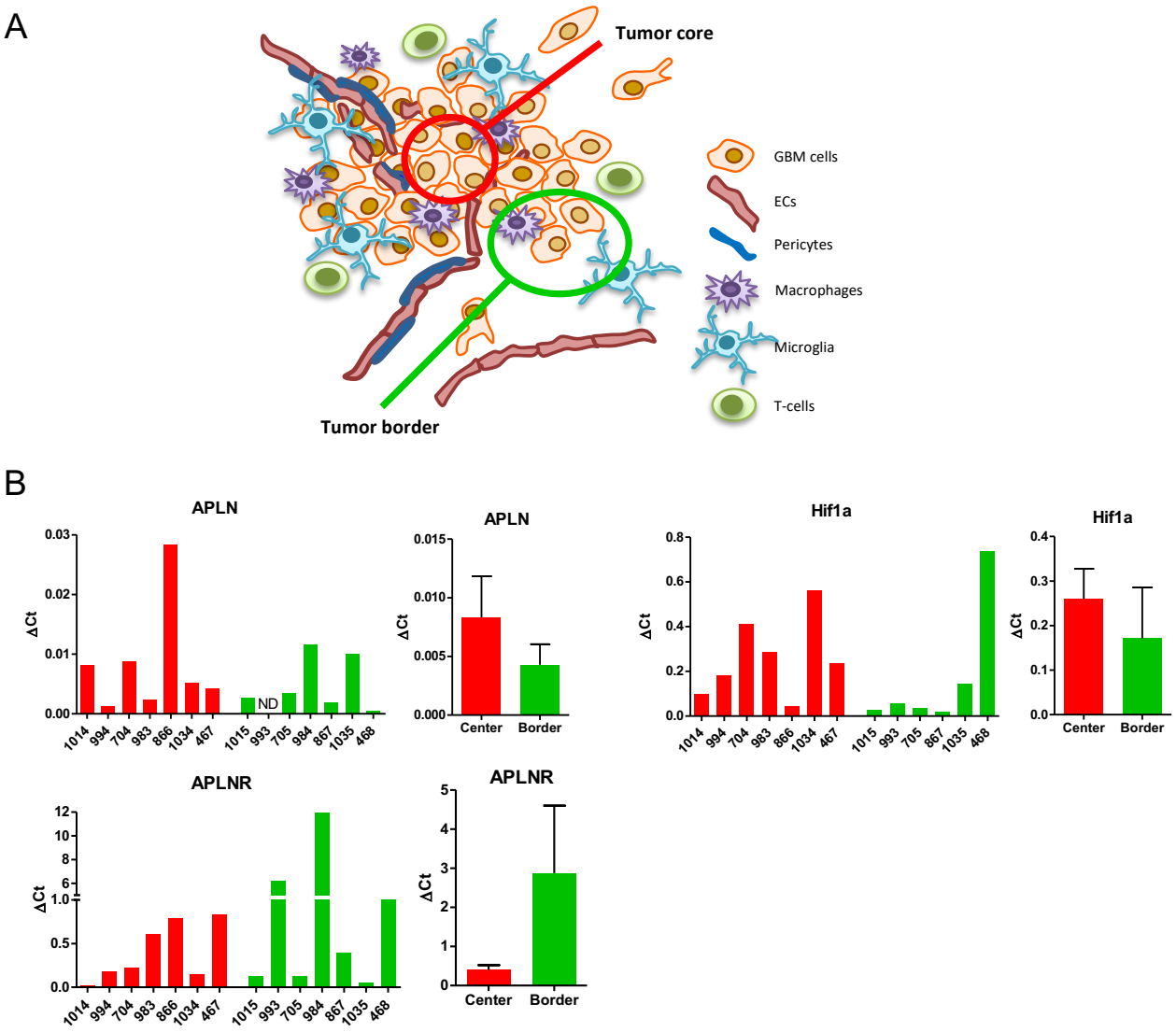

Figure 12: APLN and APLNR are heterogeneously expressed across the tumor mass – Samples classified as center and border. (A) The illustration represents the criteria for the classification of the paired samples belonging to a single tumor mass as "center" or "border" depending on their position at the time of surgical resection; (B) The qPCR analysis detected a tendency to a differential expression pattern of APLN, APLNR, and HIF1α across the GBM mass, although not significant: both APLN and HIF1α tend to an increased expression in the tumor centers, while APLNR expression tends to be higher at the tumor borders. Interestingly, APLNR expression is much higher when comparing its ΔCt to APLN ΔCt. Housekeeping gene: GAPDH. The graphs on the left show the single results, which are grouped in the graphs on the right for statistical analysis. Student's t-test, n= 7;7.

C

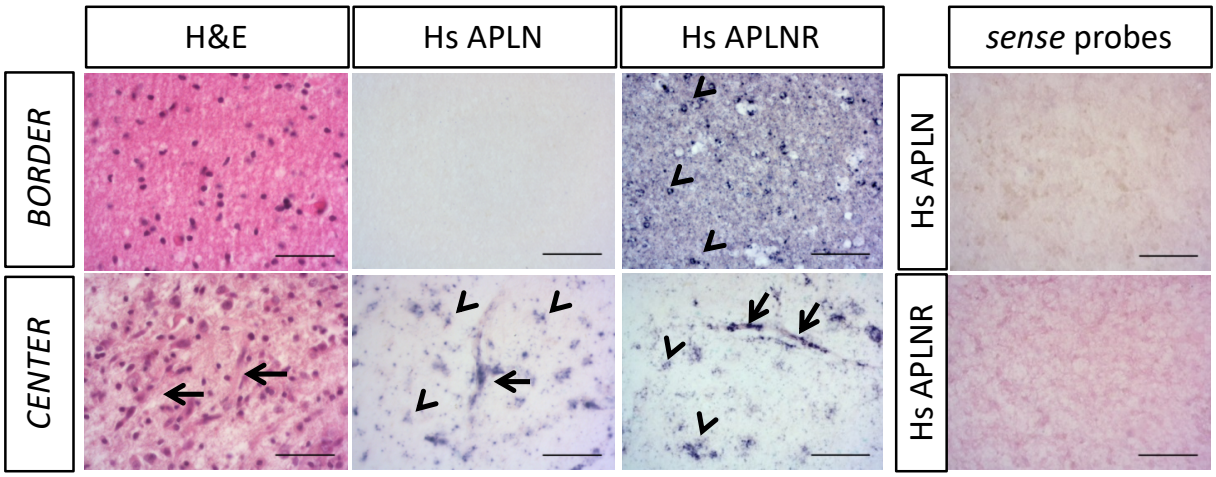

Figure 12 (continued): APLN and APLNR are heterogeneously expressed across the tumor mass – Samples classified as center and border. (C) The qualitative assessment of APLN and APLNR expression by *in situ* hybridization on a pair of center-border GBM sections supports the qPCR findings. The H&E staining indicates the presence of necrotic tissue and abundant vessels (arrows) in the tumor core, in comparison to a more-homogeneous tissue at the border. APLN expression is strongly detectable only in the tumor center, in correspondence to the presence of vessels. APLNR shows an increased cellular expression at the tumor border. Arrows indicate a positive signal on vessels, arrowheads indicate a positive signal in the tumor cells. To confirm the specificity of the hybridization, a staining with sense probes is shown; scale bar = 50μm.

7.4.2 Analysis of APLN and APLNR expression in human GBM samples classified according to the coordinates of stereotactic resection

For an enhanced local resolution of APLN/APLNR expression in GBM WHO grade IV, I next investigated a set of stereotactic GBM biopsies. These biopsies were resected along a stereotactic trajectory on the z-axis, with recorded distances in mm from the starting point of the resection, defined as zero (Figure 13A). A neuropathologist identified cell dense pleomorphic glial tumor presenting with GFAP and MAP2 positivity, IDH1 WT, 15% Ki67 positive tumor nuclei and many vascular proliferates from coordinate z = 0 to 1 mm towards the tumor border. From 6 to 9 mm along the z-axis, the biopsies contained CNS tissue with infiltrating glial tumor cells.

By *in situ* hybridization I found that APLN expression was very strong in the biopsies from z = 0 to 1 mm, with a clear signal especially in the tumor vessels (Figure 13B). APLN was almost undetectable in the outermost sections, in accordance with my previous results shown in figure 12C, which illustrates the intense APLN signal detectable in the tumor center, compared with an absent staining at the tumor border. APLNR instead, even though detectable in the sections close to the point z=0, also gave a very strong signal at the levels z = 6 to 9 mm, further away from the tumor-dense core, in the region where tumor invading cells were described in the report of the neuropathologist. These findings demonstrated that APLNR expression is present not only in the GBM neo-angiogenic areas, but in the tumor invasive regions as well. APLN and APLNR expression in the GBM samples was compared to the *in situ* hybridization performed on an healthy brain sample (called “brain” in figure 13B): here no signal from both probes was detectable.

Taken together, these results on the different patterns of APLN and APLNR localization in the tumor mass point to an additional role of the APLN-APLNR signaling in tumor progression, aside from its function in driving tumor angiogenesis. This hypothesis is supported by our results *in vivo* described at paragraph 7.3.2 (Figure 10C and D), where we demonstrated that the implantation of GMB cells with APLN loss generates more invasive tumors, thus indicating an additional role of APLN-APLNR signaling in driving GBM invasion.

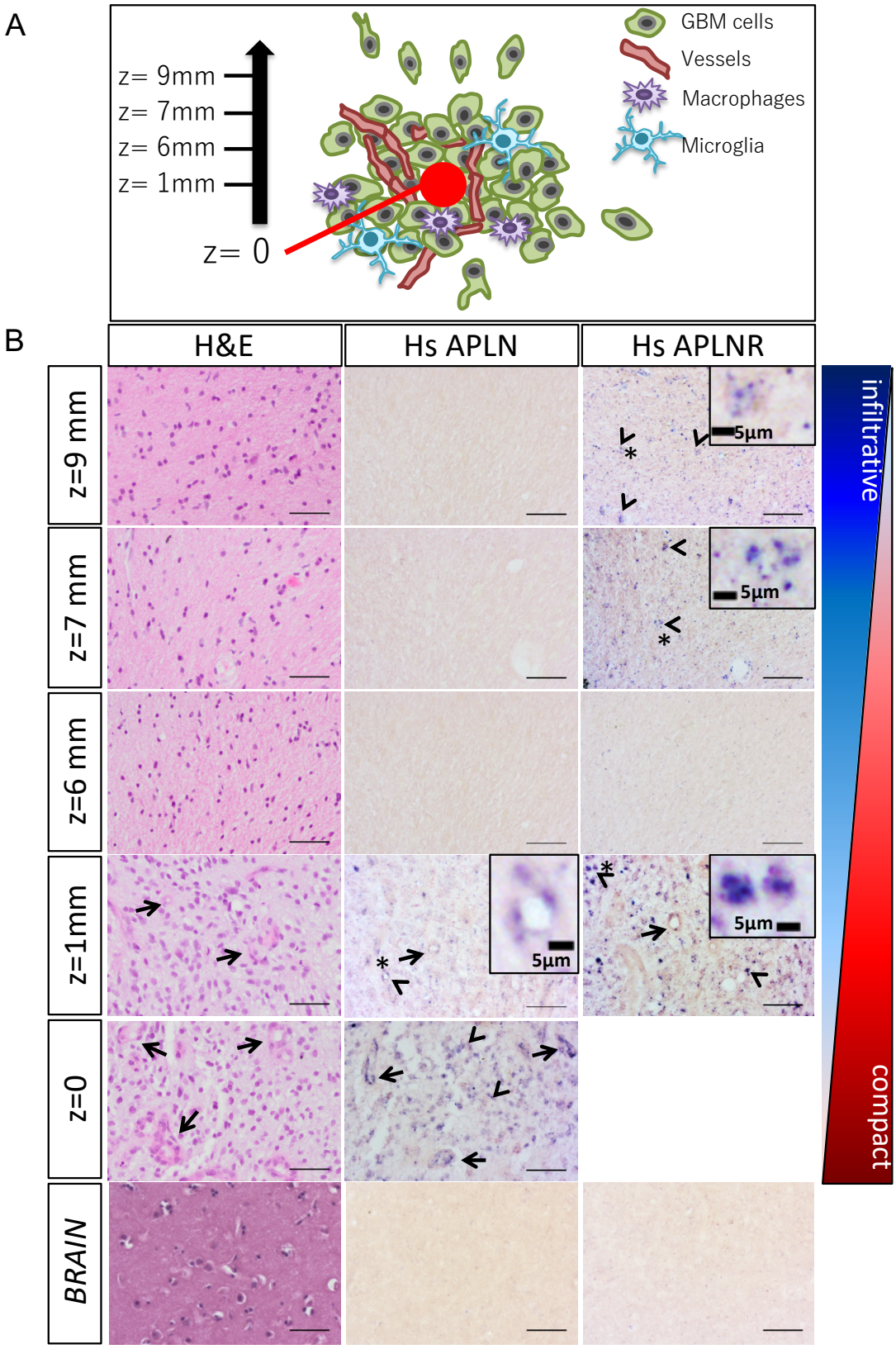

Figure 13: APLN and APLNR are heterogeneously expressed across the tumor mass in a stereotactic tumor sample. (A) The illustration represents the relative positions of the GBM sections in the tumor mass, from the deepest point z=0 to the outermost z=9 mm; (B) APLN expression is observable in the core sections, rich of vascular proliferations (arrows), but not in the outermost ones. APLNR is detectable along the axis from z=0 to z=9. Arrowheads indicate a positive signal at the single cell level and asterisks indicate the enlarged areas. Scale bar in the overview = 50µm.

7.5 APLNR is detectable *in vivo* by immunofluorescence in the GBM mass and in the invading tumor cells – Analysis of GBM mouse xenografts

To better characterize APLNR detectability and expression at tumor periphery and verify its presence in the invasive cells of our GBM mouse models, I analyzed the xenografts of four models with fluorescent immunostainings.

The immunofluorescence analysis allowed me to have a better resolution of the receptor at the single-cell level and to verify its presence in the tumor mass but also in the cells detaching from it, in order to have a comparison for the findings obtained on human GBM samples with *in situ* hybridization.

For this study, I stained the xenografts originated by the implantation of either GBM14 APLN-KD, GBM14 NSC, p53-KO PDGFB, or cdkn2a-KO EGFRvIII cells in either WT or APLN-KO mice (Figure 14). Importantly, all the implanted GBM cells expressed GFP and were easily identifiable on mouse sections. The choice of these cell types was based on the differences in their growth behavior, showing either a more invasive or compact phenotype.

As shown in the overview panels of the staining in figure 14A, APLNR was expressed not only at the border of the tumor mass, but also in the non-tumor cells (non GFP-positive), where the staining presented itself with a specific and distinguishable pattern and appeared generally nuclear. Where a more compact tumor mass was obtained, it showed an intense APLNR signal that was heterogeneous. Whether this heterogeneity correlates with the presence of more or less newly generated tumor vessels would be an interesting question for further studies. In these different GBM xenografts, the GBM cells invading the brain parenchyma express APLNR as well, as shown in the different examples at figure 14B. Interestingly, the localization of APLNR detected in the invading GBM cells, contrary to what I observed in the non-tumor cells, did not always co-localize with the nuclear staining, but was in the cytoplasmic region as well.

Therefore, as shown in the human biopsies, APLNR, which is abundantly expressed in the tumor mass, is expressed as well by some of the invading tumor cells, with a pattern that does not coincide with the one observed in non-tumor cells.

This difference may hint to a specific role of the receptor in the behavior and physiology of GBM cells, or to the important role covered by the up-regulated APLN-APLNR pathway in the development of glioblastoma.

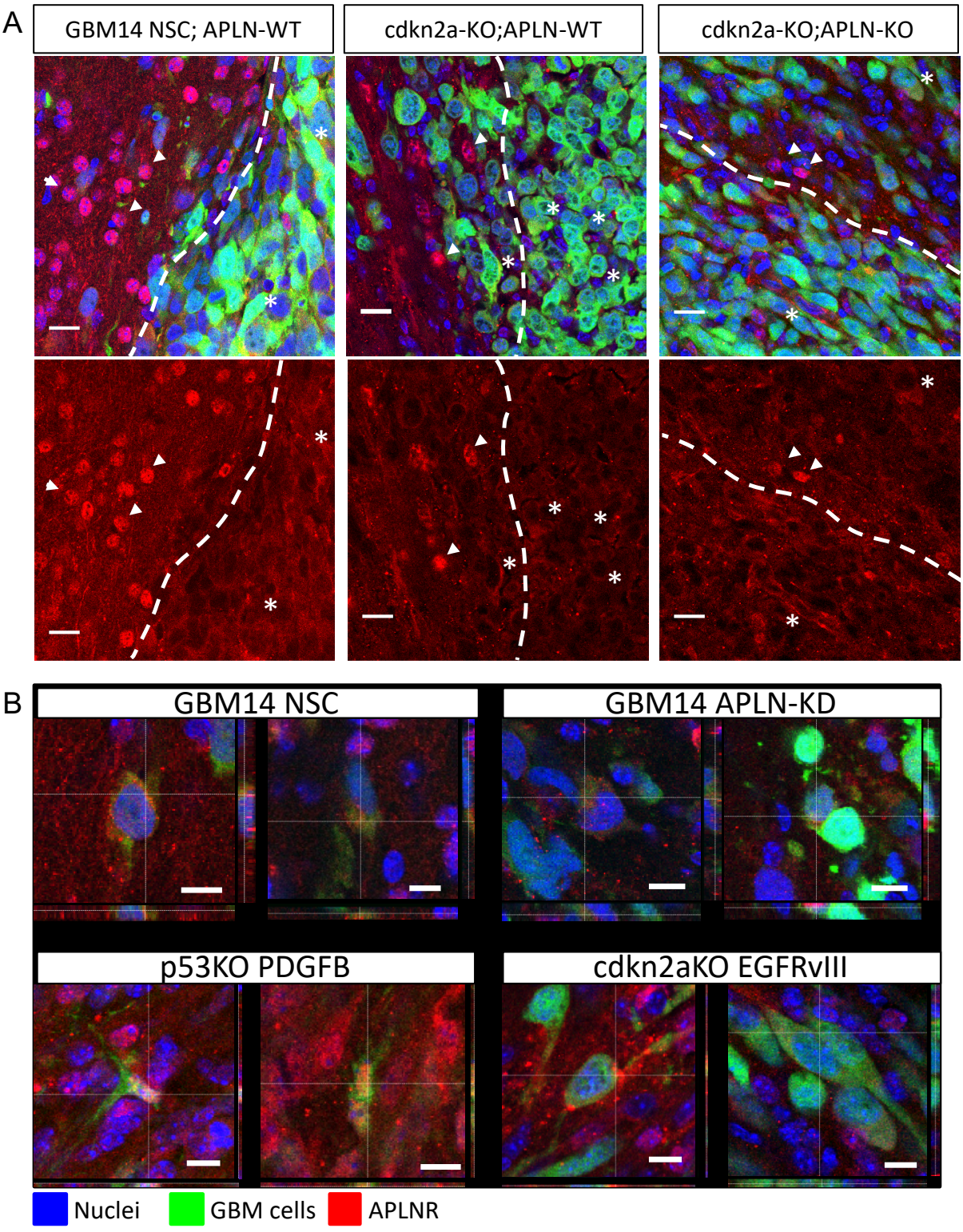

Figure 14: APLNR is expressed at the border of the GBM mass and in the invading GBM cells. (A) The overviews show the interfacing areas between the green GBM mass and the normal brain tissue, tracked by the dashed line. The border of the tumor mass expresses APLNR in a heterogeneous fashion. Single cells in the healthy parenchyma (arrowheads) show a positive and characteristic APLNR signal as well, different from the one originated by GBM cells in the tumor mass (indicated by asterisks). Scale bar = 20µm; (B) Not only the GBM cells in the tumor mass, but also the ones invading the brain parenchyma, show a heterogeneous APLNR signal that is not restricted to the cell nucleus. Scale bar = 10µm.

7.6 The APLN-APLNR signaling drives the invasion of tumor cells *in vitro*

7.6.1 *Apelin-13 enhances the invasion of the U87 APLN-KD cells*

To gain insight on the mechanisms of APLN-driven GBM cells invasion I used an *in vitro* assay established as a 3D environment constituted by rat tail collagen. The set-up of the experiment is illustrated in figure 15A.

Because previous studies reported the role of APLN as chemoattractant for various cells, as 293T cell line and ECs [86, 89], I used this *in vitro* assay to evaluate the invasive behavior of the tumor cells according to their status of endogenous APLN expression, which influences the autocrine APLN-APLNR signaling, and the exposure to an external source of APLN, which would induce a paracrine signaling. In fact, as we observed *in vivo* (Figure 10C), the presence of an weak autocrine APLN-APLNR signaling seemed to be a key factor in the generation of the invasive GBM behavior.

In the first group of experiments, I assessed the *in vitro* invasive ability of U87 APLN-KD and NSC cells, which were previously originated by transducing the human GBM cell line U87 MG with lentiviral particles. Despite the fact that U87 cells are normally cultured under adherent conditions, to perform this assay I kept them in DMEM F12 to obtain a spheroid phenotype. Each sphere was seeded into a well of a 24-well plate in the collagen matrix and its invasion was observed over a period of 7 days [149]. The invasion rate of the U87 APLN-KD and NSC cells at basal conditions (standard medium) was comparable (Figure 15B).

Next, to model the complex situation in a tumor *in vivo*, I added a WT U87 MG sphere to each well as an *in vitro* stable source of growth factors and chemokines, APLN included. I observed that the APLN-deficient U87 cells showed a much higher invasive behavior in comparison to the U87 NSC control cells when a U87 MG sphere was present in the collagen matrix (Figure 15C). When the exogenous apelin-13 peptide was added to the collagen mix, instead of the WT U87 MG sphere, I also observed a significantly higher invasion of the U87 APLN-KD cells compared to the U87 NSC cells (Figure 15D). Hence, in both experimental setups, the loss of endogenous APLN contributed to the invasive tumor phenotype observed in response to the U87 MG-derived growth factors or to the exogenous apelin-13 specifically.

These results were in accordance with the *in vivo* situation, where the U87 APLN-KD cells implanted into APLN-WT mice were significantly more invasive that the U87 NSC cells (Figures 15E).

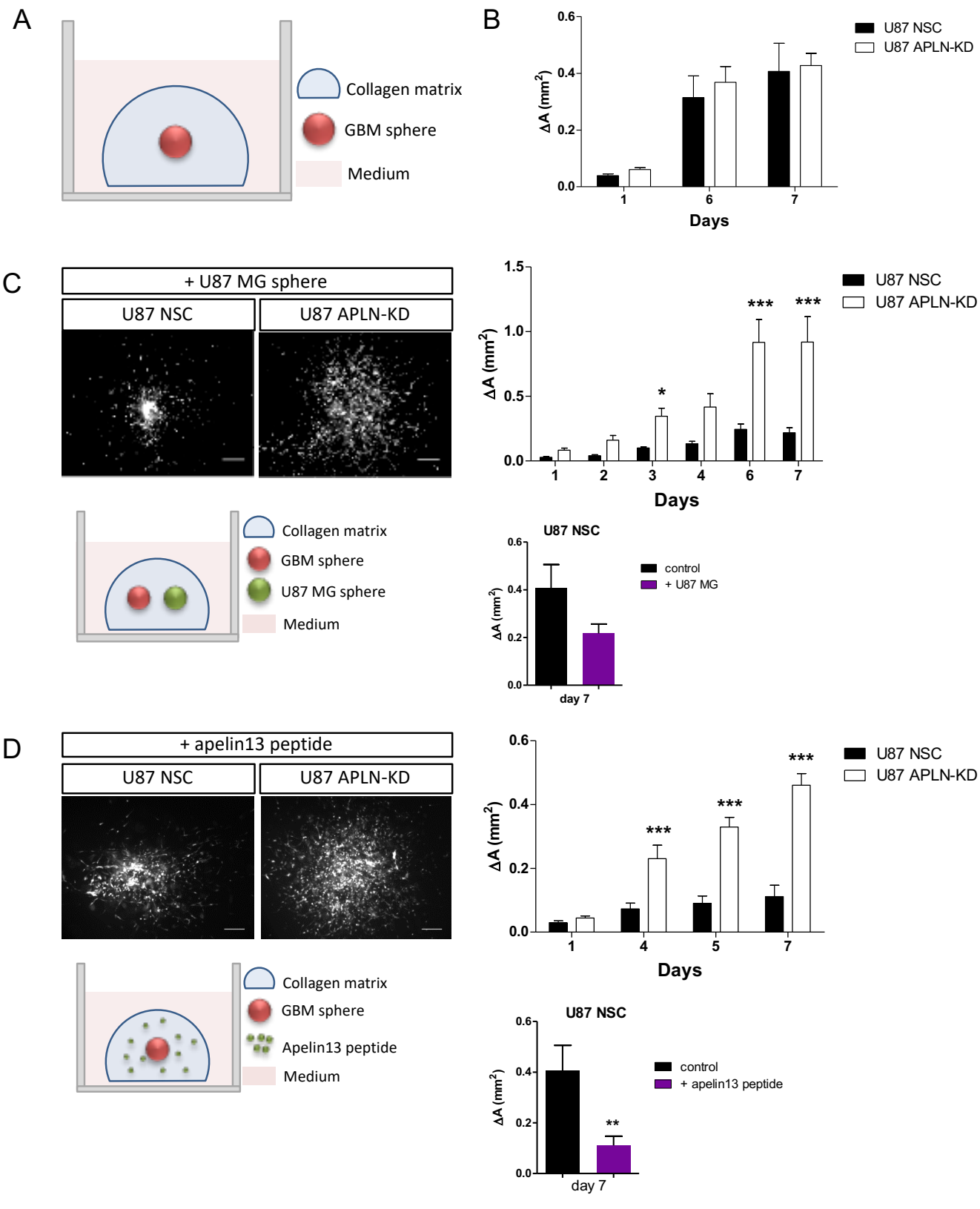
A
Collagen matrix
GBM sphere
Medium
B
U87 NSC
U87 APLN-KD
ΔA (mm²)
0.6
0.4
0.2
0.0
1
6
7
Days
C
+ U87 MG sphere
U87 NSC
U87 APLN-KD
Collagen matrix
GBM sphere
U87 MG sphere
Medium
1.5
1.0
0.5
0.0
*
***
***
1
2
3
4
6
7
Days
U87 NSC
control
+ U87 MG
day 7
D
+ apelin13 peptide
U87 NSC
U87 APLN-KD
Collagen matrix
GBM sphere
Apelin13 peptide
Medium
0.6
0.4
0.2
0.0
***
***
***
1
4
5
7
Days
U87 NSC
control
+ apelin13 peptide
**
day 7

E

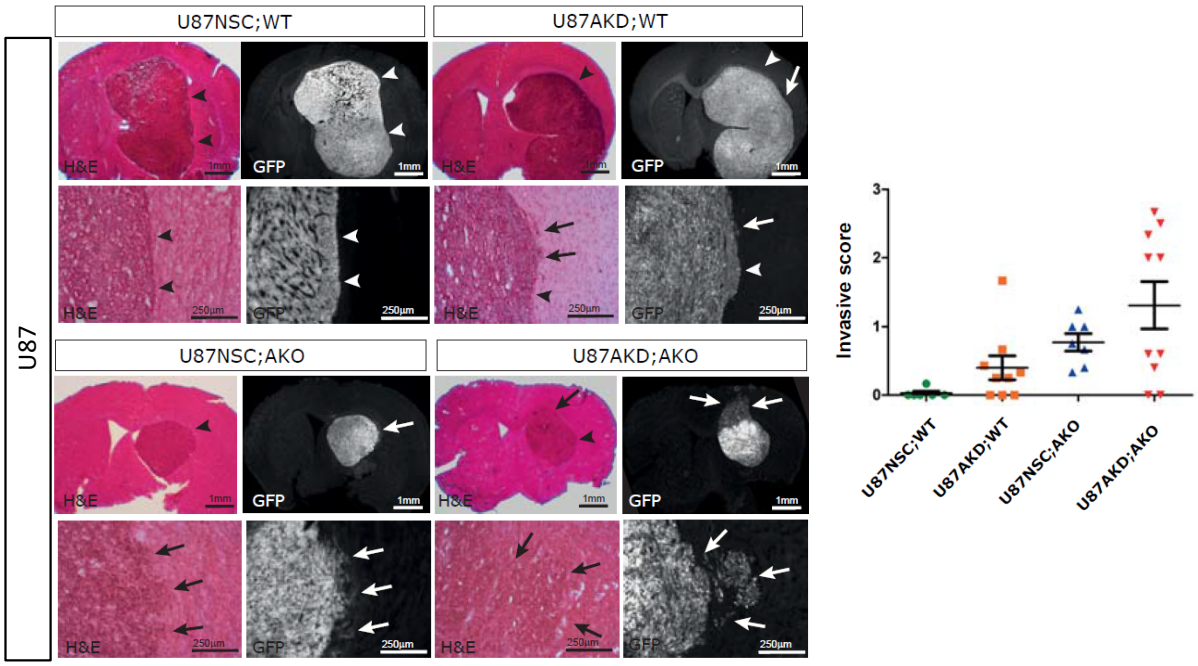

Figure 15: Invasion assays for the human GBM cell line U87. (A) The scheme shows the experimental set-up; (B) U87 APLN-KD and NSC cells invade at a comparable rate in control conditions with standard medium DMEM F12, n=13-14;17-20; analysis was performed with two-way ANOVA; (C) Top graph: U87 APLN-KD invade significantly more than NSC cells when exposed to an U87 MG sphere; two-way ANOVA n=4-9;3-6. Bottom graph: U87 NSCs exposed to a WT U87 MG sphere invade less, but not significantly, than in control conditions; Student's t-test, n=13;9; (D) Top graph: U87 APLN-KD cells show enhanced-invasive behavior when the peptide apelin-13 is added to the collagen mix; two-way ANOVA, n=15;15. Bottom graph: with the addition of exogenous apelin-13, U87 NSC cells invade less than in control conditions. Student's t-test; n= 13;15; (E) *In vivo* orthotopical implantation of U87 APLN-KD and NSC cells was performed: after scoring the GFP-positive cells for their invasiveness, we found that the U87 cells with APLN loss invaded more than the NSC cells, in accordance with my *in vitro* findings. Arrows indicate the tumor borders. One-way ANOVA with Newman Keuls post-hoc test; n=15, 15, 10, 13. Statistical significances: *p ≤ 0,05, **p ≤ 0,005, ***p ≤ 0,0005, scale bar on cell invasion assays = 250µm.

7.6.2 Apelin-13 enhances the invasion of the GBM14 APLN-KD cells

In a second set of experiments, I investigated the invasive ability of GBM14 cells using the same 3D-invasion assay (Figure 16A). First, I compared GBM14 APLN-KD and NSC cells in basal conditions (with standard DMEM F12 medium) and found no differences in their invasive behavior (Figure 16B). Next, I added a WT U87 MG sphere to each well in the same fashion illustrated in figure 15C, to provide an *in vitro* source of growth factors (APLN included), and detected a more invasive behavior in the GBM14 APLN-KD cells compared to the controls (Figure 16B). The same observation was made when the peptide apelin-13 was added to the collagen mix, instead of a WT U87 MG sphere (Figure 16C).

These findings correlate with the *in vitro* results on the U87 cells and the *in vivo* data presented in figure 10A.

Together, the invasion assays showed that, when exogenous factors including APLN are present, the invasion rate of the cells that had lost endogenous APLN expression significantly increases. Thus, the APLN-APLNR signaling not only regulates GBM angiogenesis *in vivo*, but it is also able to directly control GBM cell invasion.

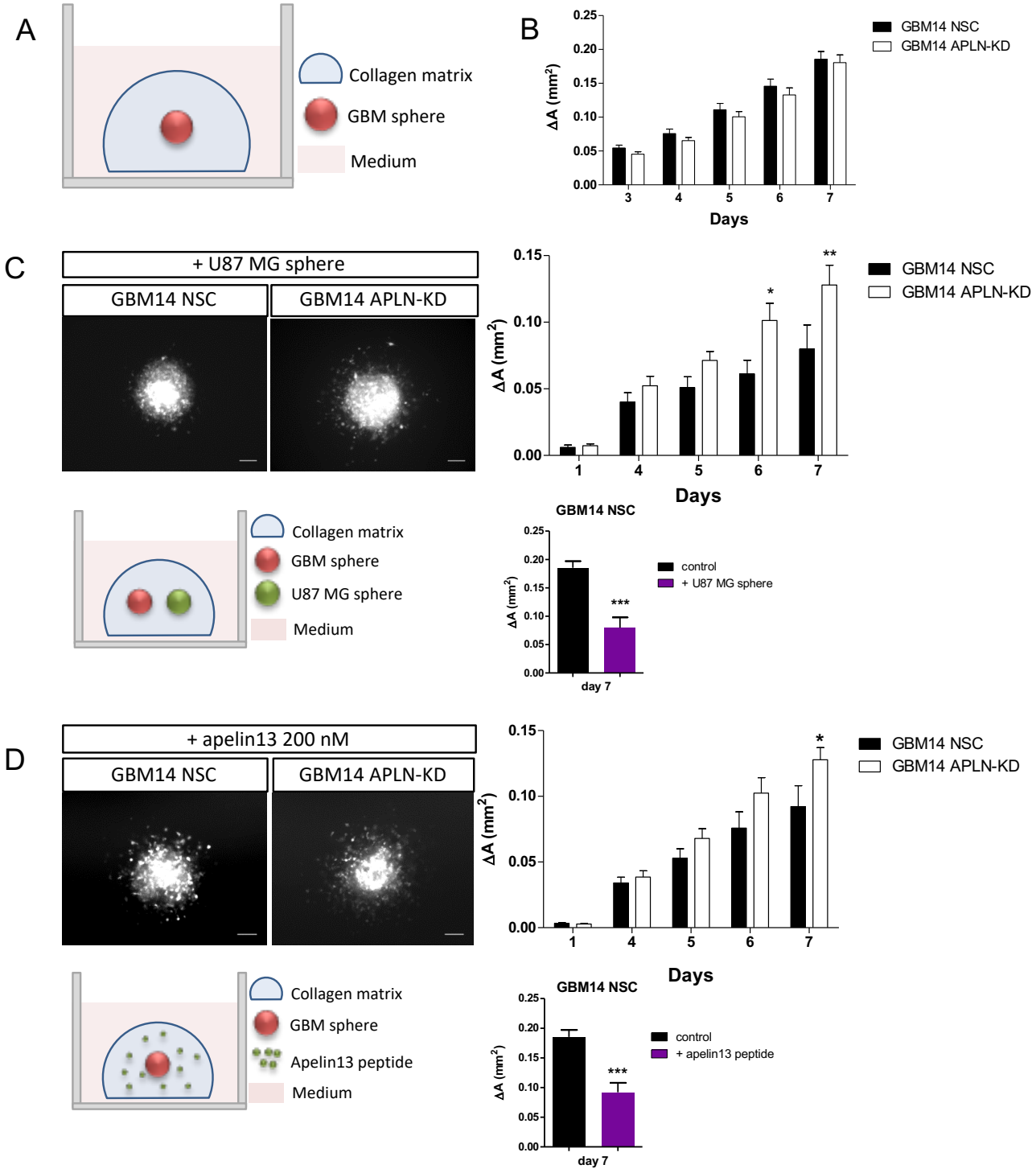

Figure 16: Invasion assays for the human primary GBM cells GBM14. (A) The scheme shows the experimental set-up; (B) GBM14 APLN-KD and NSC cells invade at a comparable rate in standard medium. Analysis was performed with two-way ANOVA, n=8;15; (C) Top graph: when a WT U87 MG sphere is added to the collagen mix, GBM14 APLN-KD cells invade significantly more than the controls; two-way ANOVA, n=5-7:7-9. The bottom graph shows that GBM14 NSC cells exposed to a WT U87 MG sphere invade less than in control conditions; Student's t-test, n=8;9; (D) Top graph: GBM14 APLN-KD cells show a more invasive behavior when the peptide apelin-13 is added to the collagen mix; two-way ANOVA, n=10;10-11. Similarly, the bottom graph shows that GBM14 NSC cells exposed to apelin-13 are less invasive than in control conditions; Student's t-test, n=15,10. Significances for two-way ANOVA and Student's t-test: *p ≤ 0,05, **p ≤ 0,005, ***p ≤ 0,0005, scale bar= 100µm.

7.6.3 APLNR blockade affects the invasion of GBM cells in vitro

To test if the invasion of the GBM cells was indeed APLNR-dependent, I created a receptor-blocking condition by adding the antagonistic peptide apelin-F13A [79] to the collagen matrix, in competition with the exogenous apelin-13 provided by a WT U87 MG sphere or by the addition of the apelin-13 peptide itself (Figure 17A). I tested this condition on the U87 APLN-KD cells, which had previously demonstrated the highest invasive ability *in vitro*, and observed that the addition of the apelin-F13A to an environment also enriched by the exogenous apelin peptide significantly decreased their invasive behavior (Figure 17B, C). However, this inhibitory effect was not detectable by applying the same conditions to the U87 NSC cells (Figure 17D), whose invasion on the contrary was inhibited by the addition of the apelin-F13A alone, without exogenous apelin-13 (Figure 17E). A possible explanation of this discrepancy may be the much lower invasive behavior observed in U87 NSC cells after the addition of the peptide apelin-13 (Figure 15D): thus, an even greater reduction might not be reached with the exposure to apelin-F13A.

Interestingly, the antagonistic peptide apelin-F13A added in competitive condition with apelin peptide, but not alone, was able to decrease the *in vitro* invasion of the GBM14 NSC cells (Figure 17F, G), in a similar fashion to the results obtained with U87 APLN-KD cells (Figure 17B).

Furthermore, the *in vivo* therapeutic treatment of GBM14 NSC tumors was performed: to observe the effect of the APLNR blockade on GBM growth *in vivo*, either apelin-F13A peptide or the artificial cerebrospinal fluid (aCSF) were infused intratumorally. The results obtained on tumor invasion correlated with the *in vitro* data collected on the GBM14 NSC cells and the addition of the apelin-F13A peptide was able to reduce tumor cell invasion (Figure 17H).

In the *in vivo* therapeutic approach, we also studied the effect of the intratumoral infusion of apelin-F13A on the growth of GBMs originated by the very invasive p53-KO PDGFB mouse cells. To verify the *in vitro* reproducibility of this experiment, I performed some invasion assays with the p53-KO PDGFB cells and the addition of exogenous apelin-13 and/or apelin-F13A. As shown in figure 17I and J, respectively, the *in vivo* and *in vitro* administration of apelin-F13A was able to significantly reduce tumor invasion. The addition of the peptide apelin-13 alone significantly enhances cell invasion, in comparison with the control conditions (Figure 17K).

In conclusion, the *in vitro* invasion assays demonstrated that endogenous APLN reduces GBM invasion through an autocrine APLN-APLNR signaling, that exogenous APLN enhances the invasive behavior of the GBM cells presenting a loss of endogenous APLN, and that the blockade of the APLNR with the inhibitory peptide apelin-F13A is able to attenuate, in some circumstances, the invasion of the GBM cells. Aside from the inhibition of tumor invasion, the *in vivo* study on the intratumoral infusion of apelin-F13A demonstrated a significant decrease of GBM angiogenesis too, in comparison to the aCSF-treated controls [147]. Given the promising results in decreasing tumor invasion *in vitro* and in the reduction of tumor invasion and angiogenesis obtained in the *in vivo* therapeutic approach, the blockade of the APLNR may be a beneficial strategy to treat some glioblastomas depending on their level of APLN and APLNR expression.

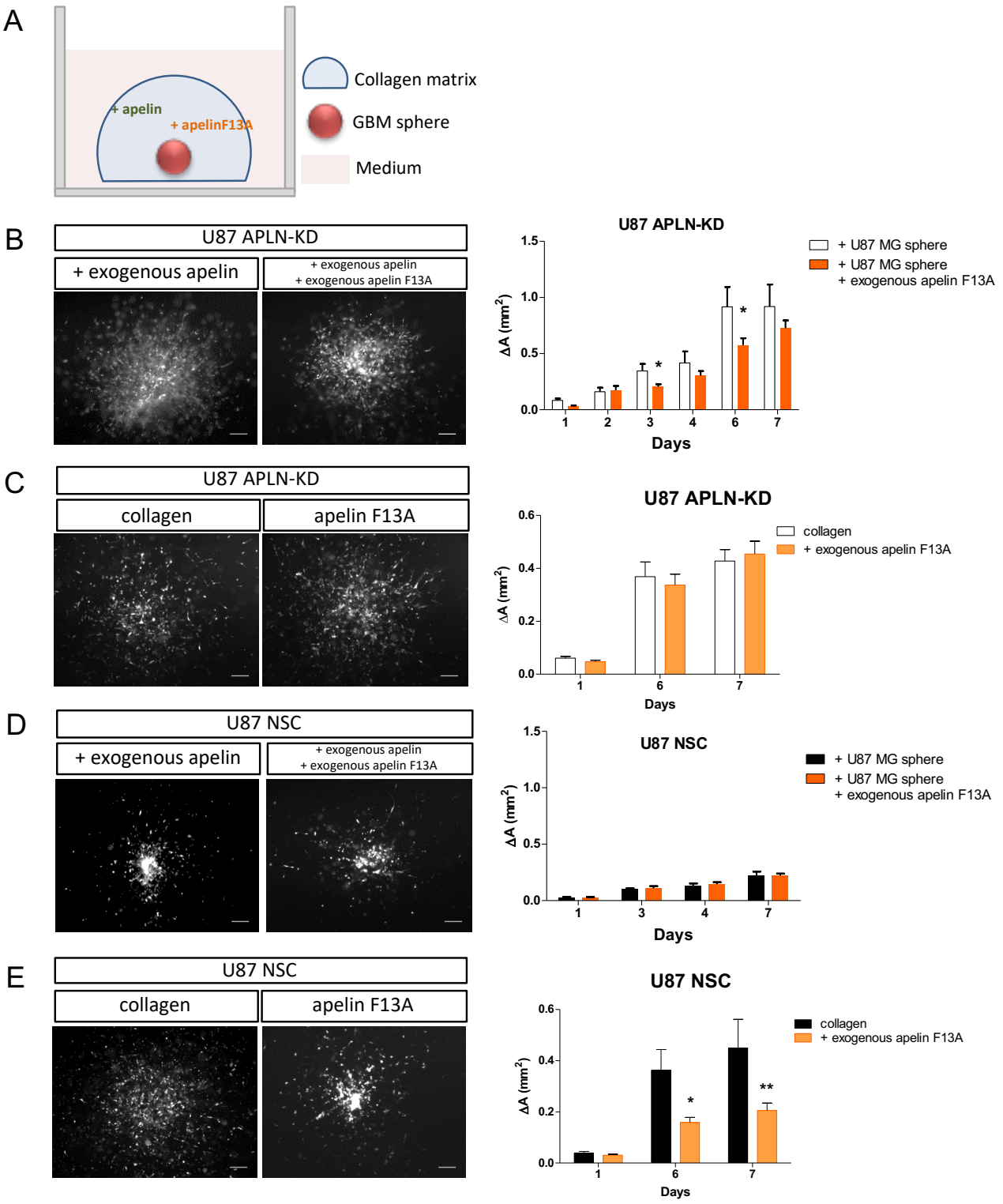

Figure 17: The blockade of the APLNR affects the invasion of the GBM cells *in vitro*. (A) Apelin-F13A was added to a collagen drop together with either a U87 MG sphere or apelin-13 peptide (B) Apelin-F13A negatively affects the invasive rate of U87 APLN-KD cells when added in competition with exogenous apelin-13 but (C) not when added alone. N=3-6;5-9 and n=17-20;19-21; (D) The effect of apelin-F13A on U87 NSC cells is the opposite: it does not alter cell invasion when added in competition with apelin-13, but (E) significantly reduces U87 NSC invasion when added alone. N=9;7 and n=13-14;14-15. Analysis was performed with two-way ANOVA, *p ≤ 0,05, **p ≤ 0,005, scale bar = 200µm.

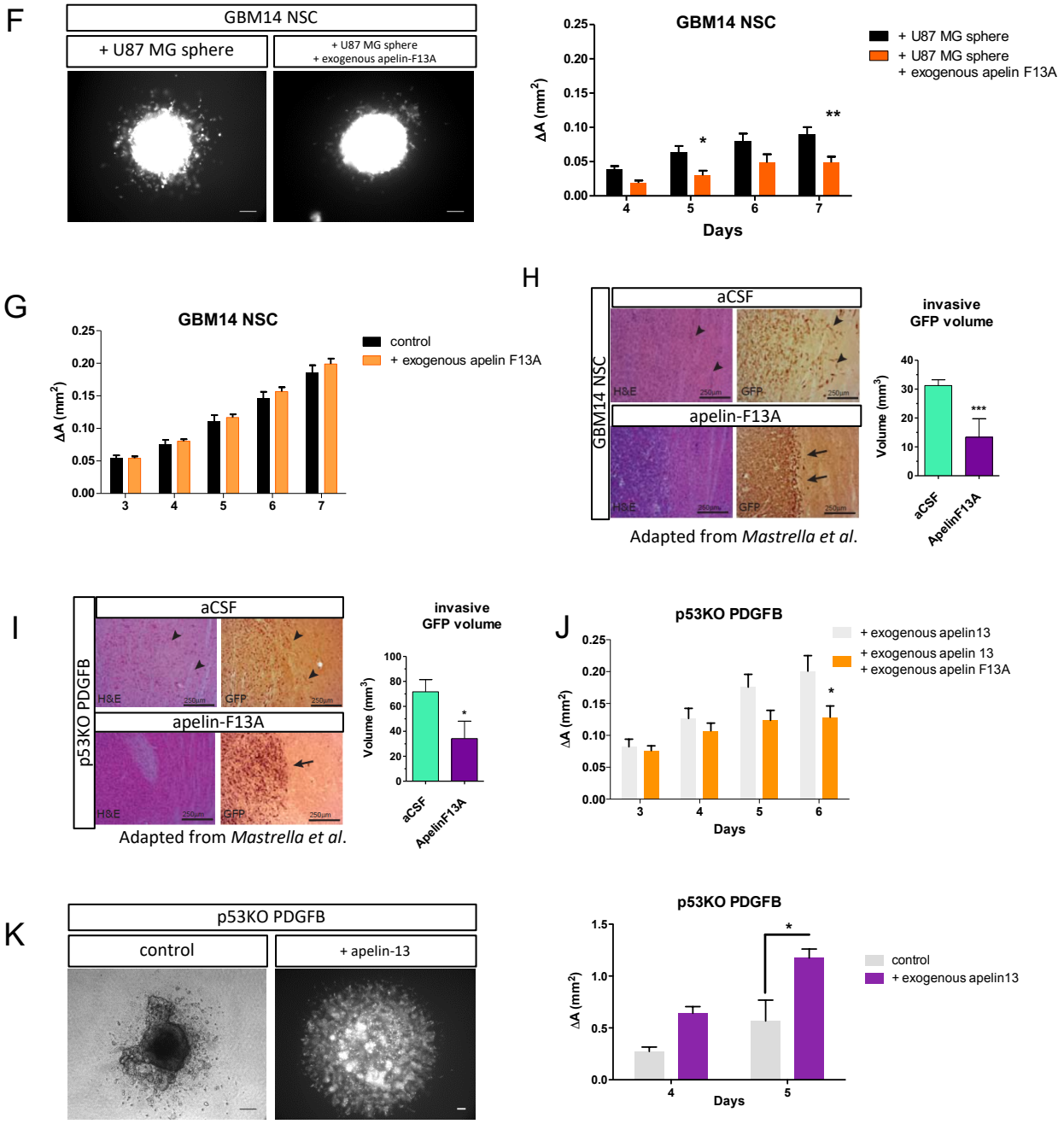

Figure 17 (continued): The blockade of the APLNR affects the invasion of the GBM cells *in vitro*. (F) GBM14 NSC invasion is reduced with the addition of apelin-F13A in competitive conditions, n=12;13; (G) The exposure of GBM14 NSC cells to apelin-F13A only does not affect their invasive behavior, n=8;12; (H) The *in vitro* results on the exposure of the GBM14 NSC cells to apelin-F13A recapitulate the *in vivo* results: when apelin-F13A is administered intratumorally, it significantly reduces GBM cell invasion. Figures from *Mastrella et al.* [147]; Student's t-test, n=6;5; (I) The intratumoral infusion of apelin-F13A *in vivo* reduces the invasive ability of the p53-KO PDGFB cells. Figures from *Mastrella et al.* [147]; Student's t-test, n= 8;6; (J) *In vitro*, the invasion of p53-KO PDGFB cells decreases after exposure to apelin-F13A and apelin-13; n=7; 4; (K) The administration of apelin-13 alone enhances p53-KO PDGFB cell invasion; n=14;14. Analysis was performed with two-way ANOVA, *p ≤ 0,05, **p ≤ 0,005, scale bar = 100μm.

7.6.4 The peptides apelin-13 and apelin-F13A show no effects on the proliferation of GBM cells

To test if the differences in GBM cell invasion that I observed *in vitro* could be due to an enhanced/decreased proliferation ability induced by the peptides apelin-13 and apelin-F13A, I investigated the proliferation of GBM14 and U87 cells *in vitro* with the MTT assay after the addition of apelin-13 or apelin-F13A 200 nM on the day of seeding. As shown in figure 18A and B, I did not find any significant effects on cell proliferation induced by the addition of apelin-13 or apelin-F13A on U87 and GBM14 APLN-KD cells. Figure 18B shows a slightly increased proliferation of the GBM14 NSC cells after exposure to apelin-F13A for 96 hours. However, the invasion rate of the GBM14 NSC cells after exposure to apelin-F13A showed no effect or a decreased ability to invade (Figure 17F, G) in comparison with the control conditions, hence confirming that the result on cell proliferation does not change the read-out of the cell invasion assays.

In conclusion, the observed differences in cell behavior presented in figures 15, 16, and 17 are attributable to a direct effect of the peptides on cell invasion and not to an induced change of cell proliferation.

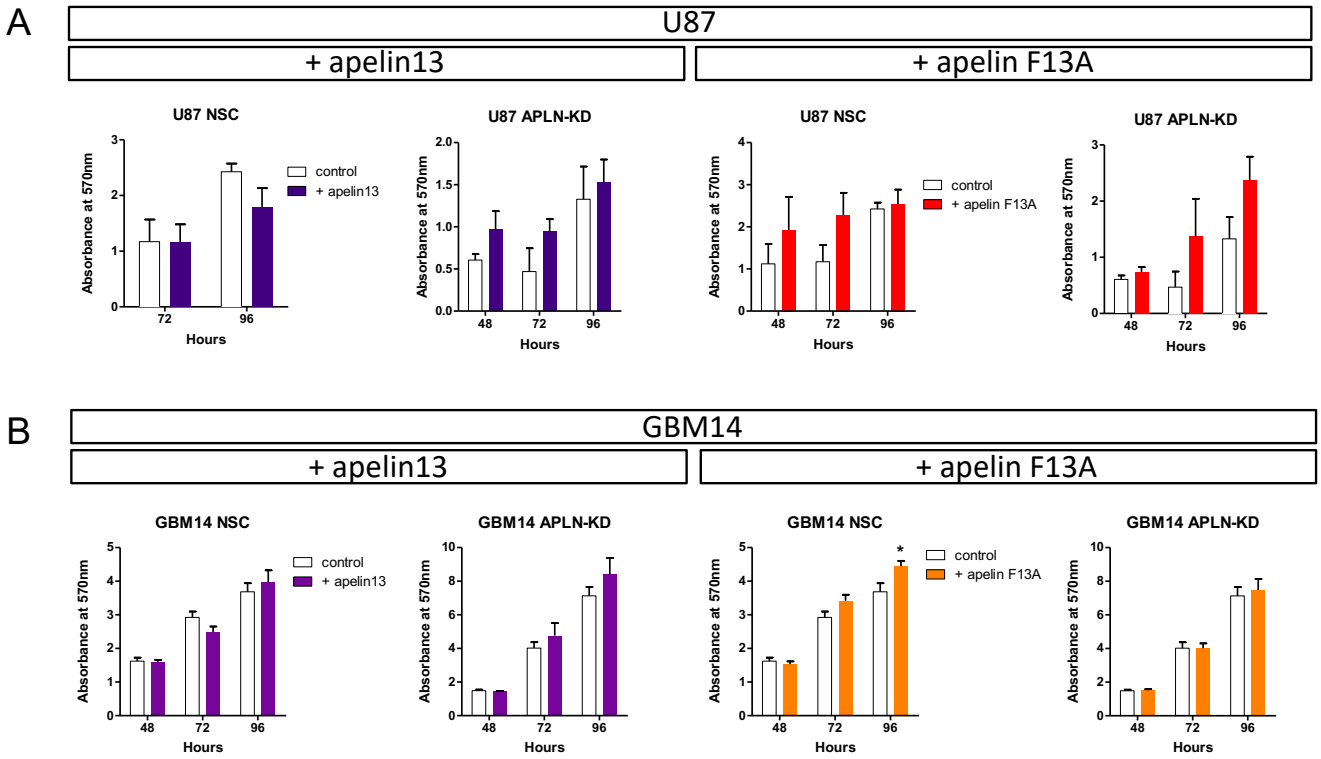

Figure 18: The effects of the peptides apelin-13 and apelin-F13A on the proliferation of GBM cells. (A) The MTT assays proves that the addition of apelin-13 or apelin-F13A 200nM does not affect U87 cell proliferation; (B) Similarly, no effect is shown by the addition of apelin-13 or apelin-F13A to GBM14 APLN-KD cells. Only the GBM14 NSC cells proliferate more when exposed to apelin-F13A for 96 hours. This result, however, is not reflected by an increased invasive behavior of these cells after the addition of apelin-F13A. 6 replicates/experiment; two-way ANOVA. *$p \leq 0{,}05$.

7.6.5 Generation and characterization of primary human and mouse GBM cells with APLNR loss

The above-mentioned *in vitro* and *in vivo* results on cell invasion after the blockade of APLNR hint to its possible role in the regulation of cell behavior. Thus, to test the specific role of the receptor in driving tumor invasion, I generated primary human GBM14 cells and mouse p53KO PDGFB cells depleted of APLNR expression (Figure 19). In the human cells, the loss of the receptor was obtained by transducing GBM14 cells with lentiviral vectors carrying a shRNA against the Hs APLNR mRNA. To obtain the most efficient knock-down I used two vectors, each carrying a shRNA (V3LHS_634451 or V3LHS_34449) targeting two different sequences on the human APLN gene. After cell recovery and selection with puromycin, I identified the construct V3LHS_634451 as the most promising for a significant reduction of APLNR expression compared to the parental group (Figure 19A). When verifying the specificity of the knock-down, I found that actin was not significantly affected in the APLNR-KD cells (Figure 19B). All the qPCR results were obtained by three independent experiment, with three replicates each. The cell proliferation assay, performed on a period of 4 days where the absorbances at 48, 72, and 96h were normalized on 24h, demonstrated that the APLNR-KD cells proliferated at the same rate as the NSC and control groups (Figure 19C). In addition, I observed that a constant viability was maintained by the three cell types over a period of 96 hours, with normalization of the absorbance of APLNR-KD and NSC cells on the parental groups (Figure 19D).

The generation of p53-KO PDGFB APLNR-KD and p53-KO PDGFB NSC cells was performed by cell transduction with lentiviral vectors carrying a shRNA against the Mm APLNR or a non-silencing shRNA, respectively. For the generation of the APLNR-KD cells, I tested two vectors (V2LMM_218787 and V3LMM_517943) carrying different shRNAs. Initially, the generation of the NSC cells was performed according to the standard protocol, by adding 500 µl of virus-containing medium. However, after cell recovery and selection with puromycin, I found that APLNR expression was significantly reduced in the control group, similarly to the reduction observed in the APLNR-KD cells (Figure 19E). In the attempt to find a concentration that would give a good control without side effects of infection, which may result in cell cytotoxicity and unspecific targeting [150], I tested different dilution of the NSC viral particles (Figure 19F). After this second transduction as well, the NSC cells showed reduced expression of the APLNR, independently from the concentration of the viral particles used. Both GAPDH and actin were tested as housekeeping genes (Figure 19E and F, respectively). Actin expression was not altered in the p53KO-PDGFB APLNR-KD cells

compared to the parental ones (Figure 19G). Before further characterization of the p53-KO PDGFB APLNR-KD cells, a reliable control group must be obtained.

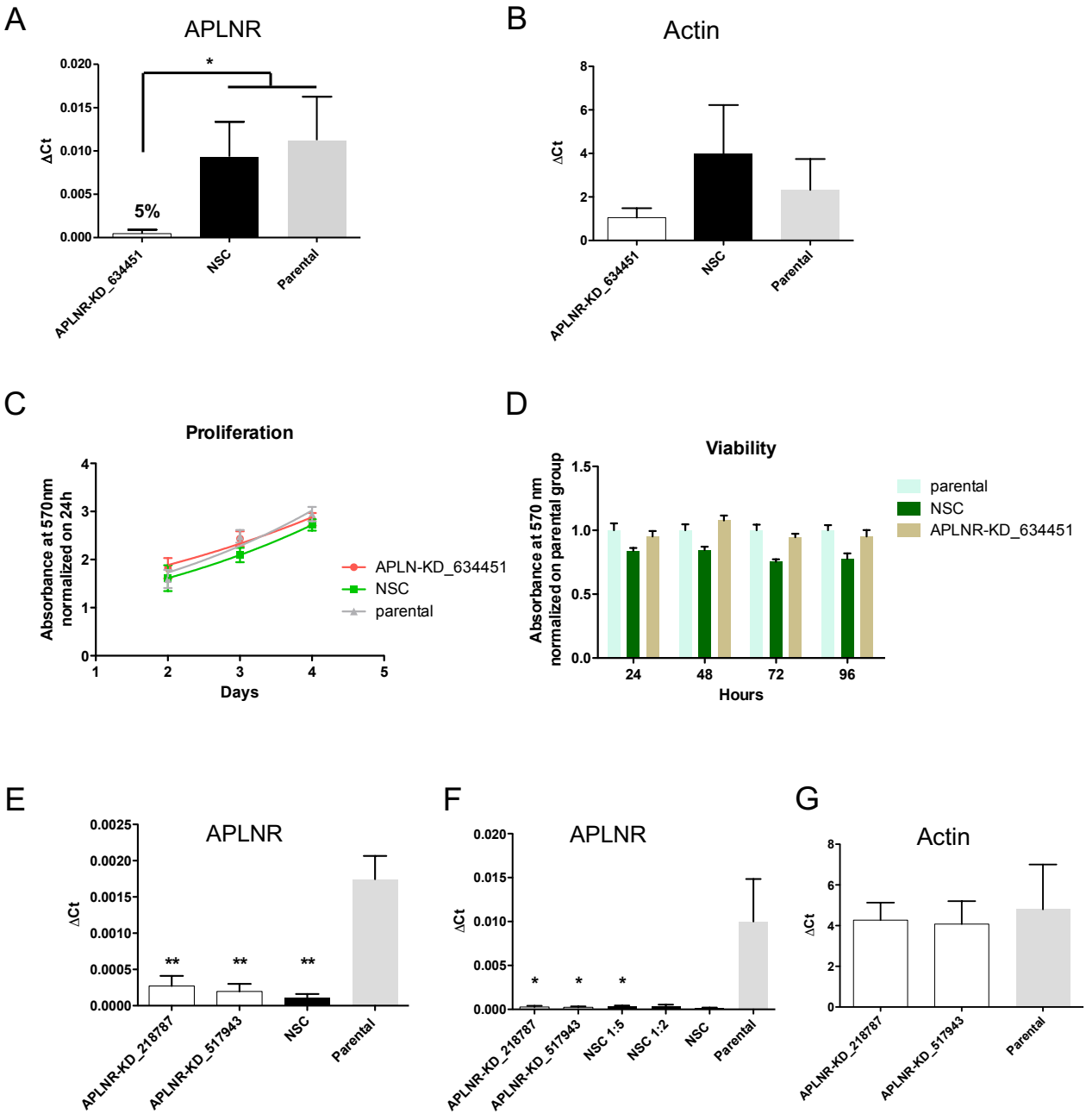

Figure 19: Generation and characterization of the primary human and mouse GBM cells with APLNR loss. (A) APLNR is knocked-down (to the 5%) in the GBM14 cells transduced with the V3LHS_634451 construct, in comparison with NSC and parental groups. HPRT1 was used as housekeeping gene. Student's t-test, *p ≤ 0,05, n=9; (B) Actin expression is not affected by the transduction. All results are normalized to HPRT1 and analyzed with one-way ANOVA with Newman Keuls post-hoc test, n=9; (C) No differences in proliferation are detectable with the MTT assay between the three groups. N= 18, two-way ANOVA; (D) Each group maintains a constant variability over a period of 4 days. N=18; (E) The two shRNA constructs used to transduce the p53-KO PDGFB cells show a successful knock-down of APLNR expression. This reduction, however, is also induced by the NSC shRNA; cells compared to the parental group with Student's t-test test, **p ≤ 0,005, n≥9; (F) Different dilutions of the NSC viral particles were tested; cells were compared to the parental group with Student' s t-test test, *p ≤ 0,05, n≥9. Both GAPDH (E) and actin (F) were assessed as housekeeping genes. (G) Cell transduction did not alter actin expression in p53-KO PDGFB APLNR-KD cells; normalization on GAPDH, one-way ANOVA with Newman Keuls post-hoc test, n= 9, 9, 6.

7.7 Apelin-13 peptides specifically target APLNR-expressing GBM14 cells

In collaboration with the research group of Prof. Dr. Ernst Wagner from the Department of Pharmacy of the LMU Munich, I tested the binding and fusion abilities of apelin-13-bound polyplexes carrying a Cy5-small interfering RNA (siRNA), and the binding and up-take abilities of apelin-13-GFP peptides in GBM14 cells. Polyplexes are an efficient method to deliver siRNAs and are obtained thanks to the interaction of the positively-charge polymers with the negatively-charged RNA [151].

The purposes of these experiments were to evaluate the specificity of the apelin-13 binding and to provide insights on the mechanism of apelin circulation in intracellular compartments. If functional, APLN could serve to specifically target APLNR-expressing cells for different therapeutic protocols. G protein-coupled receptors (GPCRs), which control numerous physiological processes, are often used as drug targets. The understanding of their intracellular re-distribution mechanisms is a key step for the generation of efficient therapeutic interventions [152, 153], as the receptor signaling can continue after its internalization [153, 154]. Immunofluorescence and spatial-intensity distribution analysis are used to evaluate the intracellular processes following receptor activation [152, 155].

To be able to visualize and quantify the processes of protein binding and up-take, I used two different methods: in the first model, I exposed the GBM14 cells to polyplexes presenting either apelin-13, apelin-F13A, apelin-13 scrambled (apelin-13scr), or no ligand, and carrying a Cy5-linked siRNA to visualize and quantify the binding and fusion events of the polyplexes to the cell membrane; in the second model, I exposed the GBM14 cells to either GFP-linked apelin-13, GFP-linked apelin-F13A, GFP-linked apelin-13scr, or to a condition of competition where both apelin-13 and GFP-linked apelin-13 were used. As positive control I plated the GFP-linked oligomer 728 [156]. For a better visualization, I co-stained the cells with the membrane marker WGA and the nuclear marker DAPI (Figure 20). The analysis of the images obtained by exposure to the Cy5-polyplexes revealed a high-level of unspecific binding and fusion, detectable when apelin-13scr-polyplxes or non-targeted polyplexes were used (Figure 20A). Even though both binding and up-take of apelin-13-polyplexes were higher than apelin-13scr-polyplexes, the processes were very well detectable in all the tested conditions. The discussions of these results with the group of Prof. Dr. Wagner confirmed possible unwanted unspecific binding of the polyplexes due to their lipid nature. Therefore, for the study of the specificity of

apelin-13 binding and up-take I decided to continue with the administration of the GFP-linked peptides described in the second model.

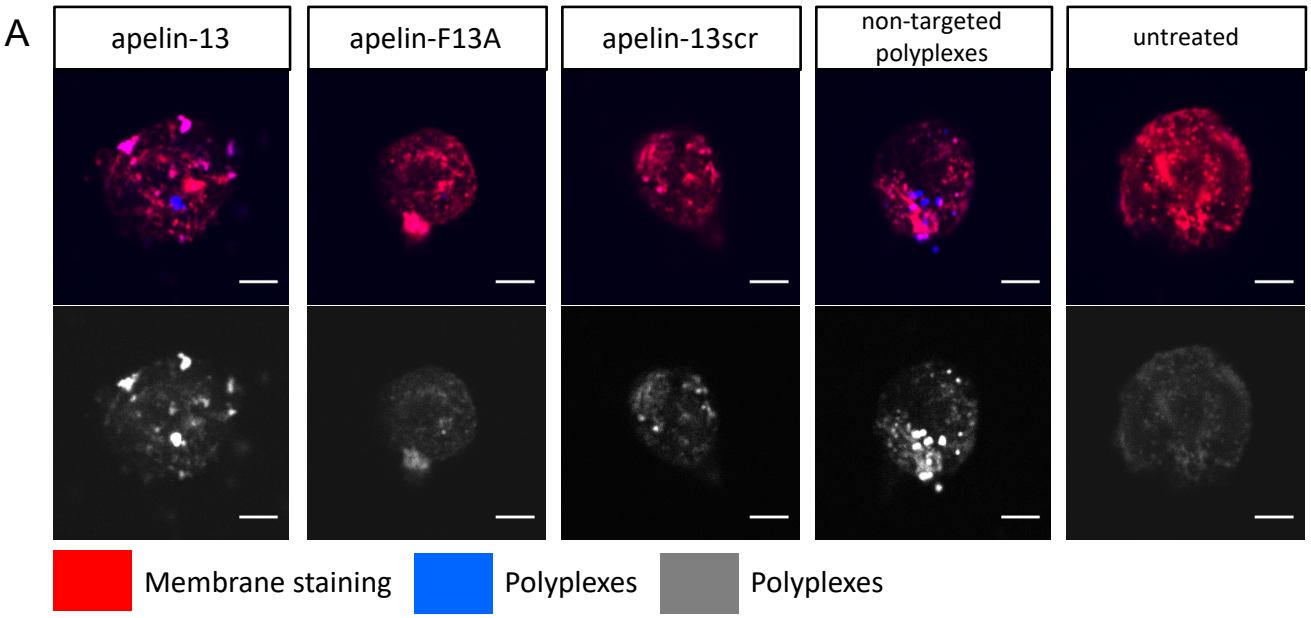

Figure 20: The specific up-take of apelin-13 peptides by GBM14 cells. (A) GBM14 cells exposed to Cy5-polyplexes: the lipid nature of the polyplexes causes unspecific binding observable with apelin-13scr-linked and non-targeted polyplexes. The membrane signal is in red. Scale bar = 10 µm.

The quantification of the number of cells presenting bound or up-taken GFP-apelin-13 was performed on 6 confocal pictures/condition taken at the level of the cell nucleus in the z-axis. As shown in figure 20B, GFP-apelin-13 specifically targeted the APLNR-expressing GBM14 cells leading to a significant higher number of GFP-positive cells in comparison to GFP-apelin-13scr (Figure 20B). GFP-apelin-F13A did not show any significant differences in binding and up-take abilities compared to GFP-apelin-13 (Figure 20B). Moreover, with the condition of competition I demonstrated that, not only the peptides GFP-apelin-13 specifically target the GBM14 cells, but the presence of highly-concentrated non-GFP linked apelin-13 is able to compete with GFP-apelin-13 and reduce its fluorescent signal, demonstrating once more its binding specificity (Figure 20B).

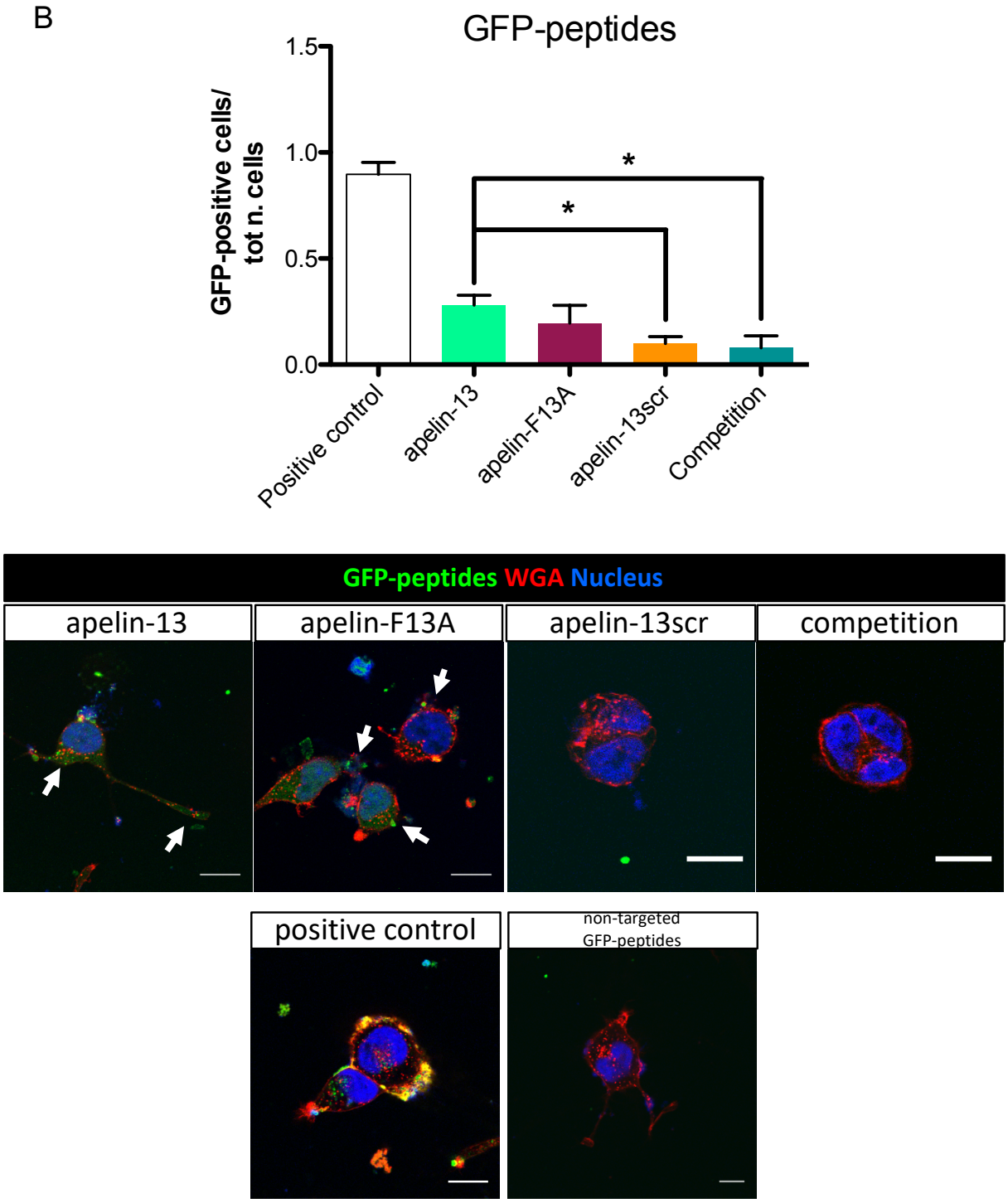

Figure 20 (continued): The specific up-take of apelin-13 peptides by GBM14 cells. (B) The quantification of GBM14 cells presenting GFP-fluorescence revealed a specificity of apelin-13 binding and up-take, in comparison to apelin-13scr and when administered in competition to non-GFP labelled apelin-13 peptide. Six stacks/condition were taken, and the central layer of each stack was quantified counting the number of cells presenting GFP fluorescence. One-way ANOVA with with Newman Keuls post-hoc test, *p ≤ 0,05; the enlargements show example of WGA-labelled cells (red) with a GFP-positive signal indicated by the arrows. Scale bar = 15 µm.

Interestingly, the observations at the confocal microscope showed that in the cells exposed to GFP-apelin-13 numerous intracellular vesicles were detectable, especially in the perinuclear region (visible in figure 20C). The green signal coming from apelin-13 sometimes merged with the red membrane marker, as shown in the enlargement of figure 20C, indicating the co-localization of apelin-13 with the intracellular vesicles. In addition, I observed many of these vesicles in the nuclear regions, where also a GFP-signal alone was detectable. The nuclear transport of vesicles that internalized apelin-13 together with its receptor APLNR would support the findings of others [157] on the nuclear trans-localization of APLNR and its intracellular redistribution in consequence to an APLN signaling, showing that the bound apelin-APLNR complex is transported as a whole.

C

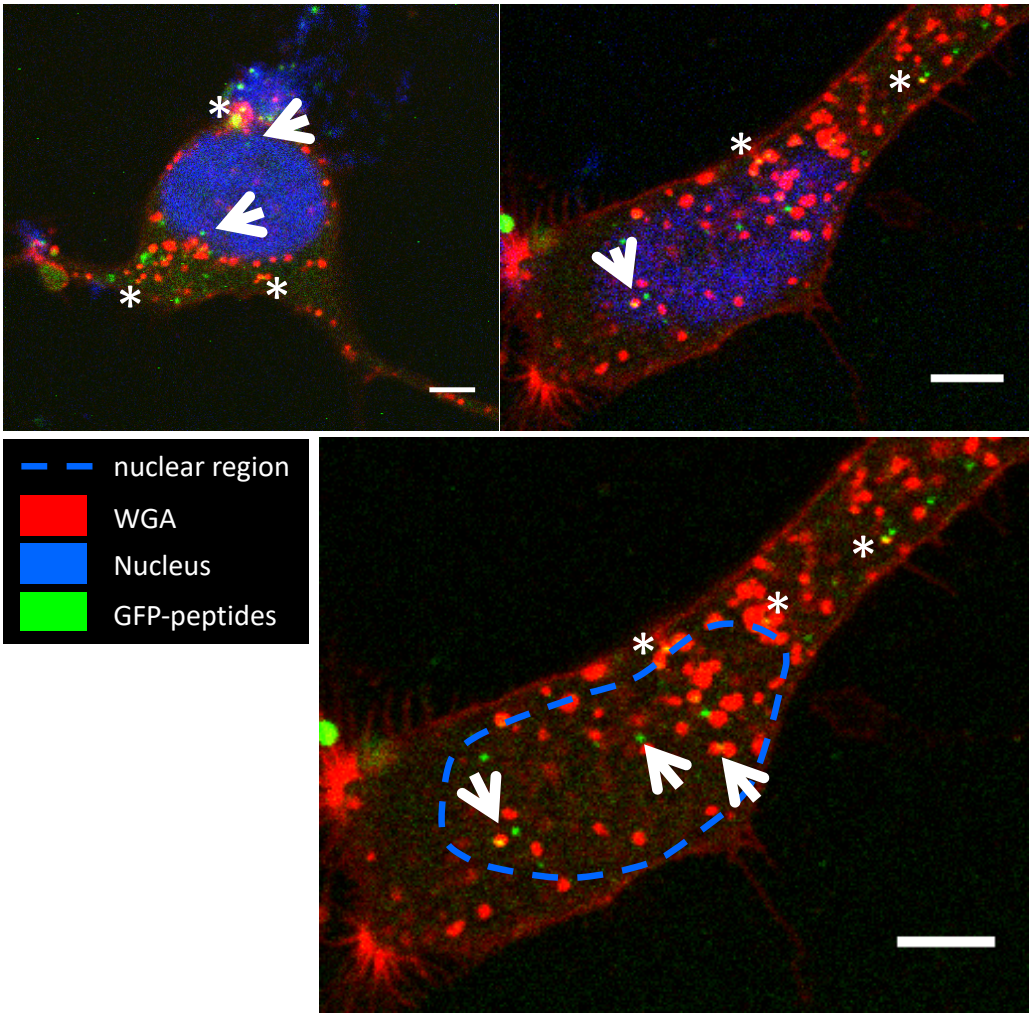

Figure 20 (continued): The specific up-take of apelin-13 peptides by GBM14 cells. (C) The enlargements show perinuclear and nuclear GFP-positive signal (arrows), sometimes in co-localization with the red membrane staining (asterisks), indicating an intracellular circulation of the internalized peptides. Scale bar = 5µm. All pictures were obtained at the confocal microscope.

Anti-angiogenic treatment of GBM

7.8 The therapeutic blockage of the VEGF signaling pathway in GBM affects the expression of APLN and APLNR

So far, the use of anti-angiogenic therapies targeting VEGF signaling for the treatment of GBMs did not show any long term benefits and improvements in patient OS [50]. GBM escapes the angiogenic blockade by up-regulating alternative chemokines involved in vessel formation or by switching to a more invasive phenotype [50-53, 56]. In addition, glioma-supporting cells release interleukins, cytokines, and growth factors that help tumor recurrence [126]. Thus, anti-angiogenic interventions alone cannot be successful unless a more-widespread targeting that considers multiple pathways of escape is applied.

In this project, I demonstrated that APLN and APLNR expression controls GBM angiogenic phenotype *in vivo* and that it has an additional role in driving *in vitro* GBM invasion. Therefore, I considered the possibility that the APLN-APLNR pathway would take part in GBM recurrence and invasion after the administration of anti-angiogenic therapies.

To assess this, I evaluated the expression status of APLN and APLNR after VEGF signaling blockade in three sets of samples belonging to different independent experiments where an anti-VEGFA antibody or a VEGFR-blocking small chemical compound had been used.

The first set of samples included patient samples obtained from tumor resections before and after the treatment with bevacizumab (Figure 21A). I extracted the RNA from these tissues and analyzed APLN and APLNR expression comparing it to the expression levels detected in two healthy brain samples. In the pre-treatment sample I found an up-regulated expression of both APLN and APLNR compared to the heathy brains, thus confirming a function of the pathway in the biology of GBM. APLN and APLNR expression was down-regulated after bevacizumab treatment indicating reduced tumor angiogenesis. However, APLN expression in the core sample after treatment remained higher in comparison to the healthy brains, indicating the persistent presence of tumor tissue.

The second set of samples available included mouse-derived GBM xenografts obtained from the RCAS/t-va model treated with a murine anti-VEGFA antibody [24, 158] (Figure 21B). Briefly, this model allows the reproduction of a GBM that "spontaneously" originates from neural precursor cells expressing the t-va receptor under a defined promoter when infected by the RCAS virus carrying an oncogene. The tumor generated reproduces the histological and pathological features of grade IV glioma. I isolated the RNA from 4 treated and 4 control

samples and analyzed the expression of APLN, APLNR, and KDR by qPCR (Figure 21B). While APLN and KDR expression were rather reduced after the administration of anti-VEGFA antibodies, APLNR was significantly upregulated in the treated mice compared to the controls. In this thesis I have previously demonstrated that a decreased APLN expression correlates with lower levels of tumor angiogenesis (Figure 8 and 10), while APLNR expression and activation may control tumor invasion (Figure 10, 13, and 17). Therefore, these findings on a decreased APLN expression and increased APLNR expression after treatment with anti-VEGFA antibodies support the decreased vessel area and increased tumor volume reported in the RCAS/t-va GBM model [24].

In the third set, samples were obtained from a subcutaneous tumor mouse model originated by the human GBM line U87 and treated with sunitinib and temozolomide to test new combinations of anti-angiogenic and chemotherapeutic compounds in GBMs [159] (Figure 21C). In the qPCR analysis of these samples I could distinguish between genes deriving from the tumor (human) or the microenvironment (mouse). APLN and APLNR expression in the tumor cells did not show any differences in any of the therapeutic regimens (sunitinib or temozolomide as monotherapy, sunitinib and temozolomide combined, and control). In the microenvironment, however, APLNR was significantly up-regulated when the combined treatment with sunitinib and temozolomide was administered (Figure 21C). The authors reported an increased vascular resistance with upregulation of alternative angiogenic factors as angiopoietin-1 and tie-1 as consequence of the combined treatment of sunitinib + temozolomide [159]. The unchanged expression of APLN in the tumor microenvironment is consistent with the observed resistance of the tumor vasculature, which is also supported by the presence of increased levels of APLNR in the brain parenchyma.

Taken together, these results obtained from three independent sets of experiments demonstrated that the expression of APLN and APLNR is affected by the therapeutic blockade of the VEGF signaling pathway. The synergistic effects of the blockade of VEGF signaling on the APLN-APLNR signaling shown in figure 21A could lead to a promising therapeutic efficacy of the anti-angiogenic treatments; however, as demonstrated in figure 21B and C, this is not always the case and the blockade of one angiogenic pathway may lead to unexpected adverse effects by enhancing tumor invasion or alternative angiogenic signaling. Thus, a more comprehensive understanding of all the mechanisms co-operating in the tumor microenvironment is crucial for an optimal anti-angiogenic intervention in GBM.

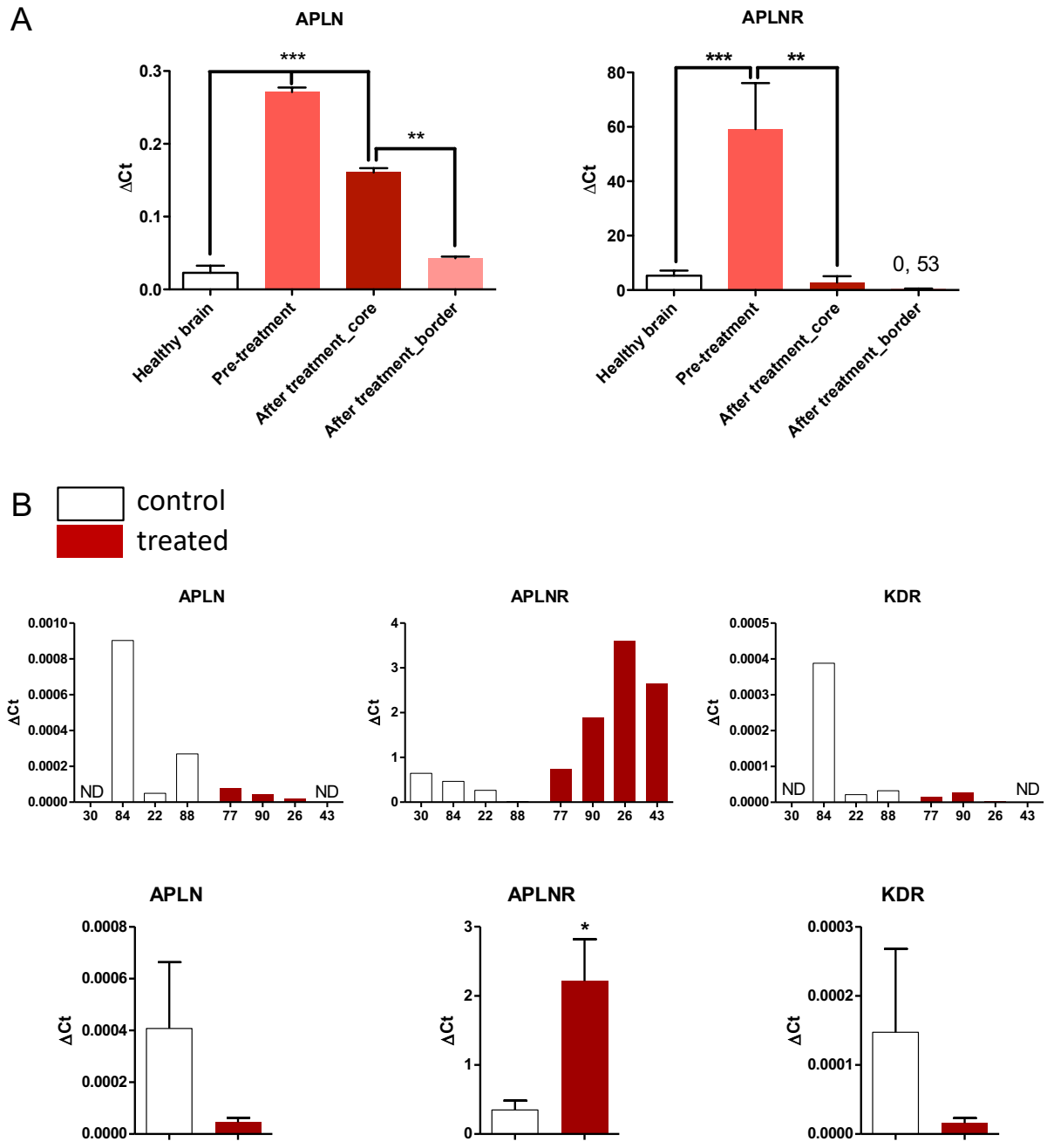

Figure 21: Analysis of APLN/APLNR expression after administration of anti-VEGF agents. (A) qPCR analysis of GBM samples resected before and after bevacizumab treatment. The pre-treatment sample shows upregulation of both APLN and APLNR expression in comparison to the healthy controls. APLN upregulation is maintained after the treatment while APLNR expression is down-regulated. Results are normalized on GAPDH, n=6; healthy brain n=12. One-way ANOVA with Newman Keuls post-hoc, **p ≤ 0,005, ***p ≤ 0,0005; (B) qPCR analysis of gene expression in GBM mouse xenografts obtained by the RCAS/t-va GBM model and treated with anti-VEGFA antibodies or a vehicle control. While APLN and KDR expression is lower after the treatment, APLNR expression is significantly higher in comparison to the vehicle-treated samples. The upper graphs show the single results, which are grouped and analyzed with Student's t-test in the bottom graphs; *p ≤ 0,05, 16 replicates.

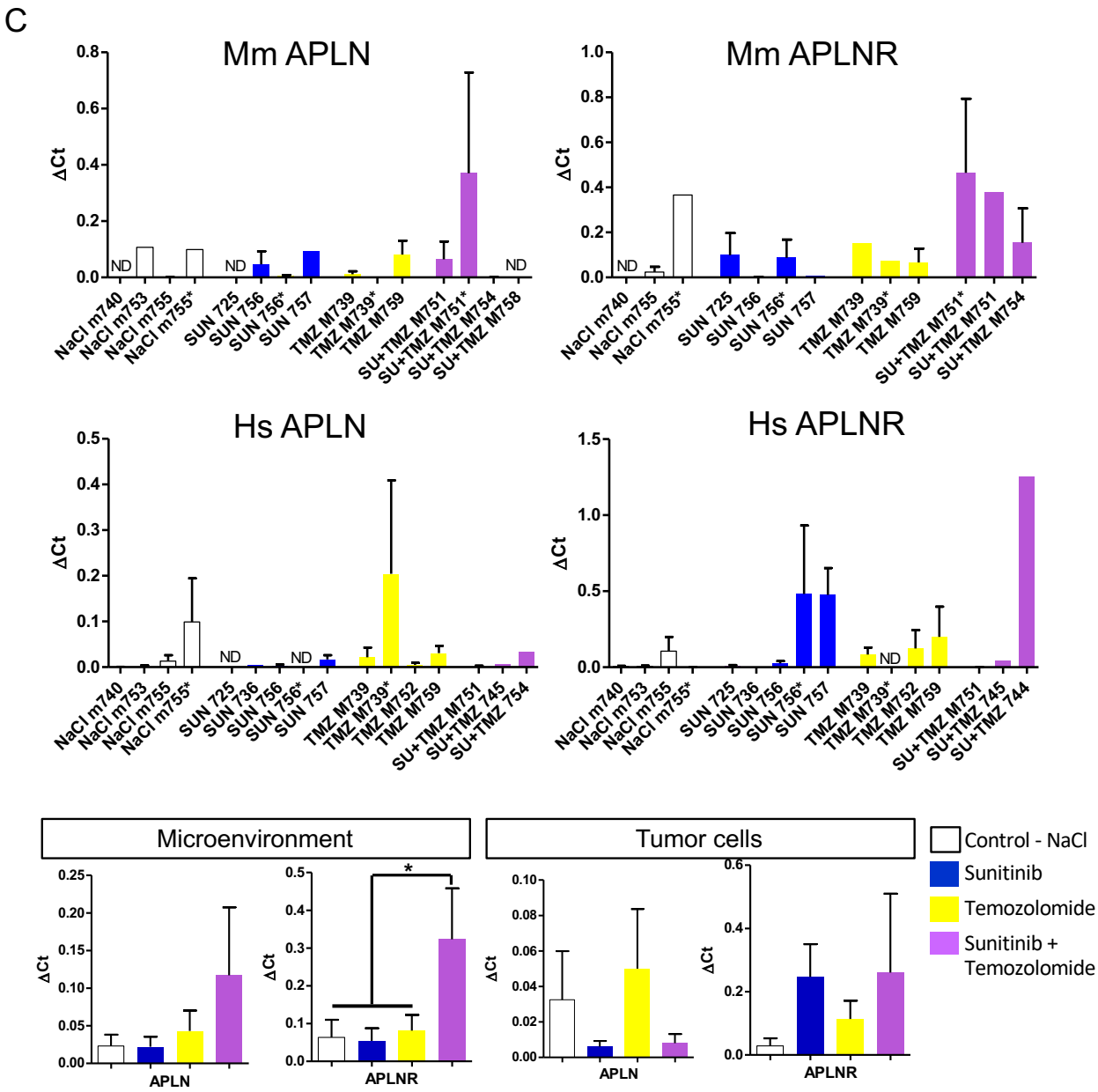

Figure 21 (continued): Analysis of APLN/APLNR expression after administration of anti-VEGF agents. (C) These samples derived from a subcutaneous U87 tumor model treated with a combination therapy of sunitinib and TMZ. The upper graphs show the single samples, which are group in the lower graphs. APLNR expression is upregulated in the tumor microenvironment after the combined treatment with sunitinib and temozolomide, in comparison to the treatment with a single-agent or the vehicle control. Results are normalized on GAPDH and analyzed with one-way ANOVA with Newman Keuls post-hoc test, *p ≤ 0,05, number of replicates ≥ 9.

The role of the APLN-APLNR signaling in the recruitment of GBM-associated myeloid cells

7.9 The infusion of the antagonistic peptide apelin-F13A does not reduce the intratumoral accumulation of myeloid cells in murine GBM models

Previous studies have demonstrated that OPN, which is strongly upregulated in GBM-associated myeloid cells, has a tumorigenic role [131, 160] and induces myeloid cells migration [131]. In addition, OPN expression is stimulated by different chemokines, APLN included [130, 132].

The role of TAMs in supporting tumor growth and angiogenesis has been extensively shown [61, 120, 121]. Our research group had already found by qPCR that cultured primary myeloid cells and the myeloid cell lines BV2 and J774 express APLNR, hence being directly responsive to APLN (data not shown). I verified by fluorescent staining the presence of APLNR in TAMs *in vivo*: as shown in figure 22A, myeloid cells were positive for iba1 (green) and APLNR (red). Thus, I confirmed that also *in vivo* myeloid cells express APLNR and may be responsive to its blockade or activation.

Therefore, to assess whether the *in vivo* blockade of APLNR may affect TAM migration to the tumor, I quantified the number of Iba1-positive cells [161] in two mouse models originated by the implantation of either GBM14 NSC or p53-KO PDGFB cells and treated with the intratumoral infusion of apelin-F13A for four and two weeks, respectively, before sacrifice. The administration of apelin-F13A was able to significantly reduce tumor volume, tumor angiogenesis, and tumor invasion in both GBM models *in vivo*.

The quantification of Iba1-positive cells was performed in three different areas per slice, which were defined in relation to their position compared to the tumor mass: intratumoral, in the tumor mass; peritumoral, lining the tumor mass; contralateral, in the tumor-free hemisphere.

In both models, when comparing the absolute densities of Iba1+ cells quantified in the intratumoral and peritumoral areas, I did not detect any significant differences between treatments (Figure 22B and C). Moreover, in the p53KO-PDGFB model a tendency for an increased number of intratumoral TAMs was found after administration of the APLNR antagonist (Figure 22C).

Therefore, even though the administration of apelin-F13A showed beneficial effects on the reduction of tumor growth, tumor vessel density, and tumor invasion, it did not decrease the

accumulation of TAMs, whose attraction instead tended to increase. In future experiments, the casual or consequential relation between TAM accumulation and the variation in tumor volume and invasion must be addressed by quantifying the number of Iba1-positive cells at different time points during *in vivo* tumor growth.

A

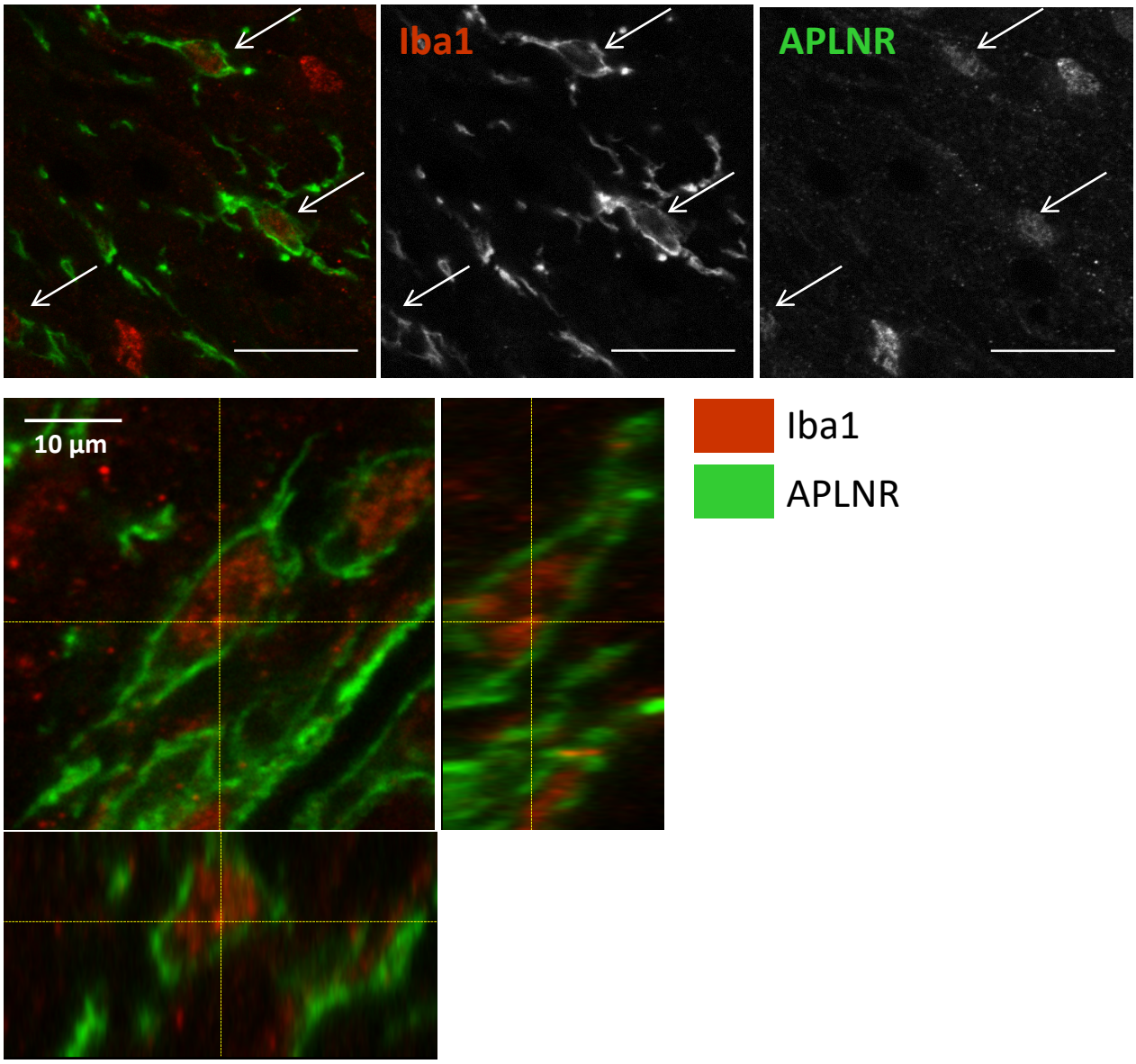

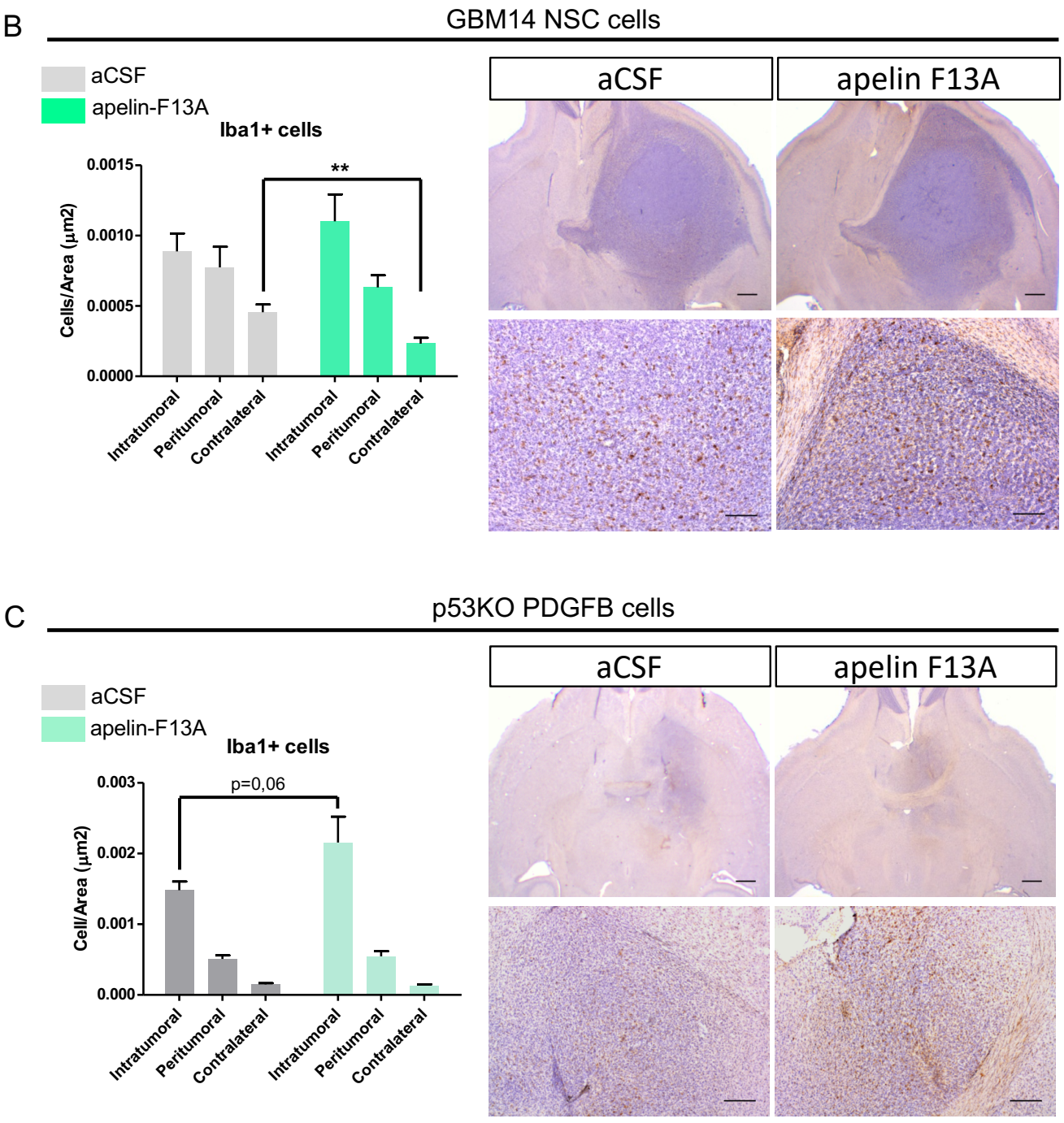

Figure 22: The effects of the blockade of the APLNR on TAMs accumulation. (A) Fluorescent immunostaining for the detection of iba1-positive cells (red) co-stained for APLNR (green). Scale bar in the overviews = 20µm; (B) Tumor-associated myeloid cells were quantified in the GBM14 NSC mouse model after 4 weeks of treatment with apelin-F13A. The graph shows that the accumulation of TAMs in the intratumoral compartment tends to increase, but not significantly, after administration of the antagonist apelin-F13A. The overview pictures show an example of the HRP staining (scale bar = 500µm), the close-ups show examples of the intratumoral staining (scale bar = 200µm). Student's t-test, n= 4;4; (C) Tumor-associated myeloid cells were quantified in the p53-KO PDGFB mouse model after 2 weeks of treatment with apelin-F13A. The graph shows that the accumulation of TAMs in the intratumoral compartment is almost significantly increased after administration of the antagonist apelin-F13A. The overview pictures show an example of the HRP staining (scale bar = 500µm), the close-ups show examples of the intratumoral staining (scale bar = 200µm). Student's t-test, n= 7;7

8. Discussion

In this doctorate thesis I present my research on the cellular expression analysis of the ligand APLN and its receptor APLNR, their histological characterization in human and mouse GBM specimens, and the role of the APLN-APLNR signaling pathway in driving GBM and myeloid cell invasion.

After a complete screening of the cultured primary GBM cells available in our laboratory, I confirmed that the expression of both ligand and receptor was detectable *in vitro* (Figure 4). The expression levels of APLN and APLNR did not correlate with any of the GBM subgroups; however, the p53 gene status had an impact on APLNR expression in our mouse GBM cells (see supplementary data figure 2): GBM cells deriving from p53-KO NPCs had a significantly higher expression of APLNR in comparison with the NPC-derived GBM cells transduced with a WT or mutated p53 construct. Notably, p53-KO PDGFB cells, which express high levels of APLNR and low levels of APLN compared to other NPCs, generate more invasive tumors than other mouse primary GBM cells when implanted *in vivo*.

Next, I confirmed the presence of ALPNR expression in WT NPCs *in vivo* by performing immunofluorescent staining on brain sections of a murine model where GFP is expressed under the nestin promoter, thus labelling the NPCs in the neurogenic niches (Figure 5). APLNR expression was detectable in some of the NPCs in the SVZ, hence indicating a possible physiological role of the APLN-APLNR signaling in controlling NPC proliferation and migration, and/or the vascular organization and maintenance of the neurogenic niche [162, 163]. As I demonstrated by qPCR and fluorescent staining, the NPCs of the SVZ express both APLN and APLNR, thus they may engage in autocrine/paracrine APLN signaling.

The histological characterization of APLN and APLNR by *in situ* hybridization in mouse GBM xenografts and in a human-derived GBM sample confirmed their expression *in vivo* in the tumor and their upregulation in the tumor microenvironment, in comparison to the tumor-free brain parenchyma (Figure 6 and 7). In addition, in the GBM mouse model, I confirmed the co-localization of APLN and VEGFA expression in the GBM tissue, as previously reported in human samples [55]. In the human GBM sample I observed differences in the expression patterns of ligand and receptor: APLN signal was particularly intense in the ECs of tumor vessels, while APLNR signal, even though detectable on vessels, was very strong in the tumor cells across the tumor mass. These differences in their distribution may indicate that ligand and receptor cover distinct roles in the processes of tumor growth and angiogenesis.

Next, I analyzed the expression of APLN and APLNR in a set of tumor samples that underwent the invasive-to-angiogenic switch [142, 143] (Figure 8): both ligand and receptor were up-regulated in the brain parenchyma of the xenografts that switched to an angiogenic phenotype, in comparison with the invasive ones. Thus, the expression of APLN and APLNR, in addition to be up-regulated in the GBM tissue, appeared to be in direct correlation with the level of GBM neo-angiogenesis.

To better understand the function of the APLN-APLNR signaling in the context of GBM growth and progression, I generated a new GBM model with APLN loss by transducing three different primary human GBM cell types with lentiviral particles carrying shRNA against the human APLN gene (Figure 9). The characterization of the transduced cells confirmed the specificity of the knock-down and their ability to proliferate at comparable levels to the control and parental groups. The analysis for stem cell frequency with the Extreme Limiting Dilution Analysis **(**ELDA) software [137] confirmed that the APLN-KD and the NSC cells presented no differences in their stem cell frequency. Similar findings on the maintenance of the stem cell frequency were reported in GBM cells with APLNR-loss-of-expression, when exposed to the standard culturing medium [164]. Therefore, according to my results and the results of others [164], APLN-APLNR signaling is not responsible for the preservation of the stemness pool *in vitro.* However, when added to the culturing medium, apelin was able to act as mitogen and increase the stem cell population of primary GBM cells, in comparison to the administration of supplement-free medium only [164].

The *in vivo* implantation of the generated APLN-KD cells was essential to evaluate the contribution of APLN, derived from the tumor or from the tumor microenvironment, to GBM angiogenesis and invasion: APLN-loss directly correlated with a reduction of GBM angiogenesis and indirectly correlated with GBM invasion [147] (Figure 10). Notably, the finding on reduced angiogenesis is in support of my results on the GBM rat model of angiogenic switch, where I demonstrated that the expression of both APLN and APLNR was up-regulated in the angiogenic GBM xenografts.

The *in vivo* experiments revealed that the implantation of APLN-KD cells into APLN-KO mice generated the most invasive tumors; the ability of the implanted GBM cells to invade an APLN-KO brain might rely not only on parallel molecular pathways that are activated in an environment with low APLN, but also on apela, which is another ligand of APLNR [165] and may be able to exert tumor invasion. The qPCR analysis performed on mouse APLN-WT, APLN-KO, and K14-APLN brain tissues confirmed the presence of apela in all three samples

(Figure 10). Further characterization is necessary to evaluate the role of apela-APLNR signaling in triggering GBM invasion.

By performing *in situ* hybridization for APLN and APLNR in patient-derived GBM samples, I demonstrated that APLN and APLNR are detectable with different distribution patterns throughout the tumor tissue (Figure 12 and 13). In particular, the ligand APLN was mainly upregulated in the tumor core cells in association with microvascular proliferations and in ECs; its receptor, although detectable in the tumor core in tumor cells and ECs, was strongly expressed on the tumor borders as well, where single invading tumor cells were present.

In conclusion, not only the staining patterns of APLN and APLNR differ at the cellular level (Figure 7), but they also have different distributions across the tumor tissue. These findings, together with the *in vivo* results on the effects of the modulation of the APLN-APLNR signaling on tumor invasion (Figure 10), indicate a possible additional role of the pathway, aside from being a driver of tumor angiogenesis.

In addition, to further characterize APLNR and verify its expression at the tumor margins in our mouse GBM models, I assessed its distribution by immunofluorescence in the xenografts generated by the implantation of different primary GFP-expressing GBM cells (Figure 14): the fluorescent signal of APLNR showed a characteristic pattern that differentiated the healthy brain parenchyma from the tumor mass. In particular, in the brain parenchyma, APLNR had a nuclear localization; on the contrary, the GBM mass showed an irregular and increased staining that was heterogenous between cell nucleus and cytoplasm. The peculiarity of the APLNR distribution in the tumor mass may indicate a different and specific role of the APLN-APLNR signaling in the context of GBM.

To gain deeper insights on the role of the APLN-APLNR pathway in driving tumor invasion, I tested the ability of the APLN-KD cells to invade *in vitro* (Figure 15 and 16). Confirming the *in vivo* results, I observed that the presence of an autocrine APLN-APLNR signaling reduced the invasive ability of the GBM-NSC cells, in comparison with the APLN-KD cells, when exposed to apelin-13 or to an U87 MG sphere.

The role of APLNR in driving a GBM invasive phenotype was confirmed *in vivo* and *in vitro* with the administration of its antagonistic peptide apelin-F13A (Figure 17). *In vivo,* the administration of apelin-F13A was able to reduce both cell invasion and tumor angiogenesis; *in vitro,* I observed a decreased invasion of the GBM cells tested when exposed to the antagonist alone or to the antagonist applied together with an external stimulus.

In conclusion, this demonstrates that the APLN-APLNR signaling drives tumor angiogenesis and invasion, and that the blockade of the receptor APLNR may be a promising strategy to inhibit GBM progression.

Next, in collaboration with the group of Prof. Dr. Wagner of the Department of Pharmacy, LMU Munich, I demonstrated that APLNR-expressing GBM14 cells are able to selectively bind and up-take GFP-linked apelin-13 in comparison to the peptide apelin-13scr, and that the level of the bound GFP-apelin-13 decreased when applied in competition with apelin-13 (Figure 20). This experiment demonstrated the possibility to specifically target APLNR-expressing cells (here GBM cells) by administration of the unaltered apelin-13 peptides.

Moreover, the confocal analysis of GBM14 cells exposed to GFP-apelin-13 demonstrated that the internalized peptides could undergo nuclear translocation in vesicular complexes, thus supporting observations of receptor intracellular circulation following stimulation with apelin-13. Further characterization of the up-take abilities of GBM cells will elucidate the possibilities to target APLNR-expressing tumor cells for therapeutic purposes.

Follow-up studies on the use of anti-angiogenic therapies reported an upregulation of alternative angiogenic signaling pathways [54, 56] and of an aggressive invasive behavior of the tumor [52]. After demonstrating a functional role of the APLN-APLNR pathway in GBM angiogenesis and invasion, I explored its expression after the administration of anti-angiogenic agents against VEGFA signaling (Figure 21). I analyzed three different sets of samples obtained by independent experiments where an anti-VEGFA antibody or a VEGFR-blocking small chemical compound had been used. In all samples, the blockade of VEGFA signaling resulted in unchanged or decreased expression of APLN in comparison with the pre-treatment or control groups. In two of these sets of samples, I observed a significant increase of APLNR expression in the tumor cells and in the tumor microenvironment, respectively, in response to the anti-VEGFA treatment (Figure 21B and C). The increased APLNR expression may indicate two different mechanism of tumor resistance to anti-angiogenic therapies: as I demonstrated in this thesis, APLNR expression is upregulated at the tumor invasive borders (Figueres 12 and 13) and its increased expression in tumor cells may correlate with an invasive behavior consequent to reduced tumor angiogenesis, as previously observed in other GBM mouse models treated with anti-VEGF signaling therapies [50-53]; on the other side, increased APLNR expression in the tumor microenvironment may indicate vascular resistance and the upregulation of angiogenic pathways alternative to VEGF. These scenarios are supported by the findings describing the two models of figure 21B and C respectively [24, 162].

An enhanced APLNR expression was not observed in one of the set of samples (Figure 21A), where APLNR expression in the tumor was strongly reduced after administration of bevacizumab, thus suggesting a better response to the therapy. This finding would not contradict the previous ones: a better outcome following anti-angiogenic treatments is observed in some patients and it is demonstrated to be subtype-dependent. In fact, previous results identified a correlation between tumor responsiveness to anti-angiogenic therapies and GBM subtype, where the proneural group is associated with a better survival outcome [49].

In addition to the up-regulation of alternative angiogenic pathways [54-57], it is believed that tumor-associated myeloid cells modulate the tumor response to anti-angiogenic therapies [166]. In this study I quantified the number of TAMs in two GBM mouse models therapeutically treated with apelin-F13A (Figure 22), which *in vivo* significantly reduced tumor volume, tumor invasion, and angiogenesis, in comparison with the control solution aCSF. The quantification of TAMs in both GBM models treated with the APLNR antagonist demonstrated that the number of tumor-infiltrating myeloid cells was unchanged, or rather tended to increase, in response to APLNR blockade. An anti-inflammatory function of the accumulated TAMs might explain the reduction in tumor volume observed in the treated animals, in comparison with controls [147]. On the other side, however, their accumulation may be due to an upregulation of attractive cues or the normalization window of tumor vessels [167] and, in a long-term perspective, translate into tumor rebound. All these are important questions that have to be addressed in future studies, by comparing the accumulation of TAMs at different stages post-implantation to follow the evolution of the process *in vivo* and verify its relation (as casual or consequential) with the variations in tumor volume.

In the present doctorate thesis, I did not only demonstrate that APLN and APLNR are overexpressed in GBM tissue, but also that the signaling and its manipulations have direct effects on tumor phenotype and on microenvironment, by regulating GBM angiogenesis and invasion.

The urgency for the discovery of efficient therapies for glioblastoma multiforme is a medical topic of high concern and numerous are the attempts (in phase I, II, and III trials) to target specific molecular pathways in combination with chemotherapy. Despite the efforts, a generalized successful strategy is not yet available and the standard regimen relies on the combined treatment of Temozolomide, radiotherapy, surgical resection, and bevacizumab, when approved [58, 168]. Unfortunately, this treatment does not give a long survival

expectancy and tumor generally recurs [169]. At more advanced stages of the disease, even though drugs extravasate in the brain parenchyma through a disrupted BBB [30], their delivery is not optimal due to the aberrant and leaky vasculature caused by an imbalanced angiogenic signaling instructed by the hypoxic regions of the tumor bulk [170]. The use of anti-angiogenic agents in a tumor such as glioblastoma multiforme, which is characterized by numerous microvascular proliferations and co-opts the existing vasculature to grow [31], seemed a promising strategy to inhibit its progression [167]. Unfortunately, the treatment of GBM with a single anti-angiogenic agent did not give the expected results [60], but, despite tumor resistance, it is thought that the inhibition of the unbalanced angiogenic signaling may have a positive effect by inducing a window of vessel normalization that allows a better delivery of other medical interventions [33].

In addition, mouse studies on GBM and in other well-vascularized tumors demonstrated an improved efficacy of the administration of a combination of anti-angiogenic drugs, which target parallel pathways like PIGF and ang-2, thus blocking possible alternative routes for tumor rebound [54, 171, 172]. In our study we demonstrated how the administration of the anti-VEGFR2 antibody DC101 in combination with apelin-F13A was able to significantly reduce both angiogenesis and invasion *in vivo*, in comparison to the single- or the control treatments [147]. Support comes from a recent study on the administration anti-angiogenic therapy in TMZ-resistant GBMs: the knock-down of the APLNR and its pharmacological blockade with a novel bi-cyclic peptide led to impaired *in vitro* and *in vivo* tumor growth and improved mouse survival [164].

To improve the outcome of GBM therapies the tumor subtype must be taken into consideration: the proneural and classical subtypes are characterized by the expression of numerous angiogenic markers and APLN expression level correlates with angiogenesis in both groups, but not in the mesenchymal one [147]. As previously discussed, the proneural GBM subtype gives a better outcome in patient OS after treatment with bevacizumab [49]. Therefore, further efforts must be done to identify and test different possible combined targets and a personalized therapy that takes into account the individual genetic variability [173].

8.1 Outlook

The promising results that I obtained in the study of APLN-APLNR signaling must be further extended in order to complete the characterization of the pathway and to fully understand the consequences of its targeting. The human primary GBM14 cells with APLNR loss, which I generated by transducing human primary GBM cells with lentiviral particles carrying shRNAs against the APLNR gene (Figure 19), will be an important tool to further explore the role of the receptor in driving tumor invasion, *in vivo* and *in vitro*. Moreover, the evaluation of the apela-APLNR signaling pathway as a possible alternative route for tumor rebound might open new unexpected strategies for GBM treatments.

In addition, the study of receptor internalization and re-distribution following apelin binding may lead to new information on a possible correlation between receptor localization and an observed cellular phenotype, e.g. tumor invasion. Furthermore, the specific targeting of tumor cells that overexpress APLNR might reveal alternative therapeutic approaches for the treatment of GBMs.

The differences in the expression pattern of APLNR between tumor mass and brain parenchyma could be investigated more in depth to be exploited as a future diagnostic tool to identify GBM tissue.

The results obtained in the GBM mouse models demonstrated that the blockade of the APLN-APLNR signaling is an efficient strategy to treat glioblastoma multiforme and to achieve not only a reduction of tumor angiogenesis, but also of tumor invasion. Notably, this double-efficiency in the reduction of both tumor processes is a fundamental step, which many current therapies fail to achieve, in order to avoid tumor rebound.

All in all, I believe that to pursue the study of the APLN-APLNR signaling will provide important insights to develop successful strategies for GBM treatment.

9. Supplementary Information

9.1 Quality assessment of extracted RNA

To verify the reliability of the Trizol RNA extraction method and the quality of the extracted RNA, I ran some of the samples with the Agilent Bioanalyzer, which interprets RNA integrity depending on its migration pattern. The analysis assigns an RNA integrity score (RIN) that goes from 0 (bad quality) to 10 (excellent quality) for a quantitative conclusion in relation to the shape of the bands displayed along the migration path. A concentration of the extracted RNA is also indicated to verify the quantification measured with the standard photometer method. As shown in the example of figure S1, the electropherogram presents numerous peaks of reference used by the software to calculate the RNA concentration, which is measured according to the total area covered by the migrated RNA. The two highest peaks on the right represent the ribosomal RNA 18s and 28s, respectively. On the left of those peaks, the so called "fast-region" contains small RNA-fragments, including digested RNA and the ribosomal subunits 5S, 5.8S. A signal in this region indicates low-quality RNA. Instead, a broad peak in the post-region or the detection of peaks in the inter-region may indicate genomic DNA contamination. The RIN value is obtained taking all these variables into consideration.

The elecropherogram of my cellular samples confirmed the good quality of the Trizol extraction protocol and of the extracted RNA (RIN between 9.4 and 9.7) (Figure S1). In the analyzed samples obtained from the cultured primary GBM cells (GBM13, GBM14, and NCH644) and the GBM cell line U87, very low RNA digestion and no genomic DNA contamination were detectable. The peaks of the ribosomal subunits 18s, 28s, and 5S were clearly depicted in the migration paths.

The RNA extraction was successfully performed and gave intact RNA to be further process for analysis by qPCR.

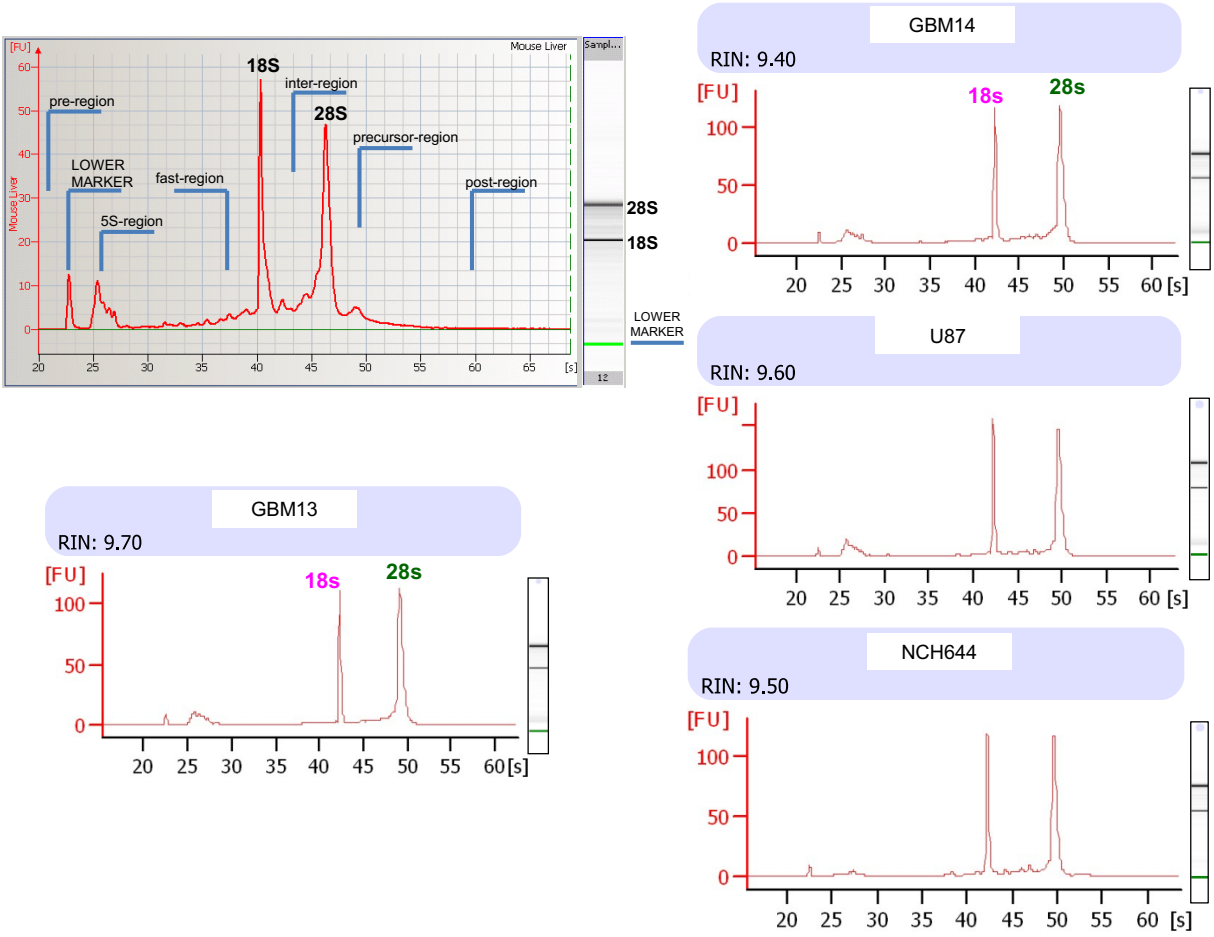

Figure S1: Quality assessment of the extracted RNA. On the top left, an illustrative example of an electropherogram of a high-quality RNA sample obtained with the Agilent Bioanalyzer. The high peaks in the center represent the ribosomal subunits 18s and 28s, respectively. On their left, the fast-region shows possible degraded RNA, while between the peaks and in post-region possible contamination with genomic DNA is displayed. The other four electropherograms represent the analysis of high-quality RNA (RINs between 9.4 and 9.7) that I extracted from four different cell pellets of the human primary GBM cells GBM13, GBM14, NCH644, and the human GBM cell line U87. The migration patterns do not show any RNA degradation or genomic DNA contamination, thus indicating that the extraction protocol was correctly performed and was a reliable method for gene expression analysis.

9.2 APLNR expression in p53-KO mouse GBM cells

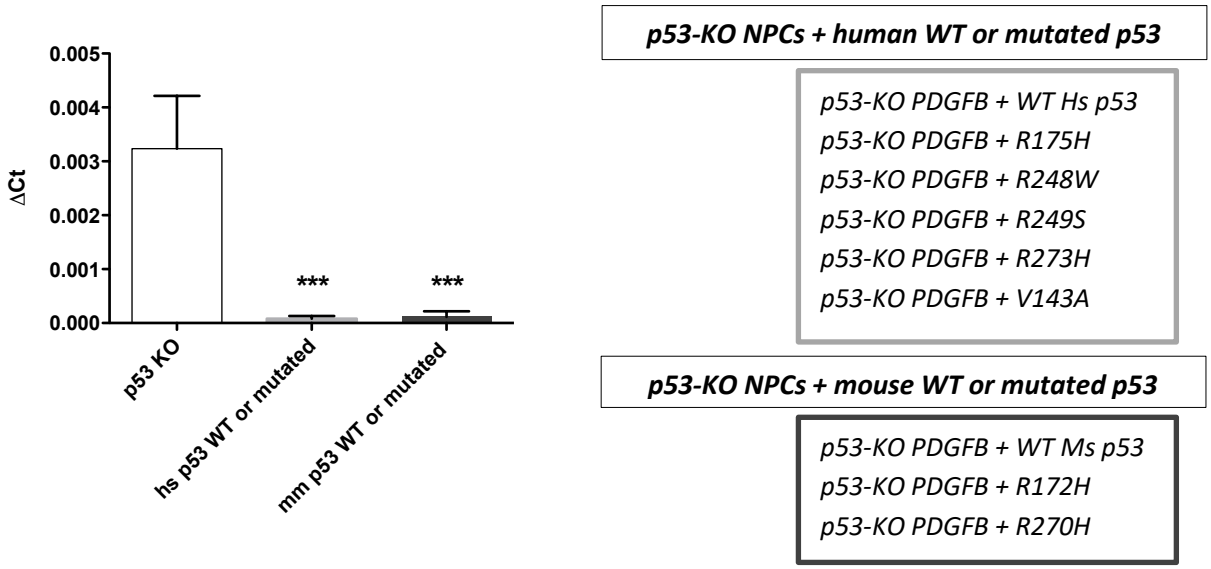

Figure S2: qPCR analysis of APLN and APLNR expression in primary GBM cultures. APLNR expression in mouse GBM cells shows a correlation with their p53 status: in tumor cells transduced with a mutated or WT p53 gene, APLNR expression is significantly low in comparison with the p53-KO GBM cells. Interestingly, GBM cells p53-KO *in vivo* originate higher invasive tumors in comparison to the other mouse GBM cell types represented in the two columns on the right. The graph is originated by pulling together the single data represented in figure 4D: the panels on the right list what mouse GBM cells are represented in the columns "hs p53 WT or mutated" and "mm p53 WT or mutated". All results were analyzed with one-way ANOVA with Newman Keuls post-hoc test, ***$p<0.0005$.GAPDH was used as housekeeping gene for all the experiments.

10. Acknowledgments

Prof. Dr. Hrvoje Miletic, from the University of Bergen, for the classification of the mouse xenografts used for qPCR analysis described at paragraph 7.2.

Prof. Dr. Ulrich Schüller, from the University of Hamburg, for the histological description of the GBM stereotactic sections used for *in situ* hybridization and described at paragraph *7.4.2*.

Prof. Dr. Ernst Wagner, from the Department of Pharmacy of the LMU Munich, for providing the polyplexes and GFP-peptides used in the apelin up-take experiments and described at paragraph *7.7.2*.

Mengzhou Hou, from Neurosurgical Research at the LMU Munich, for carrying on GBM cell implantations and the analysis of the *in vivo* results, described at paragraph *7.3.2* and *7.9*.

Dr. Roland Kälin and Prof. Dr. Rainer Glaß, from Neurosurgical Research at the LMU Munich, for the support and supervision provided to obtain the results described in this thesis.

11. References

1. Ostrom, Q.T., et al., *The epidemiology of glioma in adults: a "state of the science" review.* Neuro Oncol, 2014. **16**(7): p. 896-913.
2. Schwartzbaum, J.A., et al., *Epidemiology and molecular pathology of glioma.* Nat Clin Pract Neurol, 2006. **2**(9): p. 494-503; quiz 1 p following 516.
3. Ohgaki, H. and P. Kleihues, *Epidemiology and etiology of gliomas.* Acta Neuropathol, 2005. **109**(1): p. 93-108.
4. Louis, D.N., et al., *The 2016 World Health Organization Classification of Tumors of the Central Nervous System: a summary.* Acta Neuropathologica, 2016. **131**(6): p. 803-820.
5. von Neubeck, C., et al., *Glioblastoma multiforme: emerging treatments and stratification markers beyond new drugs.* Br J Radiol, 2015. **88**(1053): p. 20150354.
6. Das, S. and P.A. Marsden, *Angiogenesis in glioblastoma.* N Engl J Med, 2013. **369**(16): p. 1561-3.
7. Folkman, J., *Role of angiogenesis in tumor growth and metastasis.* Semin Oncol, 2002. **29**(6 Suppl 16): p. 15-8.
8. Mittal, K., J. Ebos, and B. Rini, *Angiogenesis and the tumor microenvironment: vascular endothelial growth factor and beyond.* Semin Oncol, 2014. **41**(2): p. 235-51.
9. Xu, R., D. Pisapia, and J.P. Greenfield, *Malignant Transformation in Glioma Steered by an Angiogenic Switch: Defining a Role for Bone Marrow-Derived Cells.* Cureus, 2016. **8**(1): p. e471.
10. Rafii, S. and D. Lyden, *Cancer. A few to flip the angiogenic switch.* Science, 2008. **319**(5860): p. 163-4.
11. Rees, J., et al., *Volumes and growth rates of untreated adult low-grade gliomas indicate risk of early malignant transformation.* Eur J Radiol, 2009. **72**(1): p. 54-64.
12. Wang, Q., et al., *Tumor Evolution of Glioma-Intrinsic Gene Expression Subtypes Associates with Immunological Changes in the Microenvironment.* Cancer Cell, 2017. **32**(1): p. 42-56 e6.
13. Brian J. Gill, e.a., *MRI-localized biopsies reveal subtype-specific differences in molecular and cellular composition at the margins of glioblastoma.* Proc Natl Acad Sci USA, 2014. **111**(34): p. 12550 - 12555.
14. Lin, N., et al., *Prevalence and clinicopathologic characteristics of the molecular subtypes in malignant glioma: a multi-institutional analysis of 941 cases.* PLoS One, 2014. **9**(4): p. e94871.
15. Verhaak, R.G., et al., *Integrated genomic analysis identifies clinically relevant subtypes of glioblastoma characterized by abnormalities in PDGFRA, IDH1, EGFR, and NF1.* Cancer Cell, 2010. **17**(1): p. 98-110.
16. Brennan, C.W., et al., *The somatic genomic landscape of glioblastoma.* Cell, 2013. **155**(2): p. 462-77.
17. Phillips, H.S., et al., *Molecular subclasses of high-grade glioma predict prognosis, delineate a pattern of disease progression, and resemble stages in neurogenesis.* Cancer Cell, 2006. **9**(3): p. 157-73.
18. Chen, J., R.M. McKay, and L.F. Parada, *Malignant glioma: lessons from genomics, mouse models, and stem cells.* Cell, 2012. **149**(1): p. 36-47.
19. Hambardzumyan, D., et al., *The role of microglia and macrophages in glioma maintenance and progression.* Nat Neurosci, 2016. **19**(1): p. 20-27.
20. See, A.P., et al., *The role of regulatory T cells and microglia in glioblastoma-associated immunosuppression.* J Neurooncol, 2015. **123**(3): p. 405-12.

21. Magana-Maldonado, R., et al., *Immunological Evasion in Glioblastoma.* Biomed Res Int, 2016. **2016**: p. 7487313.
22. Stupp, R., et al., *High-grade glioma: ESMO Clinical Practice Guidelines for diagnosis, treatment and follow-up.* Annals of Oncology, 2014. **25**.
23. Stupp, R., et al., *Optimal role of temozolomide in the treatment of malignant gliomas.* Curr Neurol Neurosci Rep, 2005. **5**(3): p. 198-206.
24. Pitter, K.L., et al., *Corticosteroids compromise survival in glioblastoma.* Brain, 2016. **139**(Pt 5): p. 1458-71.
25. Anton, K., et al., *Glioblastoma multiforme: overview of current treatment and future perspectives.* Hematol Oncol Clin North Am, 2012. **26**(4): p. 825-853.
26. Oh, J., et al., *Glioblastoma: patterns of recurrence and efficacy of salvage treatments.* Can J Neurol Sci, 2011. **38**(4): p. 621-5.
27. Mangiola, A., et al., *Invasive tumor cells and prognosis in a selected population of patients with glioblastoma multiforme.* Cancer, 2008. **113**(4): p. 841-6.
28. Carmeliet, P., *Angiogenesis in life, disease and medicine.* Nature, 2005. **438**(7070): p. 932-6.
29. Bergers, G. and L.E. Benjamin, *Tumorigenesis and the angiogenic switch.* Nat Rev Cancer, 2003. **3**(6): p. 401-10.
30. Jain, R.K., et al., *Angiogenesis in brain tumours.* Nat Rev Neurosci, 2007. **8**(8): p. 610-22.
31. Gerstner, E.R. and T.T. Batchelor, *Antiangiogenic therapy for glioblastoma.* Cancer J, 2012. **18**(1): p. 45-50.
32. Butler, J.M., H. Kobayashi, and S. Rafii, *Instructive role of the vascular niche in promoting tumour growth and tissue repair by angiocrine factors.* Nat Rev Cancer, 2010. **10**(2): p. 138-46.
33. Goel, S., A.H. Wong, and R.K. Jain, *Vascular normalization as a therapeutic strategy for malignant and nonmalignant disease.* Cold Spring Harb Perspect Med, 2012. **2**(3): p. a006486.
34. Jain, R.K., *Normalization of tumor vasculature: an emerging concept in antiangiogenic therapy.* Science, 2005. **307**(5706): p. 58-62.
35. Deeken, J.F. and W. Loscher, *The blood-brain barrier and cancer: transporters, treatment, and Trojan horses.* Clin Cancer Res, 2007. **13**(6): p. 1663-74.
36. Dubois, L.G., et al., *Gliomas and the vascular fragility of the blood brain barrier.* Front Cell Neurosci, 2014. **8**: p. 418.
37. Carmeliet, P., *Angiogenesis in health and disease.* Nat Med, 2003. **9**(6): p. 653-60.
38. Batchelor, T.T., et al., *Antiangiogenic therapy for glioblastoma: current status and future prospects.* Clin Cancer Res, 2014. **20**(22): p. 5612-9.
39. Gilbert, M.R., *Antiangiogenic Therapy for Glioblastoma: Complex Biology and Complicated Results.* J Clin Oncol, 2016. **34**(14): p. 1567-9.
40. Carmeliet P, J.R., *Molecular mechanisms and clinical application of angiogenesis.* Nature, 2011. **473**(7347): p. 298-307.
41. Plate KH, B.G., Weich HA, Risau W., *Vascular endothelial growth factor is a potential tumour angiogenesis factor in human gliomas in vivo.* Nature, 1992. **359**((6398)): p. 845-848.
42. Shweiki D, I.A., Soffer D, Keshet E., *Vascular endothelial growth factor induced by hypoxia may mediate hypoxia-initiated angiogenesis.* Nature, 1992. **359**(6398): p. 843-845.
43. Jayson, G.C., et al., *Antiangiogenic therapy in oncology: current status and future directions.* Lancet, 2016. **388**(10043): p. 518-29.
44. Gil-Gil, M.J., et al., *Bevacizumab for the treatment of glioblastoma.* Clin Med Insights Oncol, 2013. **7**: p. 123-35.

45. Cohen, M.H., et al., *FDA drug approval summary: bevacizumab (Avastin) as treatment of recurrent glioblastoma multiforme.* Oncologist, 2009. **14**(11): p. 1131-8.
46. Chinot, O.L., et al., *Bevacizumab plus radiotherapy-temozolomide for newly diagnosed glioblastoma.* N Engl J Med, 2014. **370**(8): p. 709-22.
47. *ClinicalTrials.gov*.
48. Neyns, B., et al., *Phase II study of sunitinib malate in patients with recurrent high-grade glioma.* J Neurooncol, 2011. **103**(3): p. 491-501.
49. Sandmann, T., et al., *Patients With Proneural Glioblastoma May Derive Overall Survival Benefit From the Addition of Bevacizumab to First-Line Radiotherapy and Temozolomide: Retrospective Analysis of the AVAglio Trial.* J Clin Oncol, 2015. **33**(25): p. 2735-44.
50. Ebos, J.M. and R.S. Kerbel, *Antiangiogenic therapy: impact on invasion, disease progression, and metastasis.* Nat Rev Clin Oncol, 2011. **8**(4): p. 210-21.
51. Piao, Y., et al., *Acquired resistance to anti-VEGF therapy in glioblastoma is associated with a mesenchymal transition.* Clin Cancer Res, 2013. **19**(16): p. 4392-403.
52. Paez-Ribes, M., et al., *Antiangiogenic therapy elicits malignant progression of tumors to increased local invasion and distant metastasis.* Cancer Cell, 2009. **15**(3): p. 220-31.
53. Ebos, J.M., et al., *Accelerated metastasis after short-term treatment with a potent inhibitor of tumor angiogenesis.* Cancer Cell, 2009. **15**(3): p. 232-9.
54. Scholz, A., et al., *Endothelial cell-derived angiopoietin-2 is a therapeutic target in treatment-naive and bevacizumab-resistant glioblastoma.* EMBO Mol Med, 2016. **8**(1): p. 39-57.
55. Kalin, R.E., et al., *Paracrine and autocrine mechanisms of apelin signaling govern embryonic and tumor angiogenesis.* Dev Biol, 2007. **305**(2): p. 599-614.
56. Jain, R.K., et al., *Biomarkers of response and resistance to antiangiogenic therapy.* Nat Rev Clin Oncol, 2009. **6**(6): p. 327-38.
57. Fischer, C., et al., *Anti-PlGF inhibits growth of VEGF(R)-inhibitor-resistant tumors without affecting healthy vessels.* Cell, 2007. **131**(3): p. 463-475.
58. Seystahl, K., W. Wick, and M. Weller, *Therapeutic options in recurrent glioblastoma--An update.* Crit Rev Oncol Hematol, 2016. **99**: p. 389-408.
59. Lamszus, K., et al., *Inhibition of glioblastoma angiogenesis and invasion by combined treatments directed against vascular endothelial growth factor receptor-2, epidermal growth factor receptor, and vascular endothelial-cadherin.* Clin Cancer Res, 2005. **11**(13): p. 4934-40.
60. Ferrara, N., *Pathways mediating VEGF-independent tumor angiogenesis.* Cytokine Growth Factor Rev, 2010. **21**(1): p. 21-6.
61. Lu-Emerson, C., et al., *Increase in tumor-associated macrophages after antiangiogenic therapy is associated with poor survival among patients with recurrent glioblastoma.* Neuro Oncol, 2013. **15**(8): p. 1079-87.
62. Rivera, L.B. and G. Bergers, *Intertwined regulation of angiogenesis and immunity by myeloid cells.* Trends Immunol, 2015. **36**(4): p. 240-9.
63. Hambardzumyan, D., D.H. Gutmann, and H. Kettenmann, *The role of microglia and macrophages in glioma maintenance and progression.* Nat Neurosci, 2016. **19**(1): p. 20-7.
64. Pitkin, S.L., et al., *International Union of Basic and Clinical Pharmacology. LXXIV. Apelin receptor nomenclature, distribution, pharmacology, and function.* Pharmacol Rev, 2010. **62**(3): p. 331-42.
65. Lee, D.K., et al., *Characterization of apelin, the ligand for the APJ receptor.* J Neurochem, 2000. **74**(1): p. 34-41.

66. Tatemoto, K., et al., *Isolation and characterization of a novel endogenous peptide ligand for the human APJ receptor.* Biochem Biophys Res Commun, 1998. **251**(2): p. 471-6.
67. Medhurst, A.D., et al., *Pharmacological and immunohistochemical characterization of the APJ receptor and its endogenous ligand apelin.* J Neurochem, 2003. **84**(5): p. 1162-72.
68. Kleinz, M.J. and A.P. Davenport, *Immunocytochemical localization of the endogenous vasoactive peptide apelin to human vascular and endocardial endothelial cells.* Regul Pept, 2004. **118**(3): p. 119-25.
69. Hamada, J., et al., *Evaluation of novel cyclic analogues of apelin.* Int J Mol Med, 2008. **22**(4): p. 547-52.
70. Masri, B., et al., *Apelin (65-77) activates extracellular signal-regulated kinases via a PTX-sensitive G protein.* Biochem Biophys Res Commun, 2002. **290**(1): p. 539-45.
71. Taylor, C.J., K. Motamed, and B. Lilly, *Protein kinase C and downstream signaling pathways in a three-dimensional model of phorbol ester-induced angiogenesis.* Angiogenesis, 2006. **9**(2): p. 39-51.
72. Ueda, Y., et al., *Protein kinase C activates the MEK-ERK pathway in a manner independent of Ras and dependent on Raf.* J Biol Chem, 1996. **271**(38): p. 23512-9.
73. Tatemoto, K., et al., *The novel peptide apelin lowers blood pressure via a nitric oxide-dependent mechanism.* Regul Pept, 2001. **99**(2-3): p. 87-92.
74. Eyries, M., et al., *Hypoxia-induced apelin expression regulates endothelial cell proliferation and regenerative angiogenesis.* Circ Res, 2008. **103**(4): p. 432-40.
75. Kasai, A., et al., *Apelin is a crucial factor for hypoxia-induced retinal angiogenesis.* Arteriosclerosis, thrombosis, and vascular biology, 2010. **30**(11): p. 2182-2187.
76. Lee DK, F.S., George SR, O'Dowd BF, *The fate of the internalized apelin receptor is determined by different isoforms of apelin mediating differential interaction with beta-arrestin.* Biochemical and Biophysical Research Communications, 2010. **395**(2): p. 185-189.
77. Evans, N.A., et al., *Visualizing differences in ligand-induced beta-arrestin-GFP interactions and trafficking between three recently characterized G protein-coupled receptors.* J Neurochem, 2001. **77**(2): p. 476-85.
78. Pope, G.R., et al., *Agonist-induced internalization and desensitization of the apelin receptor.* Mol Cell Endocrinol, 2016. **437**: p. 108-119.
79. Lee, D.K., et al., *Modification of the terminal residue of apelin-13 antagonizes its hypotensive action.* Endocrinology, 2005. **146**(1): p. 231-6.
80. Picault FX, C.-A.C., Projetti F, Prats H, Masri B, Audigiers Y, *Tumour co-expression of apelin and its receptor is the basis of an autocrine loop involved in the growth of colon adenocarcinoma.* European Journal of Cancer, 2014. **50**(3): p. 663-674.
81. Ma, Y., et al., *Structural Basis for Apelin Control of the Human Apelin Receptor.* Structure, 2017. **25**(6): p. 858-866 e4.
82. Inui, M., et al., *Xapelin and Xmsr are required for cardiovascular development in Xenopus laevis.* Dev Biol, 2006. **298**(1): p. 188-200.
83. Scott, I.C., et al., *The g protein-coupled receptor agtrl1b regulates early development of myocardial progenitors.* Dev Cell, 2007. **12**(3): p. 403-13.
84. Magali Saint-Geniez, B.M., et al., *Expression of the murine msr apj receptor and its ligand apelin is upregulated during formation of the retinal vessels.* Machanisms of Development, 2002. **110**(1-2): p. 183-186.
85. Kidoya, H., et al., *Spatial and temporal role of the apelin/APJ system in the caliber size regulation of blood vessels during angiogenesis.* EMBO J, 2008. **27**(3): p. 522-34.
86. Hashimoto, Y., et al., *G protein-coupled APJ receptor signaling induces focal adhesion formation and cell motility.* Int J Mol Med, 2005. **16**(5): p. 787-92.

87. Hosoya, M., et al., *Molecular and functional characteristics of APJ. Tissue distribution of mRNA and interaction with the endogenous ligand apelin.* J Biol Chem, 2000. **275**(28): p. 21061-7.
88. Cox, C.M., et al., *Apelin, the ligand for the endothelial G-protein-coupled receptor, APJ, is a potent angiogenic factor required for normal vascular development of the frog embryo.* Dev Biol, 2006. **296**(1): p. 177-89.
89. Kasai, A., et al., *Apelin is a novel angiogenic factor in retinal endothelial cells.* Biochem Biophys Res Commun, 2004. **325**(2): p. 395-400.
90. Kang, Y., et al., *Apelin-APJ signaling is a critical regulator of endothelial MEF2 activation in cardiovascular development.* Circ Res, 2013. **113**(1): p. 22-31.
91. Kuba, K., et al., *Impaired heart contractility in Apelin gene-deficient mice associated with aging and pressure overload.* Circ Res, 2007. **101**(4): p. e32-42.
92. Kasai, A., et al., *Retardation of retinal vascular development in apelin-deficient mice.* Arterioscler Thromb Vasc Biol, 2008. **28**(10): p. 1717-22.
93. Wang, Z., et al., *Elabela-apelin receptor signaling pathway is functional in mammalian systems.* Scientific Reports, 2015. **5**(8170).
94. Wang Z, Y.D., Wang M, Wang Q, Kouznetsova J, Yang R, Qian K, Wu W, Shuldiner A, Sztalryd C, Zou M, Zheng W, Gong DW, *Elabela-apelin receptor signaling pathway is functional in mammalian systems.* Scientific Reports, 2015. **5**(8170).
95. Chng, S.C., et al., *ELABELA: a hormone essential for heart development signals via the apelin receptor.* Dev Cell, 2013. **27**(6): p. 672-80.
96. Pauli, M.L.N., et al., *Toddler: An Embryonic Signal That Promotes Cell Movement via Apelin Receptors.* Science, 2014. **343**(6172).
97. Ho, L., et al., *ELABELA deficiency promotes preeclampsia and cardiovascular malformations in mice.* Science, 2017. **357**(6352): p. 707-713.
98. Kidoya, H., H. Naito, and N. Takakura, *Apelin induces enlarged and nonleaky blood vessels for functional recovery from ischemia.* Blood, 2010. **115**(15): p. 3166-74.
99. Chen D, L.J., Gu X, Wei L, Yu SP, *Intranasal Delivery of Apelin-13 Is Neuroprotective and Promotes Angiogenesis After Ischemic Stroke in Mice.* ASN Neuro, 2015. **7**(5).
100. Li, L., H. Zeng, and J.X. Chen, *Apelin-13 increases myocardial progenitor cells and improves repair postmyocardial infarction.* Am J Physiol Heart Circ Physiol, 2012. **303**(5): p. H605-18.
101. Kasai, A., et al., *Inhibition of apelin expression switches endothelial cells from proliferative to mature state in pathological retinal angiogenesis.* Angiogenesis, 2013. **16**(3): p. 723-34.
102. Kasai A, I.Y., Kinjo T, Satooka T, Matsumoto N, Yoshioka Y, Yamamuro A, Gomi F, Shintani N, Baba A, Maeda S., *Apelin is a crucial factor for hypoxia-induced retinal angiogenesis.* Arteriosclerosis, thrombosis, and vascular biology, 2010. **30**(11): p. 2182-2187.
103. Sorli SC, L.G.S., Knibiehler B, Audigier Y, *Apelin is a potent activator of tumour neoangiogenesis.* Oncogene, 2007. **26**(55): p. 7692- 9.
104. Berta J, K.I., Dobos J, Tovari J, Klepetko W, Jan Ankersmit H, Hegedus B, Renyi-Vamos F, Varga J, Lorincz Z, Paku S, Ostoros G, Rozsas A, Timar J, Dome B, *Apelin expression in human non-small cell lung cancer: role in angiogenesis and prognosis.* J Thorac Oncol, 2010. **5**(8): p. 1120-9.
105. Kidoya, H., et al., *The apelin/APJ system induces maturation of the tumor vasculature and improves the efficiency of immune therapy.* Oncogene, 2012. **31**(27): p. 3254-64.
106. Wang, Z., G.H. Greeley, Jr., and S. Qiu, *Immunohistochemical localization of apelin in human normal breast and breast carcinoma.* J Mol Histol, 2008. **39**(1): p. 121-4.

107. Wang, G., et al., *Characterization of the 5'-regulatory regions of the rat and human apelin genes and regulation of breast apelin by USF.* FASEB J, 2006. **20**(14): p. 2639-41.
108. Zhang L, T.K., Yamakawa D, Kidoya H, Takakura N, *apelin as a marker for monitoring the tumor vessel normalization window during antiangiogenic therapy.* Cancer Science, 2016. **107**(1): p. 36 - 44.
109. Heo, K.K.Y., et al., *Hypoxia-induced up-regulation of apelin is associated with a poor prognosis in oral squamous cell carcinoma patients.* Oral Oncol, 2012. **48**(6): p. 500-506.
110. Masiero, M.S.F., et al., *A core human primary tumor angiogenesis signature identifies the endothelial orphan receptor ELTD1 as a key regulator of angiogenesis.* Cancer Cell, 2013. **24**(2): p. 229-241.
111. Patel, S.J., et al., *Identification of essential genes for cancer immunotherapy.* Nature, 2017. **548**(7669): p. 537-542.
112. Prinz, M., D. Erny, and N. Hagemeyer, *Ontogeny and homeostasis of CNS myeloid cells.* Nat Immunol, 2017. **18**(4): p. 385-392.
113. Markovic, D.S., et al., *Gliomas induce and exploit microglial MT1-MMP expression for tumor expansion.* Proc Natl Acad Sci U S A, 2009. **106**(30): p. 12530-5.
114. Galarneau, H., et al., *Increased glioma growth in mice depleted of macrophages.* Cancer Res, 2007. **67**(18): p. 8874-81.
115. Charles, N.A., et al., *The brain tumor microenvironment.* Glia, 2011. **59**(8): p. 1169-80.
116. Ransohoff, R.M., *A polarizing question: do M1 and M2 microglia exist?* Nat Neurosci, 2016. **19**(8): p. 987-91.
117. Glass, R. and M. Synowitz, *CNS macrophages and peripheral myeloid cells in brain tumours.* Acta Neuropathol, 2014. **128**(3): p. 347-62.
118. Parks, W.C., C.L. Wilson, and Y.S. Lopez-Boado, *Matrix metalloproteinases as modulators of inflammation and innate immunity.* Nat Rev Immunol, 2004. **4**(8): p. 617-29.
119. Ruben R. Gonzalez-Perez, B.R.R., *Tumor Angiogenesis Regulators.* 2013.
120. Murdoch, C., et al., *The role of myeloid cells in the promotion of tumour angiogenesis.* Nat Rev Cancer, 2008. **8**(8): p. 618-31.
121. Nishie, A., et al., *Macrophage infiltration and heme oxygenase-1 expression correlate with angiogenesis in human gliomas.* Clin Cancer Res, 1999. **5**(5): p. 1107-13.
122. Alfaro, C., et al., *Tumor-Produced Interleukin-8 Attracts Human Myeloid-Derived Suppressor Cells and Elicits Extrusion of Neutrophil Extracellular Traps (NETs).* Clin Cancer Res, 2016. **22**(15): p. 3924-36.
123. Noy, R. and J.W. Pollard, *Tumor-associated macrophages: from mechanisms to therapy.* Immunity, 2014. **41**(1): p. 49-61.
124. Piao, Y., et al., *Glioblastoma resistance to anti-VEGF therapy is associated with myeloid cell infiltration, stem cell accumulation, and a mesenchymal phenotype.* Neuro Oncol, 2012. **14**(11): p. 1379-92.
125. Du, R., et al., *HIF1alpha induces the recruitment of bone marrow-derived vascular modulatory cells to regulate tumor angiogenesis and invasion.* Cancer Cell, 2008. **13**(3): p. 206-20.
126. Bergers, G. and D. Hanahan, *Modes of resistance to anti-angiogenic therapy.* Nat Rev Cancer, 2008. **8**(8): p. 592-603.
127. Cotechini, T., T.R. Medler, and L.M. Coussens, *Myeloid Cells as Targets for Therapy in Solid Tumors.* Cancer J, 2015. **21**(4): p. 343-50.
128. Yuting Ma, R.C., Laetitia Aymeric, Clara Locher, Oliver Kepp, Guido Kroemer, and Laurence Zitvogel, *How to improve the immunogenicity of chemotherapy and radiotherapy.* Cancer and Metastasis Reviews, 2001. **30**(1).

129. Szulzewsky, F., et al., *Glioma-associated microglia/macrophages display an expression profile different from M1 and M2 polarization and highly express Gpnmb and Spp1.* PLoS One, 2015. **10**(2): p. e0116644.
130. Kahles, F., H.M. Findeisen, and D. Bruemmer, *Osteopontin: A novel regulator at the cross roads of inflammation, obesity and diabetes.* Mol Metab, 2014. **3**(4): p. 384-93.
131. Tardelli, M., et al., *Osteopontin is a key player for local adipose tissue macrophage proliferation in obesity.* Mol Metab, 2016. **5**(11): p. 1131-1137.
132. Liu, Q.F., et al., *Apelin-13-induced proliferation and migration induced of rat vascular smooth muscle cells is mediated by the upregulation of Egr-1.* Biochem Biophys Res Commun, 2013. **439**(2): p. 235-40.
133. *United Kingdom Co-ordinating Committee on Cancer Research (UKCCCR) Guidelines for the Welfare of Animals in Experimental Neoplasia (Second Edition).* Br J Cancer, 1998. **77**(1): p. 1-10.
134. Campos, B., et al., *Differentiation therapy exerts antitumor effects on stem-like glioma cells.* Clin Cancer Res, 2010. **16**(10): p. 2715-28.
135. Schindelin, J., et al., *Fiji: an open-source platform for biological-image analysis.* Nat Methods, 2012. **9**(7): p. 676-82.
136. Schindelin, J., et al., *The ImageJ ecosystem: An open platform for biomedical image analysis.* Mol Reprod Dev, 2015. **82**(7-8): p. 518-29.
137. Hu, Y. and G.K. Smyth, *ELDA: extreme limiting dilution analysis for comparing depleted and enriched populations in stem cell and other assays.* J Immunol Methods, 2009. **347**(1-2): p. 70-8.
138. Pope, G.R., et al., *Central and peripheral apelin receptor distribution in the mouse: species differences with rat.* Peptides, 2012. **33**(1): p. 139-48.
139. Yamaguchi, M., et al., *Visualization of neurogenesis in the central nervous system using nestin promoter–GFP transgenic mice. Neuroreport.* Neuroreport 2000. **11**: p. 1991–1996.
140. Zhang, J., Jianwei J., *Molecular Biomarkers for Embryonic and Adult Neural Stem Cell and Neurogenesis.* Biomed Res Int, 2015. **2015**.
141. Hanahan, D. and J. Folkman, *Patterns and emerging mechanisms of the angiogenic switch during tumorigenesis.* Cell, 1996. **86**(3): p. 353-64.
142. Sakariassen, P.O., et al., *Angiogenesis-independent tumor growth mediated by stem-like cancer cells.* Proc Natl Acad Sci U S A, 2006. **103**(44): p. 16466-71.
143. Talasila, K.M., et al., *EGFR wild-type amplification and activation promote invasion and development of glioblastoma independent of angiogenesis.* Acta Neuropathol, 2013. **125**(5): p. 683-98.
144. Dharmacon, T. *http://dharmacon.gelifesciences.com//rnai/shrna/#all*. 2017.
145. Wojcik, E.J., et al., *Kinesin-5: cross-bridging mechanism to targeted clinical therapy.* Gene, 2013. **531**(2): p. 133-49.
146. T., K.Y.a.Q., *Apelin-APJ Signaling in Retinal Angiogenesis.* Arterioscler Thromb Vasc Biol, 2008. **28**(10): p. 1687 - 1688.
147. Mastrella, G., et al., *Targeting APLN/APLNR Improves Antiangiogenic Efficiency and Blunts Proinvasive Side Effects of VEGFA/VEGFR2 Blockade in Glioblastoma.* Cancer Res, 2019. **79**(9): p. 2298-2313.
148. Kidoya H., e.a., *Apelin induces enlarged and nonleaky blood vessels for functional recovery from ischemia.* Blood, 2010. **115**(15): p. 3166-74.
149. Eskilsson, E., et al., *EGFRvIII mutations can emerge as late and heterogenous events in glioblastoma development and promote angiogenesis through Src activation.* Neuro Oncol, 2016.

150. An, D.S., et al., *Optimization and functional effects of stable short hairpin RNA expression in primary human lymphocytes via lentiviral vectors.* Mol Ther, 2006. **14**(4): p. 494-504.
151. Reinhard S, W.E., *How to Tackle the Challenge of siRNA Delivery with Sequence-Defined Oligoamino Amides.* Macromol Biosci, 2017. **17**(1).
152. Stoddart, L.A., et al., *Probing the pharmacology of G protein-coupled receptors with fluorescent ligands.* Neuropharmacology, 2015. **98**: p. 48-57.
153. Calebiro, D. and A. Godbole, *Internalization of G-protein-coupled receptors: Implication in receptor function, physiology and diseases.* Best Pract Res Clin Endocrinol Metab, 2018. **32**(2): p. 83-91.
154. Thomsen, A.R.B., et al., *Therapeutic Targeting of Endosomal G-Protein-Coupled Receptors.* Trends Pharmacol Sci, 2018. **39**(10): p. 879-891.
155. Pediani, J.D., et al., *Spatial Intensity Distribution Analysis: Studies of G Protein-Coupled Receptor Oligomerisation.* Trends Pharmacol Sci, 2018. **39**(2): p. 175-186.
156. Zhang, P., et al., *Lipo-Oligomer Nanoformulations for Targeted Intracellular Protein Delivery.* Biomacromolecules, 2017. **18**(8): p. 2509-2520.
157. Lee, D.K., et al., *Agonist-independent nuclear localization of the Apelin, angiotensin AT1, and bradykinin B2 receptors.* J Biol Chem, 2004. **279**(9): p. 7901-8.
158. Hambardzumyan, D., et al., *Modeling Adult Gliomas Using RCAS/t-va Technology.* Transl Oncol, 2009. **2**(2): p. 89-95.
159. Czabanka, M., et al., *Combined temozolomide and sunitinib treatment leads to better tumour control but increased vascular resistance in O6-methylguanine methyltransferase-methylated gliomas.* Eur J Cancer, 2013. **49**(9): p. 2243-52.
160. Chen, Q., et al., *An osteopontin-integrin interaction plays a critical role in directing adipogenesis and osteogenesis by mesenchymal stem cells.* Stem Cells, 2014. **32**(2): p. 327-337.
161. Greter, M., I. Lelios, and A.L. Croxford, *Microglia Versus Myeloid Cell Nomenclature during Brain Inflammation.* Front Immunol, 2015. **6**: p. 249.
162. Kai Nie, Z.M., and Francis G. Szele, *Proliferation but Not Migration Is Associated with Blood Vessels during Development of the Rostral Migratory Stream.* Dev Neurosci, 2010. **32**(3): p. 163-172.
163. Molnár, H.B.S.a.Z., *Neurogenic niches in the brain: help and hindrance of the barrier systems.* Front Neurosci, 2015. **9**(20).
164. Harford-Wright, E., et al., *Pharmacological targeting of apelin impairs glioblastoma growth.* Brain, 2017. **140**(11): p. 2939-2954.
165. Perjes, A., et al., *Characterization of apela, a novel endogenous ligand of apelin receptor, in the adult heart.* Basic Res Cardiol, 2016. **111**(1): p. 2.
166. Rivera, L.B., et al., *Intratumoral myeloid cells regulate responsiveness and resistance to antiangiogenic therapy.* Cell Rep, 2015. **11**(4): p. 577-91.
167. Carmeliet, P. and R.K. Jain, *Principles and mechanisms of vessel normalization for cancer and other angiogenic diseases.* Nat Rev Drug Discov, 2011. **10**(6): p. 417-27.
168. R. Stupp, M.B., M. J. van den Bent, J.-C. Tonn & G. Pentheroudakis, *High-grade glioma: ESMO Clinical Practice Guidelines for diagnosis, treatment and follow-up.* Annals of Oncology, 2014. **25**.
169. Miranda, A., et al., *Breaching barriers in glioblastoma. Part I: Molecular pathways and novel treatment approaches.* Int J Pharm, 2017. **531**(1): p. 372-388.
170. Huang, W.J., W.W. Chen, and X. Zhang, *Glioblastoma multiforme: Effect of hypoxia and hypoxia inducible factors on therapeutic approaches.* Oncol Lett, 2016. **12**(4): p. 2283-2288.
171. Fischer, C., et al., *Anti-PlGF inhibits growth of VEGF(R)-inhibitor-resistant tumors without affecting healthy vessels.* Cell, 2007. **131**(3): p. 463-75.

172. Koh, Y.J., et al., *Double antiangiogenic protein, DAAP, targeting VEGF-A and angiopoietins in tumor angiogenesis, metastasis, and vascular leakage.* Cancer Cell, 2010. **18**(2): p. 171-84.
173. Xu, Y.Y., et al., *Development of targeted therapies in treatment of glioblastoma.* Cancer Biol Med, 2015. **12**(3): p. 223-37.

LMU LUDWIG-MAXIMILIANS-UNIVERSITÄT MÜNCHEN

Dean's Office
Medical Faculty

Affidavit

Mastrella Giorgia

Surname, first name

[redacted]

Street

[redacted]

Zip code, town

Germany

Country

I hereby declare, that the submitted thesis entitled

APLN-APLNR signaling controls tumor angiogenesis and glioblastoma cell invasion

is my own work. I have only used the sources indicated and have not made unauthorised use of services of a third party. Where the work of others has been quoted or reproduced, the source is always given.

I further declare that the submitted thesis or parts thereof have not been presented as part of an examination degree to any other university.

Munich, 24th December 2019

Place, date

Mastrella Giorgia

Signature doctoral candidate